Answers to reviewer 1 (Paper-IOP16-NHESS)

We would like to thank the anonymous reviewer for the valuable comments, suggestions and questions. We have considered all comments. We believe that the quality of the manuscript has increased, thanks to the comments of the reviewer and acknowledge how answering the raised questions has been crucial for a better exposition of our key messages.

1 - GENERAL COMMENTS

R1C1. First of all, it contains numerous purely speculative assertions that are not at all substantiated. This is reinforced by the fact that results are often given before they are demonstrated (this should be reversed). More rigorous justifications are needed to make the discussion paper a compelling study.

We have corrected all speculative answers and hypothesis in the manuscript, as well as reorganized the conclusions to be given after presenting the corresponding results only.

We would like to add, that this case study belongs to a series of modelling experiments performed in our group which are object of an on-going publication. In these modelling experiments we analysed the impact of nudging GPS-ZTD on several heavy precipitation events of the HyMeX period as well as the statistics of the complete autumn season. This is why at times in the manuscript some statements are introduced which are not justified. These statements arise from further analysis on the period which are not presented in the paper. This has been corrected accordingly to show only information relative to IOP16.

R1C2. Second, as justly stated by the authors at the end of their concluding section, their study relies on one case only. This undermines the results concerning the sensitivity study to the assimilation of GPS ZTD data

We have adapted the manuscript to clearly state that the withdrawn conclusions correspond to the presented case only (IOP16). This is done for example at lines L579-580.

In connection with the previous answer, we will submit in the coming weeks a publication with analyses on heavy precipitation and the impact of the GPS-ZTD nudging for the whole season. The selected case study object of this paper is a relevant event of the period since the GPS-ZTD showed very interesting impacts on convective development, as explained in the manuscript. The simulations presented in this paper are used, together with other simulations and observational data, in the analyses of this future publication on the seasonal time scale.

To let the readers know about the broader scope of these studies we have adapted the following section.

2.2.2 The GPS-ZTD Nudging Sensitivity Experiments (L244-246)

IOP16, the case study of this paper, is one of them which is especially interesting given the large reduction of maximum precipitation (-20 %) induced by the GPS-ZTD nudging over the investigation area of Corsica in the course of 26 h. The remaining cases of the autumn 2012 period and analyses on the complete season are part of a series of modelling studies from our working group, including a PhD thesis by Caldas-Alvarez (2019). IOP16 is also suitable to assess the benefit of atmospheric moisture corrections with GPS-ZTD nudging given the important role of the local orographic and instability factors in triggering and maintaining convection rather than the large-scale upper level forcing.

R1C3. *all the more since the different runs start much earlier than the event itself. In doing so, it is difficult to link the impact of the assimilation of ZTD-GPS data to the simulated precipitation. Differences observed during the chosen event might simply be due to the chaotic nature of the atmosphere. In any case, such a configuration does*

not help understand where and when the assimilation of GPS ZTD data has the most impact on precipitation. authors should start the different runs shortly before the event starts

This is in connection with the previous answers. We believe that analysing one case study from a seasonal simulation can be useful to relate the findings for this one case study with the analysis of the whole Autumn period. In addition, we think that starting the simulation 50 days before the event allows us to study the hypothesis that correcting the atmospheric moisture also during previous events (not only during the selected case study) would bring a larger improvement for precipitation. In this sense we wanted to profit from the availability of the unique GPS-ZTD data set, that covers the whole SOP1 period and part of 2013 (1-Sep-2012 to 20-Nov-2013). Moreover, the earlier initialization introduces a spin up time for slower processes such as soil-atmosphere interactions that are affected by precipitation during previous events.

Since we consider relevant the question raised by the reviewer, how different the impact will be depending on the initialization day, we performed additional simulations starting only a few days before the event using the same settings and forcing data but initialized on the 20-Oct-2012. This date was selected to ensure the representation of the large moisture evapotranspiration over north Africa (20 to 21-Oct), demonstrated in Fig. 6 of the manuscript.

a)

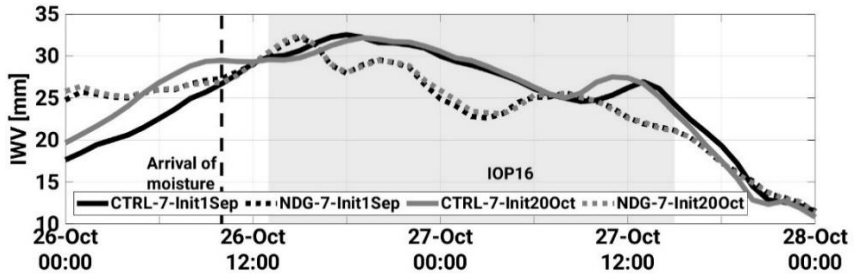

b)

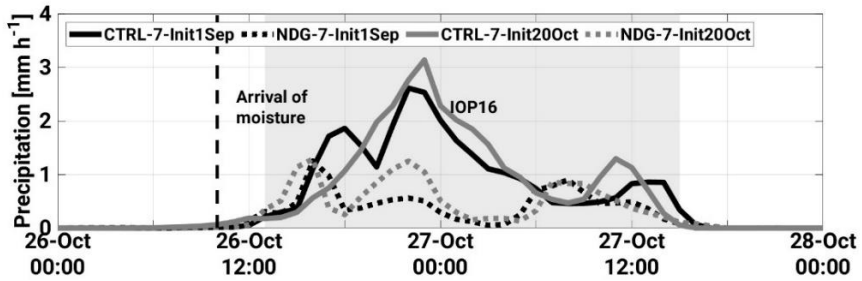

c)

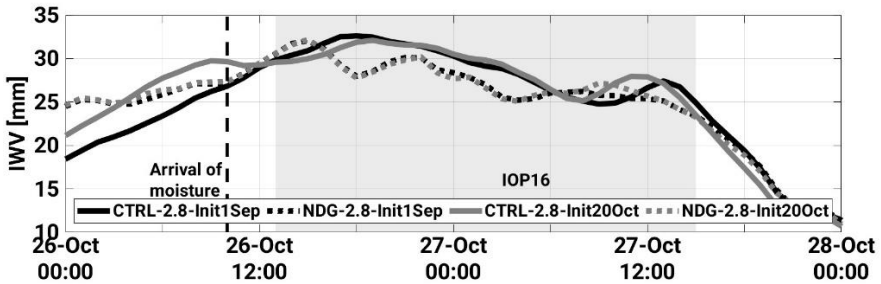

d)

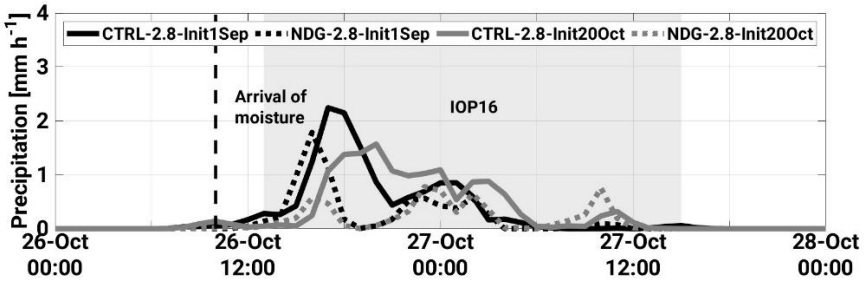

Figure 1. Spatially averaged IWV (a, c) and Precipitation (b, d) for the 7 km simulations (a, b) and the 2.8 km (c, d) during the event. The area of the spatial averages is Corsica. The model output has been upscaled to a common coarser grid of 8 km to allow for comparison. The period shown is 26-Oct 0000 UTC to 28-Oct 0000 UTC.

Regarding IWV, the shorter simulations show differences in that the IWV increase happens 1 to 2 h earlier in the CTRL runs initialized on the 20-Oct (Init20Oct). This holds for both resolutions. The NDG runs show, however, no perceptible differences for the temporal evolution of spatially averaged hourly IWV. On the contrary, precipitation shows relevant differences for both resolutions (Fig. 1b and Fig.1.d). NDG-7-Init20ct shows two maxima instead of three with somewhat larger precipitation intensities. NDG-2.8-Init20Oct shows a delayed (1 h) onset of precipitation and lower precipitation rates as compared to CTRL-2.8-Init1Sep.

A plausible explanation for these findings, as stated by the reviewer, is the chaotic nature of the atmosphere that is affected by all perturbations in earlier stages. This analysis will be added in the annex of the manuscript as supplementary information for the readers. We prefer not to include it in the body of the paper, since it deviates from the objective for the article.

We believe using the longer simulations, i.e. started on the 1-Sep-2012, have the advantage of relating the findings with those of our planed publication on the complete autumn season and that they benefit from the whole duration of the GPS-ZTD data set. Therefore, we will present in our manuscript the analyse with these simulations as in the first version but will add a supplementary subsection within *4-Nudging Effects on Convection* where the sorter simulations will be introduced and analysed. This will be done to present the results of the 1h vs. 10min frequency comparison (see comment R1C5).

R1C4. authors should include some estimation of the impact duration of the GPS-ZTD data assimilation by running some free runs and determining when they converge

Our simulations span the whole autumn season to cover the duration of the HyMeX SOP1 and the availability of the GPS-ZTD data. This is why it is not possible to answer when would the assimilated and the free runs converge. Our scientific question was *how is convective precipitation impacted by a continuous correction of IWV in the model?* The modelling set up was planned in a different way to usual data-denial assimilation experiments (Borderies, et al., 2019; Benjamin, et al., 2010; Mahfouf, et al., 2015) in that these experiments data assimilation is performed during a given time window to obtain the initial conditions for a future step of first guesses. These data-denial experiments allow to study how long the impact of an observation type stays in the system as the analysed runs converge with the forecasts, but our set-up was not conceived to provide information on this.

R1C5. the benefit of a sub-hourly frequency versus, e.g., at hourly frequency, has not been demonstrated (coming from my sentence "modelling experiments demonstrated the benefit of sub-hourly GPS-ZTD nudging to improve the modelling of precipitation")

Thanks for this comment. We acknowledge that the sentence was misleading. We wanted to express that our experiments nudging GPS-ZTD with a 10-min frequency showed an improvement for this case study. This has been corrected in the manuscript.

We agree that this is an interesting aspect, thus we have performed supplementary simulations to investigate more in detail this issue. We run the 20-Oct-2012 to 28-Oct-2012 0000 UTC period as in the comment R1C3, applying the GPS-ZTD nudging with a frequency of 1 h, as opposite to the 10 min frequency. All other settings are the same as NDG-7-Init20Oct and NDG-2.8-Init20Oct respectively. Hereafter we name these simulations simply as CTRL-7, CTRL-2.8, NDG-7, NDG-2.8, NDG-7-1h and NDG-2.8-1h. These six simulations have been initialized on the 20-Oct-2012

a)

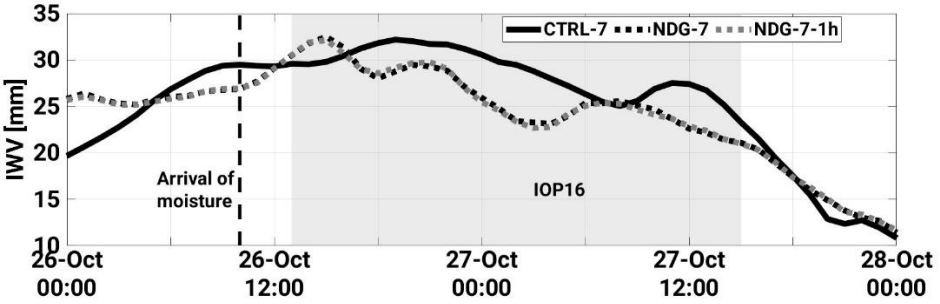

b)

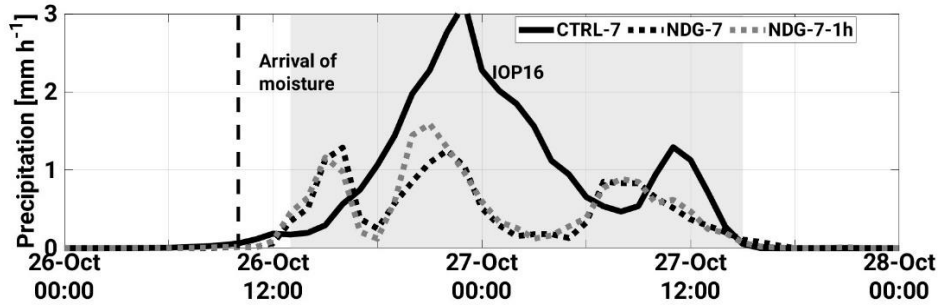

c)

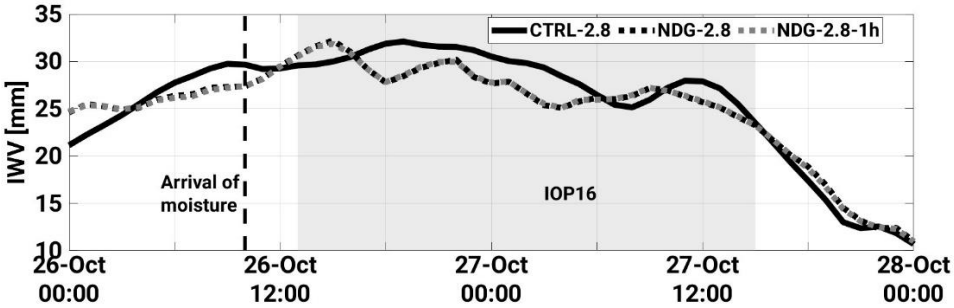

d)

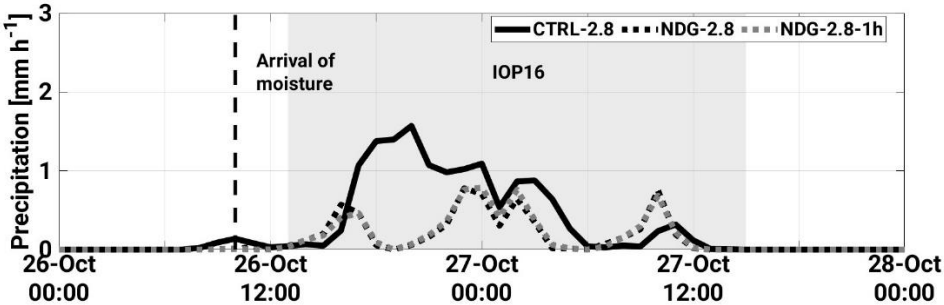

Figure 2. Spatially averaged IWV (a, c) and Precipitation (b, d) for the 7 km simulations (a, b) and the 2.8 km simulations (c, d) during the event. The area for averaging is Corsica. The model output has been upscaled to a common coarser grid of 8 km. The period shown is 26-Oct 0000 UTC to 28-Oct 0000 UTC. The comparison is between the runs using a temporal nudging frequency of 10 min (NDG-7, NDG-2.8) against nudging at a temporal frequency of 1h (NDG-7-1h, NDG-2.8-1h).

The results show no differences on the temporal evolution of IWV. This holds for 7 km and 2.8 km. This can be explained by the fact that we calculate the spatially averaged IWV at sharp hours (i.e. 0000 UTC, 0100 UUTC, 0200 UTC, etc.), precisely is at those times when the GPS-ZTD data is assimilated in the NDG-7-1h and the NDG-2.8-1h runs.

For precipitation, there is a slight impact for the 7 km runs, but not for the 2.8 km. The NDG-7-1h simulation shows a somewhat larger precipitation than NDG-7 at 2000 UTC on the 26-Oct (Fig. 2b) corresponding to an increase from 30 mm to 50 mm at the western shore of the island (Fig.3.b and Fig. 3.c).

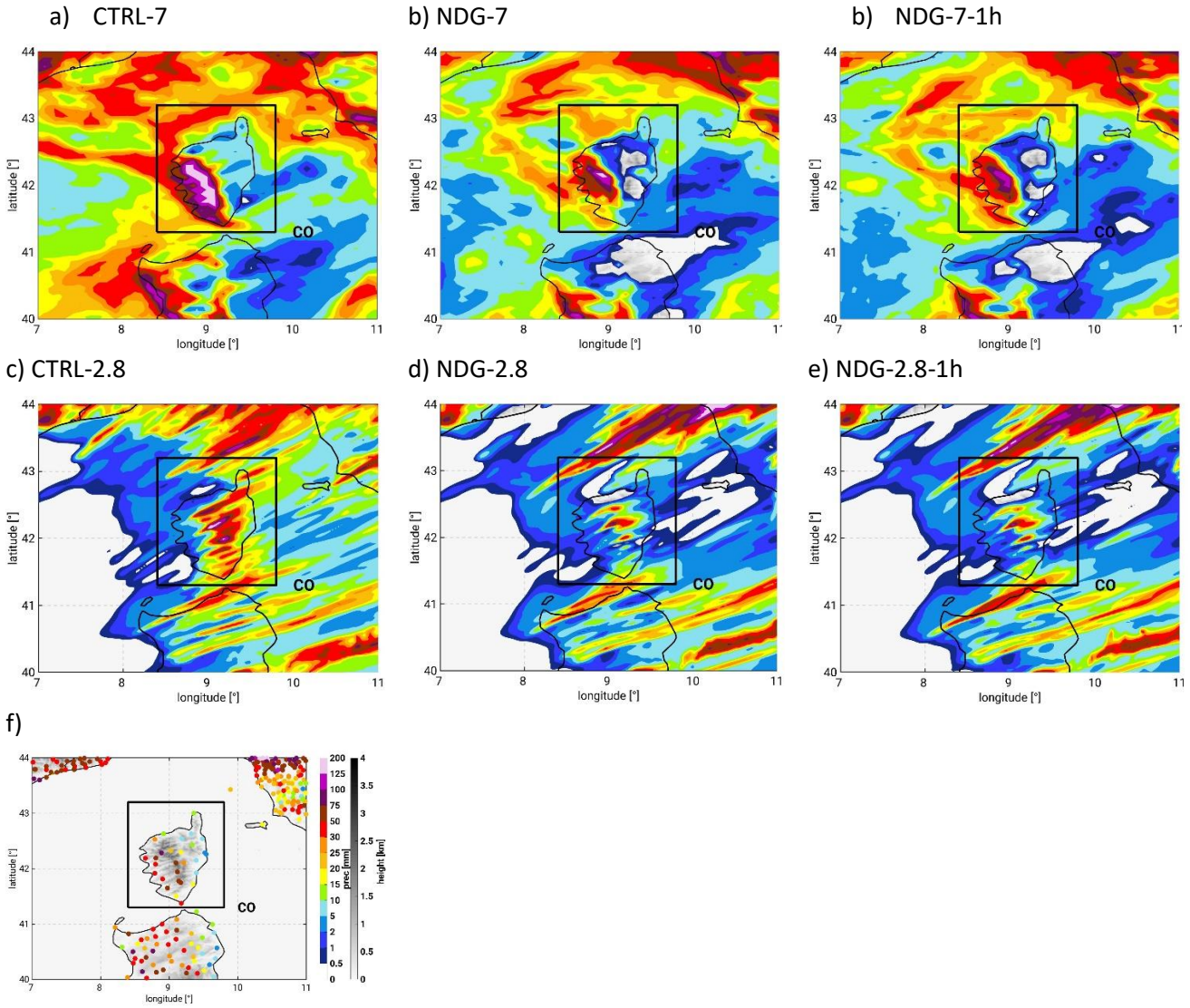

Figure 3. COSMO-CLM accumulated precipitation over Corsica between 26-Oct 1300 UTC and 27-Oct 1500 UTC i.e. during the period of precipitation over the island and RG.

To delve further into which aspects of precipitation representation have been improved, we present in Table 1 further validation metrics using the Rain Gauges (RG) as reference.

Table 1 shows the RMSE of the anomalies of hourly precipitation rates (first column), the differences (OBS-MOD) of the standard deviations of hourly precipitation (second column) and the spatially averaged differences of accumulated precipitation during the whole event, i.e. between 26-Oct 1300 UTC and 27-Oct 1500 UTC (third column). The last three metrics are obtained after interpolating the COSMO-CLM precipitation values to the location of the RG stations. On the other hand, columns four and five of Table 1, show differences of the standard deviation and maximum value of precipitation for COSMO-CLM over land without interpolation. That means, we have obtained all 27h-accumualeted precipitation values simulated by COSMO-CLM over land and have calculated the standard deviation and the maximum. We have done the same for all RG measurements and the

differences are shown. We do this to avoid double-penalty problems due to a possible misrepresentation of the maxima location (Wernli, et al., 2008; Gilleland, et al., 2009). The formulas used are included in Table 2.

Table 1. Metrics of the precipitation validation against RG. The model precipitation has been interpolated to the location of the RG for the first three columns and all precipitation values simulated by COSMO-CLM over the island of Corsica are used in the last two columns. This is done to avoid double-penalty problems due to a shifting of the precipitation maxima. N is the number of RG stations and M the total number of grid points over land. The units are mm.

	Interp. To RG location			Distributions without interpolation	
[mm]	**RMSE** (h)	$\boldsymbol{OBS_\sigma - MOD_\sigma}$ (1h)	$\boldsymbol{\overline{OBS} - \overline{MOD}}$ (27h)	$\boldsymbol{OBS_\sigma - MOD_\sigma}$ (27h)	$\boldsymbol{OBS_{max} - MOD_{max}}$ (27h)
CTRL-7-Init20Oct	3.3	-0.85	-19.1	-33	-170
NDG-7-Init20Oct	2.5	0.73	12.5	-5	-79
NDG-7-1h- Init20Oct	2.5	0.95	12.2	-4	-50
CTRL-2.8-Init20Oct	3.6	-0.15	9.5	-3	-74
NDG-2.8-Init20Oct	2.6	1.64	23.8	11	-16
NDG-2.8-1h- Init20Oct	2.5	1.64	23.6	10	-17

Table 2. Precipitation validation metrics.

RMSE (1h)	$\sqrt{\sum_{i(1h)}^{N}((OBS_i - \overline{OBS}) - (MOD_i - \overline{MOD}))^2}$
$\boldsymbol{OBS_\sigma - MOD_\sigma}$ (1h)	$\sqrt{\frac{1}{N}\sum_{i(1h)}^{N}(OBS_i - \overline{OBS})^2} - \sqrt{\frac{1}{N}\sum_{i(1h)}^{N}(MOD_i - \overline{MOD})^2}$
$\boldsymbol{\overline{OBS} - \overline{MOD}}$ (27h)	$\frac{1}{N}\sum_{i(27h)}^{N} OBS_i - \frac{1}{N}\sum_{i(27h)}^{N} MOD_i$
$\boldsymbol{OBS_\sigma - MOD_\sigma}$ (27h)	$\sqrt{\frac{1}{N}\sum_{i(27h)}^{N}(OBS_i - \overline{OBS})^2} - \sqrt{\frac{1}{M}\sum_{j(27h)}^{M}\left(MOD_j - \overline{MOD}\right)^2}$
$\boldsymbol{OBS_{max} - MOD_{max}}$ (27h)	$\max(OBS_i) - \max(MOD_j)$

Overall, we see that nudging GPS-ZTD data is beneficial for the 7 km grid with little difference between nudging with 1h frequency or 10 min. If any, we see a slight advantage in nudging GPS-ZTD data with 10 min for the representation of the hourly standard deviation rates. The same holds for the 2.8 km, assimilating with a 10min frequency shows very weak differences with respect to assimilating with 1h frequency.

These results will be included as an additional subsection in section 4.1 (Nudging effects on Precipitation).

R1C5. there is no "pure" modelling in the study since the model is constantly perturbed by the modification of its moisture field. The authors should be more specific about the usefulness of continuously nudging moisture.

We decided to perform a continuous nudging to study the scientific question "how does simulated precipitating convection respond to a sub-hourly moisture correction?". In the following version of the manuscript we state more clearly that our study is diagnostic and that we do not provide an assessment of the prognostic use of GPS-ZTD nudging. We have corrected the following parts.

In the Abstract

"In this study, we use a diagnostic approach to assess the sensitivity of precipitating convection and underlying mechanisms during a heavy precipitation event (HyMeX intensive observation period 16) to corrections of the atmospheric moisture spatio-temporal distribution."

In Section 2.2.2 of the Methods. The GPS-ZTD Nudging Sensitivity Experiments

"The Nudging scheme is used to assimilate GPS-ZTD data to assess the sensitivity of heavy precipitating convection to corrections of the spatio-temporal distribution of atmospheric moisture. We use a diagnostic approach as opposite to commonly use data-denial experiments."

As stated earlier in this document, our modelling setup differs from other data-denial assimilation experiments for instance (Benjamin, et al., 2010; Borderies, et al., 2019; Sahlaoui, et al., 2019). Hence the idea of finding new initial conditions for subsequent forecast intervals through data assimilation does not apply in our experiments.

We believe, our study is valuable we were able to show the potential of such observation nudging since, for this case study, hourly RMSE values, the maximum and standard deviation were improved using the GPS-ZTD nudging and in the 7 km grid. Furthermore, we also observed the problems of COSMO in representing the moisture vertical gradient with substantial differences between 7 km and 2.8 km and how the GPS nudging could not correct sufficiently the vertical humidity errors. We saw that for this case study, the reduction of instability and of humidity at the free-troposphere exerted the largest control for convective precipitation. The fact that we nudge our simulations to GPS values continuously for a whole season has the advantage that the corrections introduced are not only present during the event (as usually in data-denial experiments) but also in past events.

2 - SPECIFIC COMMENTS

R1C6. L47-49: The authors point out the interest of assimilating humidity data at sub-hourly frequencies. I suggest the authors study the sensitivity of the assimilation frequency by carrying out an additional experiment with a one-hour assimilation frequency. This would demonstrate to what extent a sub-hourly assimilation frequency is needed.

See section 1.

R1C7. Case study and numerical set-up: Why run experiments that last several months and study one case only? The differences seen in this specific case could be caused by a lower predictability rather than to improvements in the description of the humidity field.

See section 1.

R1C8. Case study and numerical set-up: Why is there no NDG-2.8 simulation forced by NDG-7? In theory, shouldn't this configuration yield the best results?

We decided to force the NDG-2.8 simulations with the CTRL-7 simulations to be able to compare NDG-2.8 to CTRL-2.8 directly. By doing so we were able to assess the direct impact of the GPS-ZTD nudging at the 2.8 km resolution which would have not been possible if the NDG-2.8 runs had been forced by different boundary conditions than their CTRL counterparts.

R1C9. L246-247: Can the authors please elaborate on why, "under a weak synoptic forcing, the impact of the GPS-ZTD is larger given the strongest correction of the lower to middle tropospheric humidity"?

Thanks for this comment. We acknowledge that the information of this sentence is not fully explanatory. This conclusion arises from the results we obtained in the seasonal simulations of the complete autumn period. Given the large number of heavy precipitation cases during that season and the advantage of having nudged GPS data continuously, we were able to ascertain which cases were impacted the most by the GPS-ZTD nudging. Precisely we found a larger sensitivity in the model for those cases of weak synoptic forcing such as IOP16 where the role of the local factors (i.e. latent instability, low-level moisture, wind convergence and orographic triggering) is more important for convection than the direct forcing of the large scale.

To clarify this question, we include here results of the analysis on all cases of the Autumn 2012 period. These graphs will not be included in the new version of the manuscript as they would be outside the scope of the paper but will be included in a future publication from our working group. We include them here for clarification of the raised question. Finally, in the new version of the abstract this point will be adequately explained and referenced.

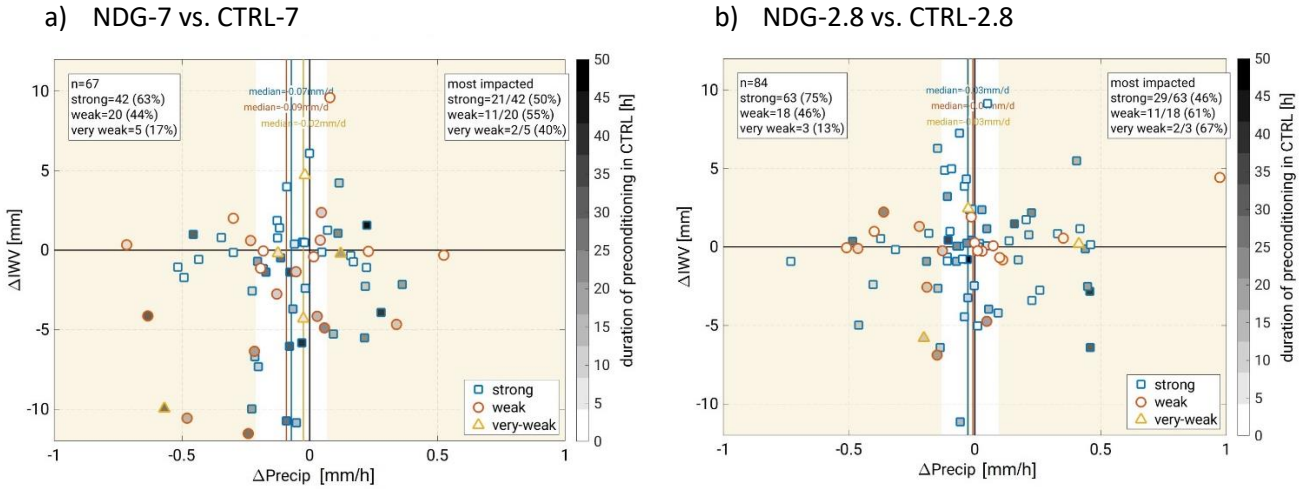

Figure 4. Scatterplot of IWV and precipitation variations due to the GPS-ZTD nudging for all events in the 1-Sep to 20-Nov period for the 7 km (a) and the 2.8 km (b). Each, dot accounts for one event. The events are detected by averaging hourly precipitation values over 8 study regions, of the HyMeX campaign (Ducrocq, 2015) and selecting those with average precipitation reaching 0.4 mm/h. The differences in precipitation and IWV (ΔPrecip, ΔIWV) are obtained after subtracting the average precipitation of NDG to CTRL. The degree of synoptic forcing (strong, weak, very weak) is calculated following the convective-adjustment time-scale criteria of Keil et al. (2013). The gray-scale color bar shows the duration of the event in the CTRL-7 and CTRL-2.8 runs respectively. The yellow shaded areas at the sides denote the areas of the upper and lower quartiles of precipitation variations. The upper-left and upper-right text boxes show statistics on the shown events.

In Fig. 4 we show the differences of IWV and precipitation for the events of the Autumn 2012 period between CTRL and their NDG counterparts (NDG-CTRL). We can see that 67 and 84 events took place in the total of the 8 investigation areas of the HyMeX campaign in the 7 km and the 2.8 km runs respectively. We can see, that 63 % of the cases in the 7 km runs and 75 % in the 2.8 km where categorized as synoptically strongly forced by the

convective adjustment time scale criteria, being the rest of them either weakly or very weakly forced. The events lying in the upper and lower quartiles of the precipitation distribution (yellow shaded areas) show that the most impacted events where those of a weak synoptic forcing (55 % in the 7 km runs and 61 % in the 2.8 km runs). The 2.8 km runs also show two out of three cases of very weak synoptic forcing within the upper and lower quartiles.

R1C10. Section 3.3: This section contains general statements, which are true, but are not new: writing that moisture is swept by a front and/or originates from the seas and oceans is true, but it would be much more interesting to know which fraction is swept and which fraction comes from evaporation

We agree with the reviewer that a quantification of the different terms of Evaporation and moisture flux over the investigation area NA and the Mediterranean would be most interesting. We have obtained the terms, described in Lamb et al. (2012) over the investigation areas NA (North Africa) and MED (Mediterranean Sea) for this purpose, see Fig. 5.a.

The calculation of these terms entails simplifications for example, of the turbulent and microphysical processes that introduce relevant uncertainties. Hence, what we provide here is an estimation of the different contributions.

$$\Delta IWV = E + (-P) + MFC \quad (1)$$

All terms of Eq. 1 are expressed in mmh^{-1}, where positive signs of the Evaporation (E) and Integrated Moisture Flux Convergence (MFC) imply an increase of Integrated Water Vapour variations (ΔIWV>0) within the NA and MED volumes. On the contrary, if precipitation and water vapor divergence occur (MFC<0) IWV decreases (ΔIWV<0). The volumes cover the areas in Fig. 5.a where the integrations of IWV and MFC are performed from the first to the last model levels.

Fig. 5.b shows similar information to Fig.6.c of the manuscript. Intense precipitation occurs over NA on the 20-Oct-2012 with the subsequent decrease of IWV, and intense evaporation over the area on the 21-Oct and 22-Oct at midday. This is the moment when solar radiation is strongest and evaporation is intensified over this wet soil. Please note the change in the axis scales between the different panels of this figure and those of Fig.6.c of the manuscript, expressed in mmd^{-1}. The order of magnitude of those evaporations over NA is the same as those over the Mediterranean Sea, up to 0.15 mmh^{-1}. This is better seen in Fig. 5.c. The evaporated moisture is advected with the wind flow, merging with the Atlantic and Mediterranean moisture.

To quantify how much the Mediterranean Sea contributed to the changes of atmospheric moisture at that location, Fig. 5.c shows the contribution from each of the moisture equation terms over the selected volume MED. We can see that between 22-Oct and 26-Oct 1200 UTC there is a positive, homogeneous evaporation from the Sea at a rate of 0.25 mmh^{-1} that picks up from 26-Oct 1200 UTC to 0.5 mmh^{-1} by 28-Oct 0000 UTC. The time of the evaporation pick up coincides the occurrence of precipitating convection over the Mediterranean Sea west of Corsica. The intensification of the evaporation is brought by the intensified drag of horizontal winds close to sea surface.

a)

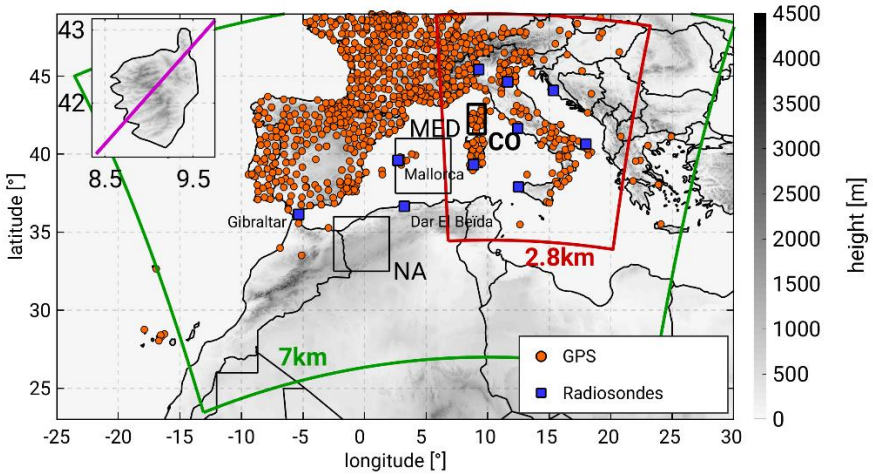

b) NA

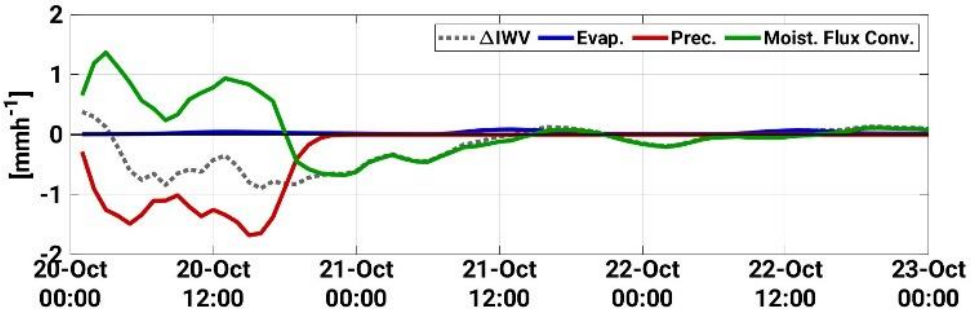

c) MED

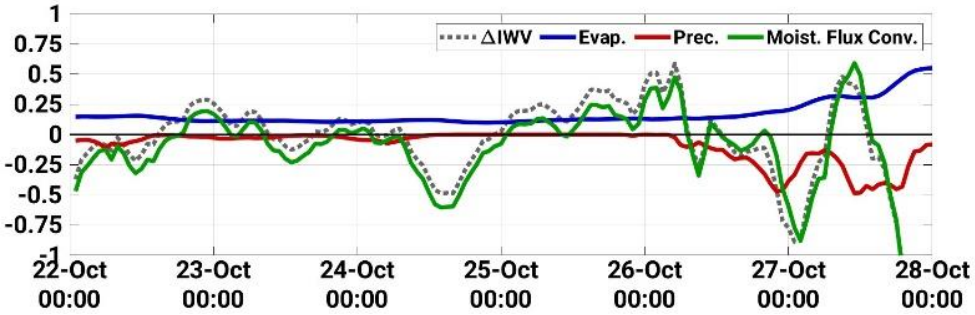

d) NA

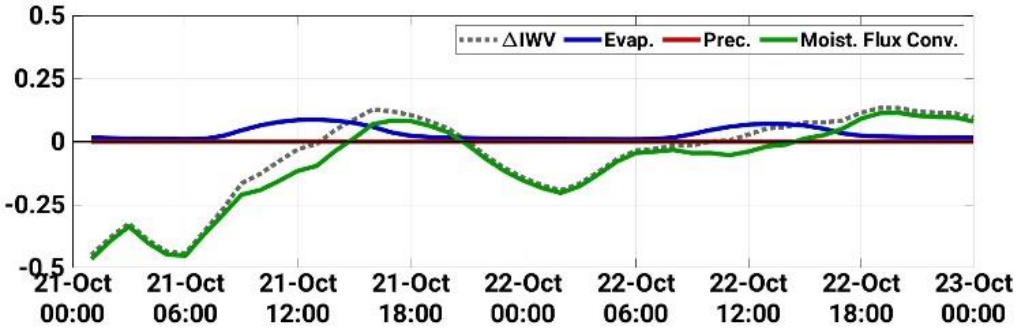

Figure 5. Analysis of the moisture budget terms. (a) Simulation domains as Fig.1 of the manuscript including the NA and MED areas for calculation of averaged evaporation, precipitation and moisture convergence. (b) Spatial average of hourly IWV variations (dotted grey), Evaporation (blue), Precipitation (red) and Moisture flux Convergence (green) in mmh^{-1}, over investigation area NA between 20-Oct and 23-Oct 0000 UTC. All variables are obtained from the CTRL-7 runs. (c) is as panel (b) but showing the averages over the investigation area MED between 22-Oct and 28-Oct 0000 UTC. (d) is as panel (b) but showing the spatial averages between 21-Oct and 23-Oct 0000 UTC. Mind the changes in the y-axis scaling.

R1C11. The CTRL-7 simulation is validated later (that would be better here or before!)

We will change this accordingly in the next version of the manuscript.

R1C12. no moisture budgets are computed,

See above

R1C13. A validation against MODIS is mentioned but not shown(?!)

We decided not to include this validation against MODIS IWV (version D3, daily product, 1°x1°, onboard Terra and Aqua) since some pixels had missing values. This is due to the inability of MODIS to retrieve IWV when there is cloud cover (Seemann, et al., 2003). Under these lines you can see the validation. Over the eastern Spanish coast and southern France on the 25-Oct-2012 and over the Alps and northern Italy on the 26-Oct-2016 there is no available MODIS data. For the areas with available MODIS data both Terra and Aqua MODIS observations overestimate IWV west of Corsica and Sardinia (25-Oct) and south of Italy (26-Oct) as compared to COSMO-CLM.

Given this issue of too many pixels showing missing values we decided not to include these figures in the manuscript and base our analysis on the model data, radiosondes and GPS.

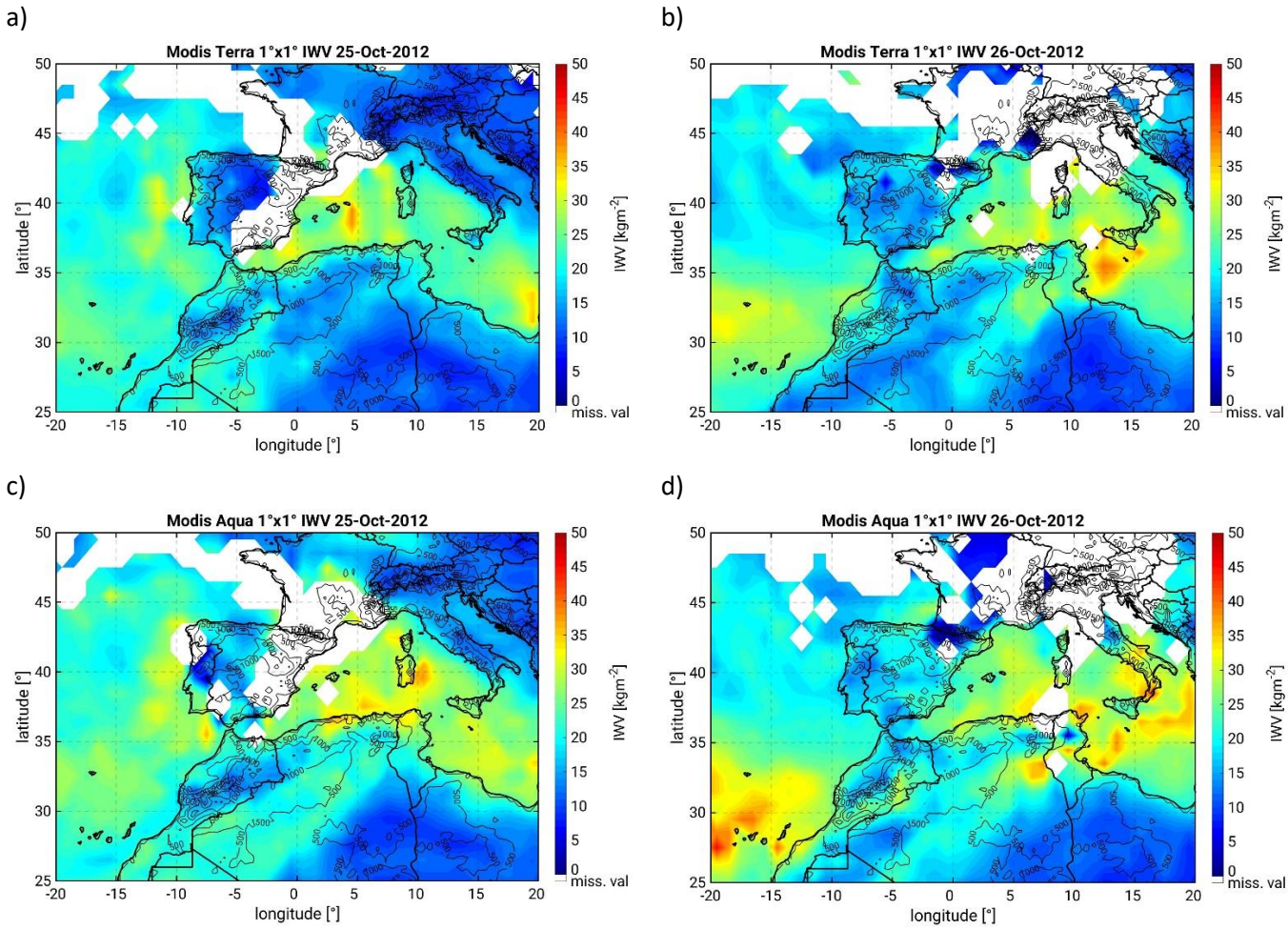

Figure 6. Daily averaged IWV measured MODIS onboard Terra (a, b) and Aqua (c, d). The spatial resolution is 1°x1°. The products used are MOD08_D3 and MYD08_D3.

R1C14. Furthermore, I suspect that labels A and B are inverted in the lower panel of Figure 6.b. If I am wrong, it means that I don't understand this panel.

The ellipses A and B try to explain which trajectories are found at which height in the GDAS-HySPLIT simulation. The fastest backward trajectories (those starting at the northwest corner of the island) are denoted with the ellipse A. On the other hand, ellipse B denotes the slower trajectories starting at the southeast corner of the matrix that reach northern Algeria in 24 h. We performed further analyses of these trajectories using the GDAS-HySPLIT model splitting the matrix of starting points. We saw that the first group of trajectories (ellipse A, reaching the Atlantic Ocean) travel for most of the 24 hours between the levels of 4000 m and 2000 m. On the other hand, the slow trajectories (ellipse B) in the last 12 h of the trajectory descend and travel at a height between 2000 m and 500 m. This is shown in the following graphs, that will be included as supplementary material in the next version of the manuscript. Moreover, a clearer explanation of the figure will be included in order to avoid the misinterpretation of this result.

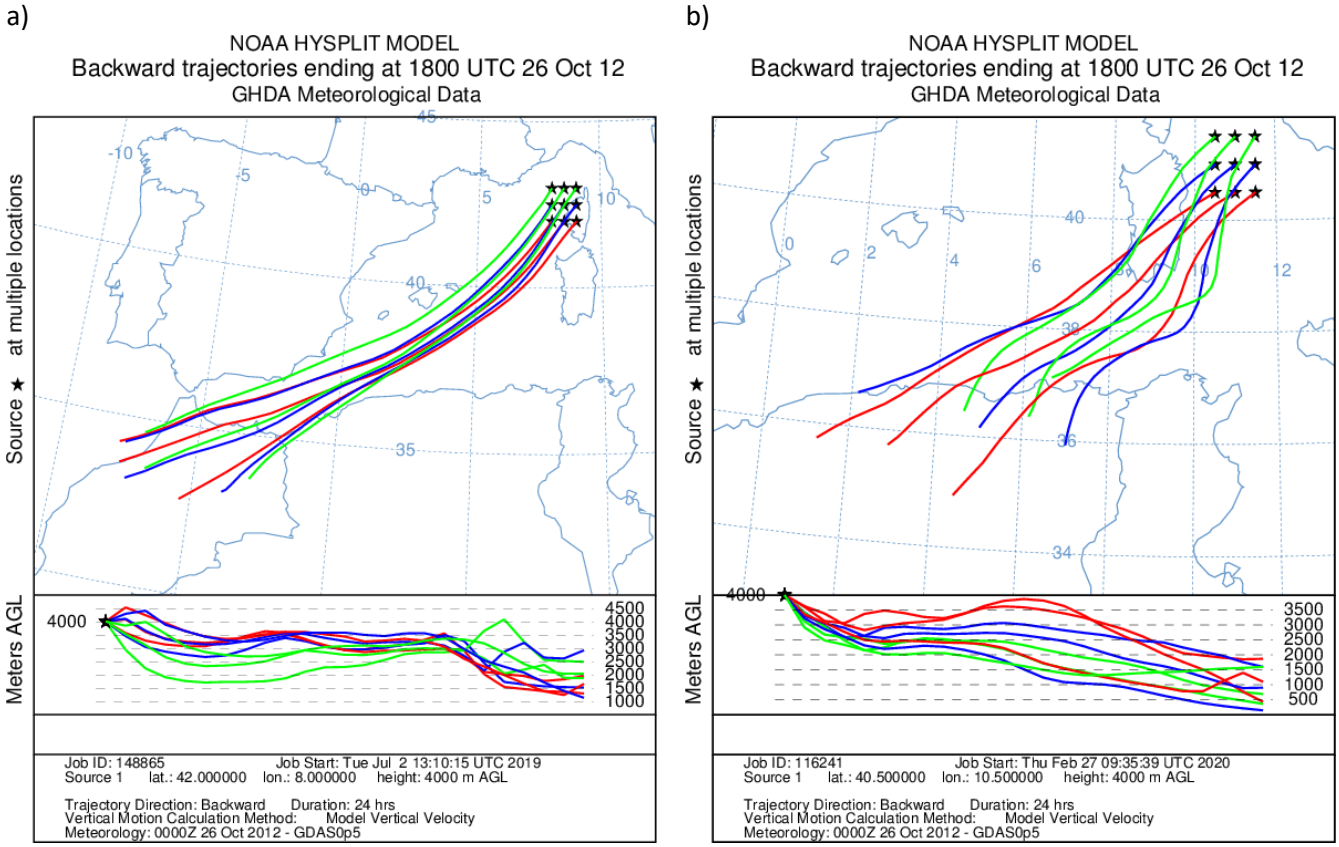

Figure 7. Lagrangian backward trajectories obtained with the HYSPLIT model, starting on the 26-Oct-2012 1800 UTC (initiation of the event over Corsica) back to for 24 h. Figure 7.a shows the northwest subset of the trajectories shown in Fig.6.d of the manuscript while Fig. 7.b shows the subset corresponding to the trajectories starting at the southeast of the investigation domain. Please not the changes of axis (longitude, latitude and height) shown between panels a and b.

R1C15. L352-353: Why does this "further promote the moisture uptake form the Sea"?

Lifting over the affected area is accompanied by strong low-level convergence close to the surface following the mass-continuity conservation law. Stronger surface winds induce larger evaporation rates over water or wet and vegetated soils (Schneider, et al., 2010; Peixoto & Abraham H. Oort, 1992). In CCLM this process is parameterized through the standard Bulk-Transfer scheme (Louis, 1979) that controls the heat and mass transfer between the surface (land or water) and the atmosphere (Schättler, et al., 2016). In this scheme, the surface water flux affects the atmosphere as lower boundary conditions for the turbulent moisture flux ($F_{q^v}^3$) within the turbulent mixing term of the model equations ($M_{q^v}^{TD}$). The turbulent moisture flux ($F_{q^v}^3$) is proportional to the horizontal wind speed over the surface ($|\overrightarrow{v_h}|$) following the next equation.

$$\left(F_{q^v}^3\right)_{sfc} = -\rho C_q^d |\overrightarrow{v_h}| \left(q^v - q_{sfc}^v\right) \quad (1)$$

Where ρ is the air density, $C_q^d$is the bulk-aerodynamical coefficient for turbulent moisture transfer, which is adapted to each surface type (water, soil type, vegetation, etc), $q_{sfc}^v$is the ground specific humidity and q^v is the humidity at the lowest model level. Hence, larger moisture flux from the surface (land, sea) to the atmosphere happens with larger horizontal wind speeds.

R1C16. L396-398: Looking only at the maximum precipitation value is not really fair because the RG network is rather sparse compared to the scale of the studied phenomenon (and simulated maximum value). At first glance,

I would say that CTRL-2.8 is better than NDG-2.8. A proper validation of numerical simulations against RG is needed.

We decided to validate our model results against the HyMEX RG data set given it has undergone several post-processing procedures (four revised versions of the product, https://mistrals.sedoo.fr/?editDatsId=904&datsId=904&project_name=HyMeX) and enjoys a large quality. We performed another validation against the CMORPH product, which has a spatial scale (8 km), similar to the model resolutions (7 km and 2.8 km) but found large discrepancies between CMORPH and RG for this case study. Therefore, we dismissed the analysis against CMORPH.

We acknowledge that a point-to-point comparison against RG entails difficulties, such as the sparse distribution over the island, as pointed out by the reviewer, and the double-penalty problem due to missed location of precipitation maxima (Wernli, et al., 2008; Gilleland, et al., 2009). This is why, in the comparison against RG (Tables 1 and 3) we perform a point-to-point comparison interpolating to the location of the stations but also analyse the maximum and standard deviation of the precipitation distributions intensities over the island. Since RG are usually employed as reference data for precipitation validation (Habib, et al., 2012; Jiang, et al., 2018) we decided to use this data set for the validation.

We show here the validation metrics similarly to Table 1 for the seasonal simulations (initialized on 01-Sep-2012). For the calculation of the metrics, hourly and accumulated precipitation values between 26-Oct 1300 UTC and 27-Oct 1700 UTC i.e. the period of precipitation over CO.

We confirm the comment of the reviewer for the 2.8 km since CTRL-2.8 outperforms NDG-2.8 in the simulation of the standard deviations of precipitation (both hourly and accumulated), accumulated precipitation and maximum. Only, the hourly RMSE is improved in NDG-2.8.

Regarding the 7 km simulations, applying the GPS-ZTD nudging is beneficial in that it improves the RMSE, and the standard deviation and maximum value of the accumulated precipitation values. This is as described in the manuscript.

These results can be explained from the precipitation reduction of the NDG-7 and NDG-2.8 simulations. CTRL-7 was overestimating excessively precipitation, whereas CTRL-2.8 showed a good representation of the maximum and accumulated amount. After a drying, only the scores of the 7 km resolution were improved, but not those of the 2.8 km.

We will adapt our conclusions and analysis in the manuscript to suit these findings. Besides, we will include Table 3 in Section 4.1 of the manuscript.

Table 3. As, Table 1 for the runs initialized on the 1-Sep-2012. The validation is done against hourly or accumulated precipitation values between 26-Oct 1300 UTC and 27-Oct 1500 UTC i.e. the period of precipitation over CO.

	Interp. To RG location			Distributions without interpolation	
	RMSE (1h)	$OBS_\sigma - MOD_\sigma$ (1h)	$\overline{OBS} - \overline{MOD}$ (27h)	$OBS_\sigma - MOD_\sigma$ (27h)	$OBS_{max} - MOD_{max}$ (27h)
CTRL-7-Init1Sep	3.1	-0.35	-10.4	-56	-185
NDG-7- Init1Sep	2.6	1.07	15.4	-0.7	-58
CTRL-2.8-Init1Sep	3.1	0.55	14.6	6	-3
NDG-2.8-Init1Sep	2.7	1.03	21.5	12	11

R1C17. L400: The authors do not really assess the accuracy of model moisture outputs: since most of the radiosonde locations are near GPS receivers, they rather assess the accuracy of GPS IWV retrievals. This most certainly explains why NDG-7 and NDG-2.8 results are so close to each other. To really assess the accuracy of model moisture outputs, free runs should be evaluated.

Only two sets of simulations can be validated against radiosondes. On the one hand, the free runs (CTRL), where no observation nudging is performed and hence are runs constrained only by the forcing data. On the other hand, the NDG runs where IWV is corrected every 10 minutes. We are assessing the accuracy of model moisture output for these two different sets of simulations.

Regarding the comment on the proximity between the GPS stations and the radiosondes. We must add that CCLM redistributes the nudged GPS information in the vertical profile specific humidity. Hence CCLM constructs a profile where errors at some levels are introduced. This is exactly what we wanted to quantify in Section 4.2 and Figures 8 and 9.

R1C18. L411: Figure 8.a shows the IWV over the CO domain, not Corsica. This is important, because the most noticeable differences among the nudging simulations may be over the sea since IWV mainly comes from GPS receivers on ground. The authors should adapt the rest of their interpretation of Figure 8.a accordingly.

Yes, thanks for this remark. Indeed, the spatial averages shown in Fig.8.a are obtained from the area CO and not Corsica. The text has been changed accordingly in the manuscript. In now reads:

Figure 8.a shows the spatially averaged temporal evolution of IWV over CO. The hours prior to precipitation initiation (26-Oct 1300 UTC) were characterized by an IWV pick up starting at 26-Oct 0000 UTC. All simulations show this, albeit the IWV amount over CO for NDG-7 and NDG-2.8 was 5 mm higher than for CTRL-7 and CTRL-2.8. This was due to represented precipitation over the island until the night of 24-Oct in the NDG runs, hence inducing a much wetter boundary layer (not shown).

R1C19. L423: Where is it evidenced that the humidity reduction takes place below 500 hPa?

How the GPS-ZTD nudging affects the vertical distribution of humidity is introduced in Section 4.2, in Figs. 8.b and Fig. 9. This is done on the one hand through box and whiskers plots over the investigation domain CO (Fig. 8.b) and on the other hand in the validation of the CCLM atmospheric moisture distribution against radiosondes (Fig 9). The sentence, as pointed out by the reviewer, could be misleading since no reference to the figures is given. We have corrected this in the manuscript. Furthermore, Fig. 8 shows how between 26-Oct-2012 1300 UTC and 27-Oct-2012 1500 UTC the specific humidity median, quartile and extreme values at 500 hPa are lower in NDG as compared to CTRL. We will revise our manuscript to read "*The humidity reduction between 26-Oct 1600 UTC and 27-Oct 0600 UTC takes mostly place at 500 hPa down to the 950 hPa level*".

R1C20. L429-447: A validation against radiosondes is presented. Which radiosonde profile has an impact on the event under consideration? They are all located either east, north, or south of Corsica, while the authors showed that moisture comes from the (south-)west.

The validation against radiosondes of Section 4.2 had for objective showing how good was the performance of the model in representing the profile of specific humidity. We selected all operational stations available during the two days of convective activity in the Mediterranean contained within the simulation domains of both resolutions. Hence the seven stations shown in Fig. 1 of the manuscript. Even if the stations are located only east of the study region on the Italian Peninsula, they are still valuable to assess the performance of the model.

R1C21. L466-467: Where is a "decrease of humidity close to ground" shown?

Thanks for this remark. In the analysis of box and whisker plots for 2m specific humidity we saw a reduction of ca. 1 gkg^{-1} and 0.5 gkg^{-1} in the NDG-7 and NDG-2.8 respectively as compared to their CTRL counterparts. This was shown for the period between 26Oct 1300 UTC and 27-Oct 1500 UTC over Corsica. We did not include this graph in our manuscript in order to make the text more concise, but we will include it as a subpanel of Fig. 8.b in the next version of our manuscript. Figure 8.b then will show as it follows

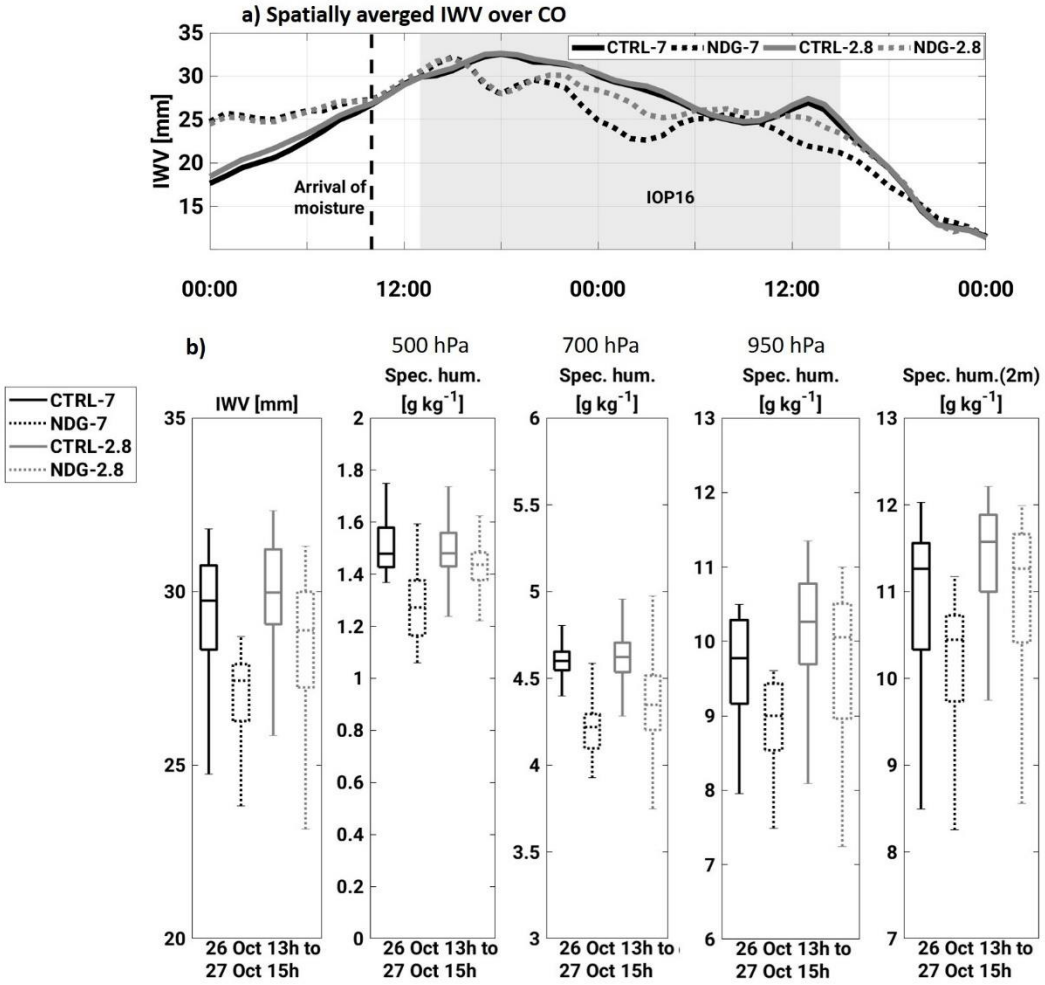

Figure 8. Spatially averaged IWV for all simulations during the event. The area for averaging is shown in Fig. 1 (CO) and the model output has been upscaled to a common coarser grid. The period shown is 26-Oct 0000 UTC to 28-Oct 0000 UTC. (b) Box and whiskers plots showing the median, the percentiles 25 and 75 and the extreme values of IWV and specific humidity at 500 hPa, 700 hPa,950 hPa and at 2m height. All box and whiskers are obtained from the distribution of values for the shown quantities between the 26-Oct 1300 UTC and 27-Oct 1500 UTC over the study region CO.

R1C22. L469-471: A simulation nudging IWV at 2.8 km and forced by NDG-7 would be useful here.

As explained in Section 1, we decided to force the NDG-2.8 runs with CTRL-7 to allow for comparison against CTRL-2.8. We believe this is the best means to assess the direct impact of the GPS-ZTD nudging in this resolution, avoiding any potential influences coming from the forcing data.

R1C23. L487: Why is the effect of the low-pressure system change exclusively seen in the 7 km simulations? Isn't the wind changed in the 2.8 km simulations, too?

We show only the results in the 7 km resolution since these runs cover the whole western Mediterranean area, as opposite to the 2.8 km runs. The 2.8 km simulation domain only covers the Italian Peninsula and the islands in order to save computational resources. The effect described in the manuscript (increase of PMSL at the centre of the low-pressure system in southern France) is only seen in the NDG-7 simulation since NDG-2.8 does not cover southern France. The following figure shows the PMSL changes in the NDG-2.8 compared to CTRL-2.8 and in the winds at 950 hPa (analogously to Fig. 12 in the manuscript for the 7 km runs).

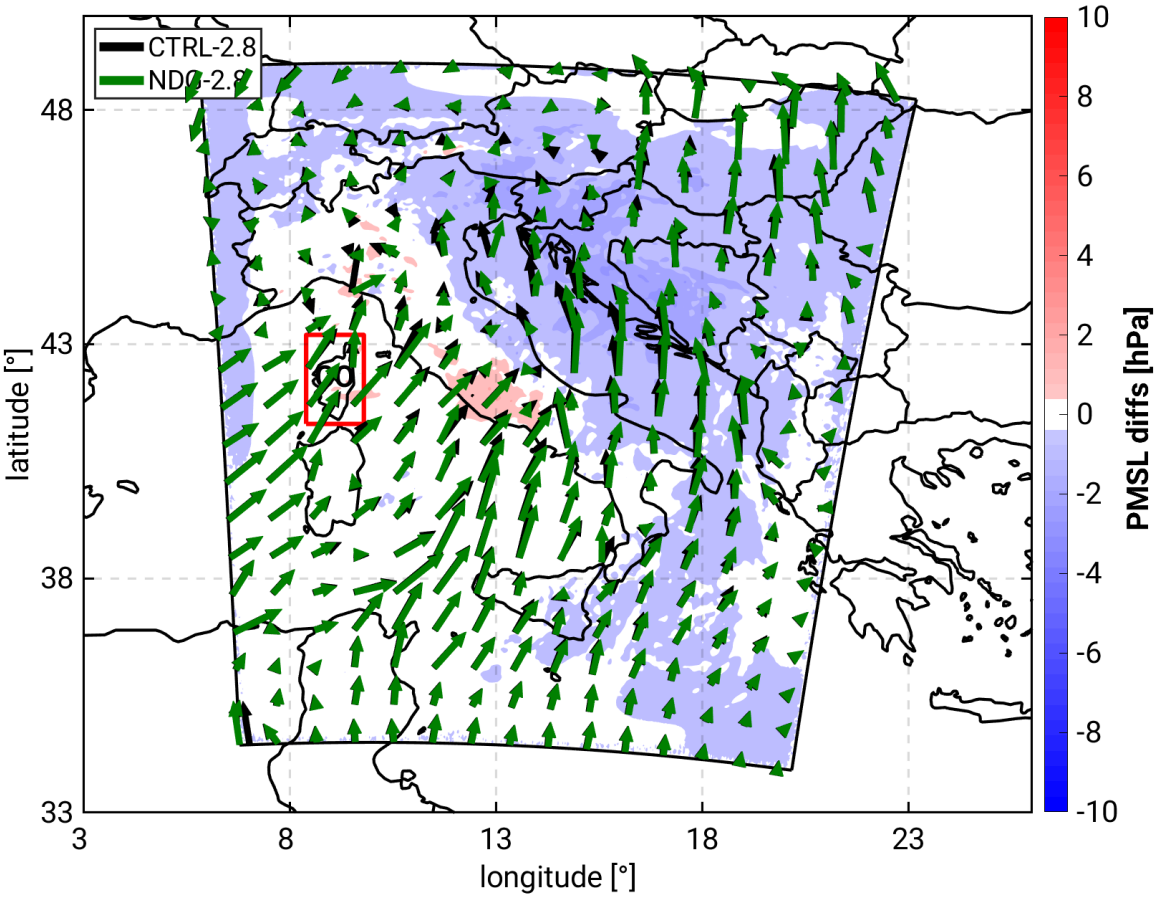

Figure 9. Spatial distribution of the differences in Pressure at the Mean Sea Level (PMSL) between NDG-2.8 and CTRL-2.8 on the 26-Oct 2300 UTC. Horizontal winds at 950 hPa are represented by black (CTRL-2.8) and green (NDG-2.8) arrows.

Fig. 9 shows that there are some areas (Adriatic Sea, the Balkans, southern Alps) with lower PMSL in the NDG-2.8 than CTRL-2.8 in extent of -2 hPa. These differences are weaker than the differences observed in the 7 km runs (up to 10 hPa) and are of opposite sign. Fig.9 clearly shows that the NDG-2.8 run does not show the same effect as NDG-7. The weakening of the low-pressure system over southern is not simulated in the NDG-2.8. There are however changes in the wind direction and intensity, mainly offshore, ahead of the western Italian and the Balkan coasts. However, these changes in wind direction and speed do not correspond to the changes observed in the 7 km runs since they do not show a clockwise veering of the direction centered in the southern French region. We will also include this graph in the supplementary material to support the analysis of the PMSL variations in Section 4.4

R1C24. L568-569: The high-temporal resolution of GPS-ZTD observations has not been shown to facilitate a better representation of the water vapour variability and a better regulation of the accumulated precipitation. To do this, different temporal resolutions should have been used.

In the general comments part, we have addressed how only little differences arise from using different nudging frequencies for spatially averaged precipitation in the 7 km for this case study over CO. These findings will be presented in the new version of the manuscript in Section 4.1 (Nudging effects on Precipitation).

3-TECHNICAL CORRECTIONS

We have accepted all corrections and comments of this section in the revised version of the manuscript. Where needed a short clarification is added here.

R1C25. L217: Is it useful to describe the vertical interpolation in the nudging scheme when it comes to assimilate GPS data?

We have adapted these lines in the manuscript to give this information in a clearer way. How the information is spread in the vertical direction is relevant since each GPS observation is used to construct a specific humidity profile that is treated as such in the nudging scheme. Hence, what is used for the nudging is this constructed profile based on the issued GPS-ZTD value. This sentence has been rewritten as: *"The vertical interpolation of the observed data is performed assuming a Gaussian decay in height differences. The vertical interpolation is also applied in the case of GPS-ZTD nudging since a profile of specific humidity is constructed from the derived GPS-IWV value. This constructed profile shall be treated by the nudging scheme as an upper-air measurement in the remainder of the process."*

R1C26. L230-231: It is unclear. What is the "iterative process"? If Eq 2 is used, it is not an iterative process, is it?

Yes, it is an iterative process that its repeated until a sufficiently low error is reached or after 20 iterations. We acknowledge that Eq. (2) in the manuscript was not written as an iterative formula and we have corrected this. This paragraph now reads.

"The observations are assigned to a grid point in the model space, provided the altitude difference of the GPS station and model surface lays within the range -150 to 600 m to allow for extrapolation and interpolation, respectively and are converted to a specific humidity profile (q_v^{mod}). This is needed given IWV is not a model prognostic variable as opposite to specific humidity. The profile is constructed by means of an iterative process that scales the observed IWV (IWV^{obs}) with the modelled one (IWV^{mod}) until a sufficiently low error is reached or up to 20 iterations. Eq. (2) describes the iterative formula. The first profile ($q_{v_i}^{mod}$) used as the first guess for the iterative process, is the modelled specific humidity profile. Hence, the profile used for nudging depends on the vertical humidity distribution simulated by the model at the beginning of the nudging time-window. "

$$q_{v_{i+1}}^{mod} = q_{v_i}^{mod} \cdot \frac{IWV^{obs}}{IWV_i^{mod}} \quad (2)$$

R1C27. L241: It is stated that the 7 km runs are forced by ECMWF analyses. How often?

Every 6 h. The forcing data has a temporal resolution of 6 h. We have included this information in the newest version of the manuscript.

R1C28. L244: The terms "large precipitation reductions" is unclear. The authors must specify which experiences they are referring to.

This sentence has been rephrased to express the information in a clearer way. In it, we were referring to a large reduction of maximum precipitation that was induced by the GPS-ZTD nudging. We have added more details so that this sentence is not out of context. The sentence now reads.

"Within the 80-day period of simulation, there were several events, which were largely affected by the GPS-ZTD nudging. IOP16, the case study of this paper, is one of them which is especially interesting given the large reduction of maximum precipitation (-20 %) induced by the GPS-ZTD nudging over the investigation area of Corsica in the course of 26 h. IOP16 is also suitable to assess the benefit of atmospheric moisture corrections with GPS-ZTD nudging given the important role of the local orographic and instability factors in triggering and maintaining convection rather than the large-scale upper level forcing."

R1C29. L298: What is an "offshore-size" convective system?

Thy is a typo. The sentence should read "Between 26-Oct 1900 UTC and 27-Oct 0100 UTC, offshore convective systems arrive at the island (see Fig.3.a)". We have corrected the text accordingly.

R1C30. L447: What is an "accuracy rate"?

The corrected sentence is: "The 2.8 km simulation was initially more accurate, but the nudging brings both to similar accuracy values".

R1C31. L454: What does "height-surface" mean? Do the authors simply mean "vertical"?

Yes, it was meant vertical cross-section. Thank you. It has been corrected in the manuscript.

R1C32. L455: What does "vertical-horizontal direction" mean?

The sentence has been changed to: "Figure 10 shows the vertical cross-sections of Equivalent Potential Temperature (θ_e), specific humidity and the wind along the direction of the mean horizontal wind (purple transect in Fig. 1) over the island at 26-Oct 1700 UTC."

4-REFERENCES

Benjamin, S. G. et al., 2010. Relative Short-Range Forecast Impact from Aircraft, Profiler, Radiosonde, VAD, GPS-PW, METAR, and Mesonet Observations via the RUC Hourly Assimilation Cycle. *Monthly Weather Review,* 4, Band 138, p. 1319–1343.

Borderies, M. et al., 2019. Assimilation of wind data from airborne Doppler cloud-profiling radar in a kilometre-scale NWP system. *Natural Hazards and Earth System Sciences,* 4, Band 19, p. 821–835.

Gilleland, E. et al., 2009. Intercomparison of Spatial Forecast Verification Methods. *Weather and Forecasting,* 10, Band 24, p. 1416–1430.

Habib, E., Haile, A. T., Tian, Y. & Joyce, R. J., 2012. Evaluation of the High-Resolution CMORPH Satellite Rainfall Product Using Dense Rain Gauge Observations and Radar-Based Estimates. *Journal of Hydrometeorology,* 12, Band 13, p. 1784–1798.

Jiang, Q. et al., 2018. Accuracy Evaluation of Two High-Resolution Satellite-Based Rainfall Products: TRMM 3B42V7 and CMORPH in Shanghai. *Water,* 1, Band 10, p. 40.

Keil, C., Heinlein, F. & Craig, G. C., 2013. The convective adjustment time-scale as indicator of predictability of convective precipitation. *Quarterly Journal of the Royal Meteorological Society,* 5, Band 140, p. 480–490.

Lamb, P. J., Portis, D. H. & Zangvil, A., 2012. Investigation of Large-Scale Atmospheric Moisture Budget and Land Surface Interactions over U.S. Southern Great Plains including for CLASIC (June 2007). *Journal of Hydrometeorology,* 12, Band 13, p. 1719–1738.

Louis, J.-F., 1979. A parametric model of vertical eddy fluxes in the atmosphere. *Boundary-Layer Meteorology,* Band 17, pp. 187-202.

Mahfouf, J.-F., Ahmed, F., Moll, P. & Teferle, F. N., 2015. Assimilation of zenith total delays in the AROME France convective scale model: a recent assessment. *Tellus A: Dynamic Meteorology and Oceanography,* 2, Band 67, p. 26106.

Peixoto, J. P. & Abraham H. Oort, 1992. *Physics of Climate.* s.l.:American Inst. of Physics.

Sahlaoui, Z., Mordane, S., Wattrelot, E. & Mahfouf, J.-F., 2019. Improving heavy rainfall forecasts by assimilating surface precipitation in the convective scale model AROME: A case study of the Mediterranean event of November 4, 2017. *Meteorological Applications,* 12.Band 27.

Schättler, U., Doms, G. & Schraff, C., 2016. *A Description of the Nonhydrostatic Regional COSMO-Model Part VII : User's Guide,* DeutscherWetterdienst, P.O. Box 100465, 63004 Offenbach, Germany: s.n.

Schneider, M. et al., 2010. Continuous quality assessment of atmospheric water vapour measurement techniques: FTIR, Cimel, MFRSR, GPS, and Vaisala RS92. *Atmospheric Measurement Techniques,* 3, Band 3, p. 323–338.

Seemann, S. W., Li, J., Menzel, W. P. & Gumley, L. E., 2003. Operational Retrieval of Atmospheric Temperature, Moisture, and Ozone from MODIS Infrared Radiances. *Journal of Applied Meteorology,* 8, Band 42, p. 1072–1091.

Wernli, H., Paulat, M., Hagen, M. & Frei, C., 2008. SAL—A Novel Quality Measure for the Verification of Quantitative Precipitation Forecasts. *Monthly Weather Review,* 11, Band 136, p. 4470–4487.

Answers to reviewer 2 (Paper-IOP16-NHESS)

GENERAL COMMENT

We would like to thank the anonymous reviewer for the valuable comments, suggestions and questions. We have considered all minor and major comments. We believe that the quality of the manuscript has increased, thanks to the comments of the reviewer and acknowledge how answering the raised questions was crucial for a better exposition of our key messages.

R2C1. The impact of evapotranspiration over North-Africa for this event is shown, even if not quantified.

We give a description on how much moisture evaporates from North-Africa between lines 344 and 361 using our model simulations and the GLEAM product (combination of different satellite measurements). We give values on how much moisture evaporates per day in the days prior to the event at Corsica. For example, on line 359 we state "*Suite to the precipitation event, daily evapotranspiration over the area reached spatial averages of 1.4 mm as shown by GLEAM, lasting for seven days, well above the mean evapotranspiration values during this season (0.5 mm). Albeit differences in the 360 magnitude of evaporation, COSMO-CLM well captures this period of anomalous evapotranspiration*".

How the moisture is further transported north towards Corsica is explained in the following paragraphs of Section 3.3.

A quantification of the contribution of evapotranspiration over north Africa in relation to the advected moisture is presented in our answers to the reviewer.

MAJOR POINTS

R2C1.a) The authors must clarify that this is a diagnostic study and not prognostic. The impact of assimilating GPS-ZTD is quantified by comparing two simulations: the first doesn't assimilate GPS-ZTD, while the second assimilates GPS-ZTD continuously. While this is an important comparison, it must be clarified that the paper doesn't assess the role of GPS-ZTD in a prognostic approach for the case study.

We agree with the reviewer that this point could be better clarified to the reader, for that reason we have included this information in several relevant places in the manuscript:

In the Abstract

"In this study, we use a diagnostic approach to assess the sensitivity of precipitating convection and underlying mechanisms during a heavy precipitation event (HyMeX intensive observation period 16) to corrections of the atmospheric moisture spatio-temporal distribution."

In Section 2.2.2 of the Methods. The GPS-ZTD Nudging Sensitivity Experiments

"The Nudging scheme is used to assimilate GPS-ZTD data to assess the sensitivity of heavy precipitating convection to corrections of the spatio-temporal distribution of atmospheric moisture. We use a diagnostic approach as opposite to commonly use data-denial experiments."

R2C1.b) Also the importance of sub-hourly data assimilation is not shown. To do that a comparison between two simulations one assimilating GPS-ZTD on an hourly basis and the other one assimilating GPS-ZTD every 10

minutes (as in the paper) should be performed. However, I understand that this requires adding new simulations, which can be avoided deleting the sentences where the importance of sub-hourly assimilation is emphasised.

We agree that this is a very interesting question that needs to be addressed in our paper.

We have performed supplementary simulations, initialized on the 20-Oct-2012 with no GPS-ZTD nudging (CTRL), 10-min frequency nudging (NDG-7 and NDG-2.8) and 1 h frequency nudging (NDG-7-1h and NDG-2.8-1h) where the temporal resolution of the GPS data is of 1 h (NDG-7-1h, NDG-2.8-1h). The only difference between the 1h nudging and the 10min nudging simulations is the frequency of assimilation. All other settings are the same. We have performed these experiments starting the simulations on the 20-Oct-2012 at 0000 UTC, to reduce the computational costs of running the complete season.

In the following we show graphs and analysis for the comparison between the runs with nudging frequency of 10 min vs. 1h.

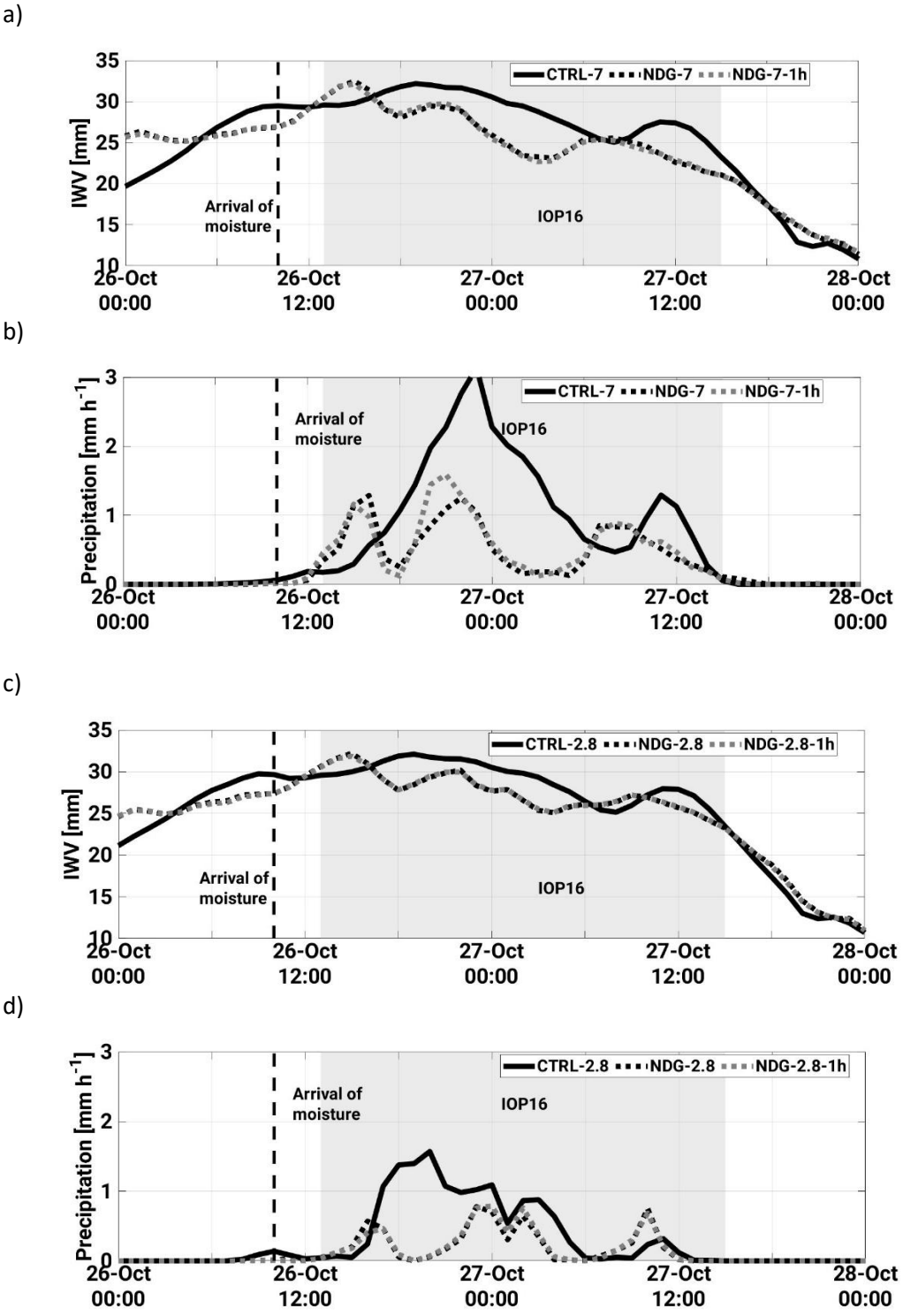

Figure 1. Spatially averaged IWV (a, c) and Precipitation (b, d) for the 7 km simulations (a, b) and the 2.8 km simulations (c, d) during the event. The area for averaging is Corsica. The model output has been upscaled to a common coarser grid of 8 km. The period shown is 26-Oct 0000 UTC to 28-Oct 0000 UTC. The comparison is between the runs using a temporal nudging frequency of 10 min (NDG-7, NDG-2.8) against nudging at a temporal frequency of 1h (NDG-7-1h, NDG-2.8-1h).

The results show no differences on the temporal evolution of IWV. This holds for 7 km and 2.8 km. This can be explained by the fact that we calculate the spatially averaged IWV at sharp hours (i.e. 0000 UTC, 0100 UUTC, 0200 UTC, etc.), precisely is at those times when the GPS-ZTD data is assimilated in the NDG-7-1h and the NDG-2.8-1h runs.

For precipitation, there is a slight impact for the 7 km runs, but not for the 2.8 km. The NDG-7-1h simulation shows somewhat larger precipitation than NDG-7 at 2000 UTC on the 26-Oct (Fig. 1b) corresponding to an increase from 30 mm to 50 mm at the western shore of the island Fig.2.b and Fig. 2.c

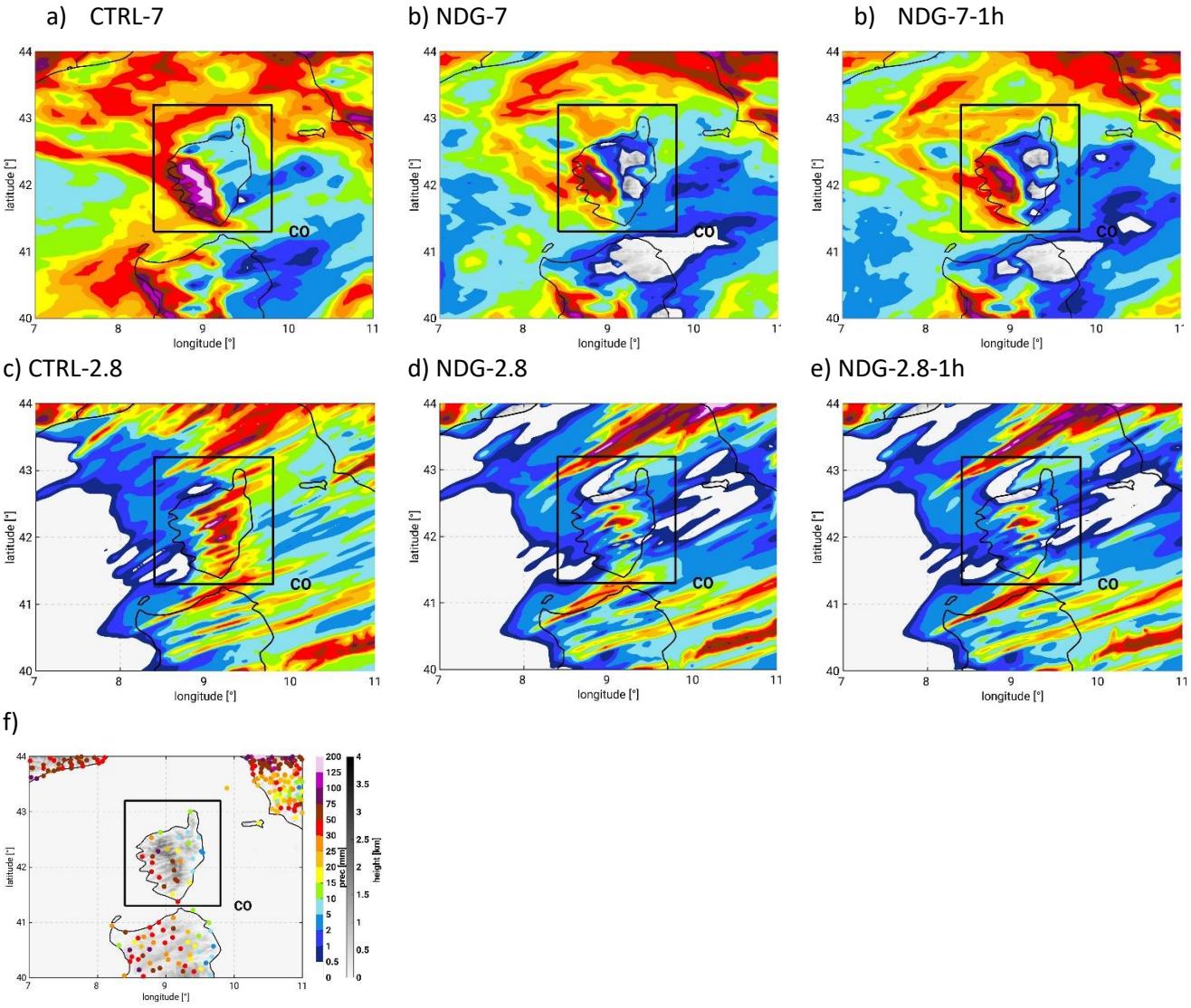

Figure 2. COSMO-CLM accumulated precipitation over Corsica between 26-Oct 1300 UTC and 27-Oct 1500 UTC i.e. during the period of precipitation over the island and RG.

To delve further into which aspects of precipitation representation have been improved we present in Table 1 further validation metrics using the Rain Gauges (RG) as reference.

Table 1 shows the RMSE of the anomalies of hourly precipitation rates (first column), the differences (OBS-MOD) of the standard deviations of hourly precipitation (second column) and the spatially averaged differences of accumulated precipitation during the whole event, i.e. between 26-Oct 1300 UTC and 27-Oct 1500 UTC (third column). The last three metrics are obtained after interpolating the COSMO-CLM precipitation values to the location of the RG stations. On the contrary, columns four and five of Table 1, show differences of the standard deviation and maximum value of precipitation for COSMO-CLM over land without interpolation. That means, we have obtained all 27h-accumualeted precipitation values simulated by COSMO-CLM over land and have calculated the standard deviation and the maximum. We have done the same for all RG measurements and the

differences are shown. We do this to avoid double-penalty problems due to a possible misrepresentation of the maxima location (Wernli, et al., 2008; Gilleland, et al., 2009). The formulas used are included in Table 2.

Table 1. Metrics of the precipitation validation against RG. The model precipitation has been interpolated to the location of the RG for the first three columns and all precipitation values simulated by COSMO-CLM over the island of Corsica are used in the last two columns. This is done to avoid double-penalty problems due to a shifting of the precipitation maxima. N is the number of RG stations and M the total number of grid points. The units are mm.

	Interp. To RG location			Distributions without interpolation	
[mm]	**RMSE** (h)	$\boldsymbol{OBS_\sigma - MOD_\sigma}$ (1h)	$\boldsymbol{\overline{OBS} - \overline{MOD}}$ (27h)	$\boldsymbol{OBS_\sigma - MOD_\sigma}$ (27h)	$\boldsymbol{OBS_{max} - MOD_{max}}$ (27h)
CTRL-7-Init20Oct	3.3	-0.85	-19.1	-33	-170
NDG-7-Init20Oct	2.5	0.73	12.5	-5	-79
NDG-7-1h- Init20Oct	2.5	0.95	12.2	-4	-50
CTRL-2.8-Init20Oct	3.6	-0.15	9.5	-3	-74
NDG-2.8-Init20Oct	2.6	1.64	23.8	11	-16
NDG-2.8-1h- Init20Oct	2.5	1.64	23.6	10	-17

Table 2. Precipitation validation metrics.

RMSE (1h)	$\sqrt{\sum_{i(1h)}^{N}((OBS_i - \overline{OBS}) - (MOD_i - \overline{MOD}))^2}$
$\boldsymbol{OBS_\sigma - MOD_\sigma}$ (1h)	$\sqrt{\frac{1}{N}\sum_{i(1h)}^{N}(OBS_i - \overline{OBS})^2} - \sqrt{\frac{1}{N}\sum_{i(1h)}^{N}(MOD_i - \overline{MOD})^2}$
$\boldsymbol{\overline{OBS} - \overline{MOD}}$ (27h)	$\frac{1}{N}\sum_{i(27h)}^{N} OBS_i - \frac{1}{N}\sum_{i(27h)}^{N} MOD_i$
$\boldsymbol{OBS_\sigma - MOD_\sigma}$ (27h)	$\sqrt{\frac{1}{N}\sum_{i(27h)}^{N}(OBS_i - \overline{OBS})^2} - \sqrt{\frac{1}{M}\sum_{j(27h)}^{M}\left(MOD_j - \overline{MOD}\right)^2}$
$\boldsymbol{OBS_{max} - MOD_{max}}$ (27h)	$\max(OBS_i) - \max(MOD_j)$

Overall, we see that nudging GPS-ZTD data is beneficial for the 7 km grid with little difference between nudging with 1h frequency or 10 min. If any, we see a slight advantage in nudging GPS-ZTD data with 10 min for the representation of the hourly standard deviation rates. The same holds for the 2.8 km, assimilating with a 10min frequency shows very weak differences with respect to assimilating with 1h frequency.

These analyses will be included as an additional subsection in section 4.1 (Nudging effects on Precipitation).

R2C2) In the section 3.3 emphasis is given to the transport of humidity from North Africa for the event. It would be interesting to give a comparison between this source of moisture and that coming from the western Mediterranean Sea to define better this contribution.

We agree with the reviewer that a quantification of the different terms of Evaporation and moisture flux over the investigation area NA and the Mediterranean would be most interesting. We have obtained the terms, described in Lamb et al. (2012) over the investigation areas NA (North Africa) and MED (Mediterranean Sea) for this purpose, see Fig. 3.a.

The calculation of these terms entails simplifications for example, of the turbulent and microphysical processes that introduce relevant uncertainties. Hence, what we provide here is an estimation of the different contributions.

$$\Delta IWV = E + (-P) + MFC \quad (1)$$

All terms of Eq. 1 are expressed in mmh^{-1}, where positive signs of the Evaporation (E) and Integrated Moisture Flux Convergence (MFC) imply an increase of Integrated Water Vapour variations (ΔIWV>0) within the NA and MED volumes. On the contrary, if precipitation and water vapor divergence occur (MFC<0) IWV decreases (ΔIWV<0). The volumes cover the areas in Fig. 3.a where the integrations of IWV and MFC are performed from the first to the last model levels.

Fig. 3.b shows similar information to Fig.6.c of the manuscript. Intense precipitation occurs over NA on the 20-Oct-2012 with the subsequent decrease of IWV, and intense evaporation over the area on the 21-Oct and 22-Oct at midday. This is the moment when solar radiation is strongest, hence evaporation is intensified over this wet soil. Please note the change in the axis scales between the different panels of this figure and those of Fig.6.c of the manuscript, expressed in mmd^{-1}. The order of magnitude of those evaporations over NA is the same as those over the Mediterranean Sea, up to 0.15 mmh^{-1}. This is better seen in Fig. 3.c. The evaporated moisture is advected with the wind flow, merging with the Atlantic and Mediterranean moisture.

To quantify how much the Mediterranean Sea contributed to the changes of atmospheric moisture at that location, Fig. 3.c shows the contribution from each of the moisture equation terms over the selected volume MED. We can see that between 22-Oct and 26-Oct 1200 UTC there is a positive, homogeneous evaporation from the Sea at a rate of 0.25 mmh^{-1} that picks up from 26-Oct 1200 UTC to 0.5 mmh^{-1} by 28-Oct 0000 UTC. The time of the evaporation pick up coincides the occurrence of precipitating convection over the Mediterranean Sea west of Corsica. The intensification of the evaporation is brought by the intensified drag of horizontal winds close to sea surface.

a)

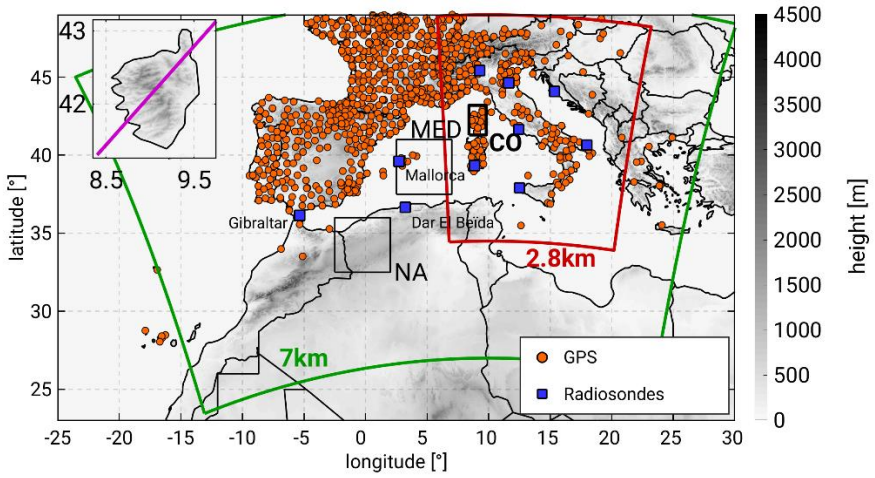

b) NA

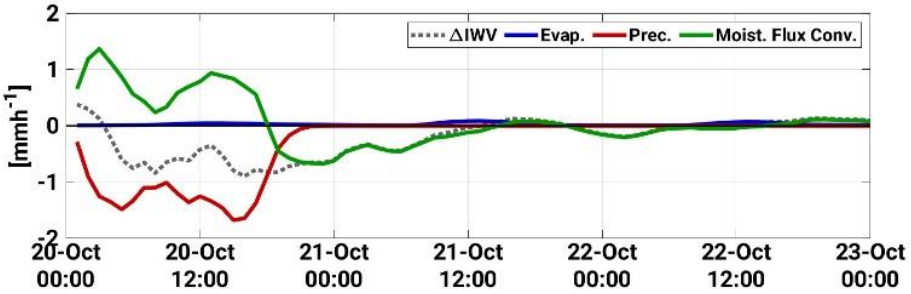

c) MED

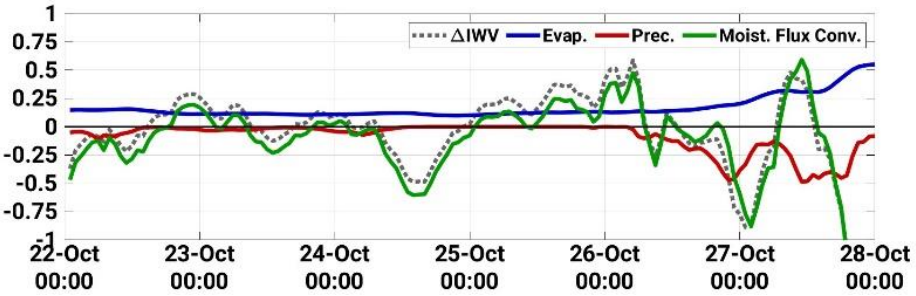

d) NA

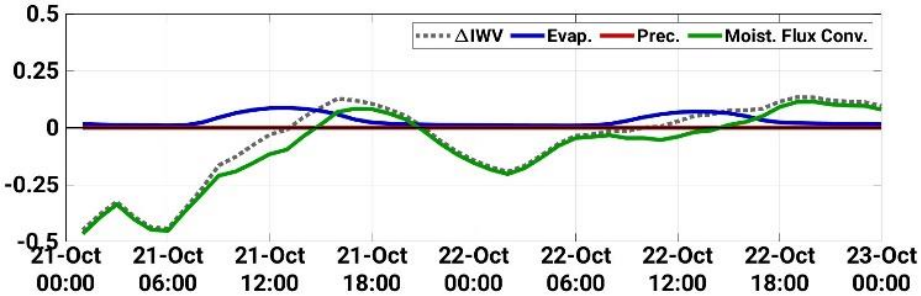

Figure 3. Analysis of the moisture budget terms. (a) Simulation domains as Fig.1 of the manuscript including the NA and MED areas for calculation of averaged evaporation, precipitation and moisture convergence. (b) Spatial average of

hourly IWV variations (dotted grey), Evaporation (blue), Precipitation (red) and Moisture flux Convergence (green) in mmh^{-1}, over investigation area NA between 20-Oct and 23-Oct 0000 UTC. All variables are obtained from the CTRL-7 runs. (c) is as panel (b) but showing the averages over the investigation area MED between 22-Oct and 28-Oct 0000 UTC. (d) is as panel (b) but showing the spatial averages between 21-Oct and 23-Oct 0000 UTC. Mind the changes in the y-axis scaling.

R2C3.a) Considering the nudging scheme there is no information on the parameters of the Second order autoregressive function. How they are determined?

We have added a short clarification in the revised version of the manuscript. In Eq. (1.b), Δr stands for the distance between the observation location and the target grid point. The other parameter, s, is the correlation scale that is defined in tables with a pressure level dependency for the different variables (Schraff & Hess, 2012). For example, for temperature (s_T) and humidity (s_q) these values are:

Table 3. Correlation scale (s) for temperature (T) and specific humidity (q) at different pressure heights

P [hPa]	1000	850	700	500	400	300	250	200	150	100	50
s_T, s_q[km]	58	66	75	83	83	83	83	91	100	100	100

The correlation scale, thus, is larger in the stratosphere than in the troposphere and lowest levels. As an example, at 500 hPa, the weight for the horizontal spreading is halved ($w_{xy} = 0.5$) at a horizontal distance of about 135 km from the station location.

The revised explanation in the manuscript reads "*The weight for spreading in the horizontal direction w_{xy}, is a second-order autoregressive function dependent on the distance between the observation and the target point (Δr) and the correlation scale (s), see Eq. (1.b). The correlation scale is dependent on the pressure level and is largest for the stratosphere (100 km) and shortest for the PBL (58 km). This implies that the horizontal weight is halved ($w_{xy} = 0.5$) at a distance of 135 km at the 500 hPa level*"

R2C3.b*) Line 217 has a comment on the vertical adjustment that doesn't apply to the specific case.*

We have adapted these lines in the manuscript to give this information in a clearer way. How the assimilated observation is adjusted in the vertical direction is indeed relevant since each GPS observation is used to construct a specific humidity profile that is treated as such in the nudging scheme. Hence, what is used for nudging is this "constructed" profile based on the issued GPS-ZTD value. This sentence has been rewritten as: *"The vertical interpolation of the observed data is performed assuming a Gaussian decay in height differences. The vertical interpolation is also applied in the case of GPS-ZTD nudging since a profile of specific humidity is constructed from the derived GPS-IWV value. This constructed profile shall be treated by the nudging scheme as an upper-air measurement in the remainder of the process."*

R2C3.c*) It also unclear how the qv profile is constructed iteratively (Lines 230-232). Do you mean that it is modified by nudging until a difference is attained or something different?*

For a certain GPS-ZTD observation at time t and location $\vec{x}$ the ZTD value is converted to IWV. This is described in the paper following Schraff and Hess (2012). Given IWV, as opposite to specific humidity, is not a prognostic variable of the model, the IWV observation has to be transformed into a profile of specific humidity. This is done for each single observation by means of an iterative process. To express this process in a more understandable way the whole paragraph has been rewritten.

"The observations are assigned to a grid point in the model space, provided the altitude difference of the GPS station and model surface lays within the range -150 to 600 m to allow for extrapolation and interpolation,

respectively and are converted to a specific humidity profile (q_v^{mod}). This is needed given IWV is not a model prognostic variable as opposite to specific humidity. The profile is constructed by means of an iterative process that scales the observed IWV (IWV^{obs}) with the modelled one (IWV^{mod}) until a sufficiently low error is reached or up to 20 iterations. Eq. (2) describes the iterative formula. The first profile ($q_{v_i}^{mod}$) used as the first guess for the iterative process, is the modelled specific humidity profile. Hence, the profile used for nudging depends on the vertical humidity distribution simulated by the model at the beginning of the nudging time-window. "

$$q_{v_{i+1}}^{mod} = q_{v_i}^{mod} \cdot \frac{IWV^{obs}}{IWV_i^{mod}}$$

MINOR POINTS

All minor corrections mentioned by the reviewer have been accepted and included in the revised version of the manuscript. When needed, a short clarification is included here.

R2C4. Line 33: During heavy precipitation events, rain rates can be much higher than 20 mm/h.

Yes, thanks for the comment. As reported for example in Röhner, et al., (2016) and Ducrocq, et al., (2014), some extreme past events have shown precipitation totals reaching 500 mm in 6 h to 12 h in the Mediterranean area. This is however very exceptional cases. We have adapted the sentence in the manuscript, now it reads.

"During these events, daily accumulated precipitation over 150 mm is not rare and precipitation rates can be well over 20 mm h^{-1} (Röhner, et al., 2016; Ducrocq, et al., 2014)"

R2C5. Line 244: Check the sentence "given the large precipitation reduction". Do you mean when you assimilate GPS-ZTD?

Yes. This sentence has been rephrased to express the information in a clearer way. In it we were referring to a large reduction of maximum precipitation that was induced by the GPS-ZTD nudging. We have added more details so that this sentence is not out of context. The sentence now reads.

"Within the 80-day period of simulation, there were several events, which were largely affected by the GPS-ZTD nudging. IOP16, the case study of this paper, is one of them which is especially interesting given the large reduction of maximum precipitation (-20 %) induced by the GPS-ZTD nudging over the investigation area of Corsica in the course of 26 h. IOP16 is also suitable to assess the benefit of atmospheric moisture corrections with GPS-ZTD nudging given the important role of the local orographic and instability factors in triggering and maintaining convection rather than the large-scale upper level forcing."

R2C6. Line 248: I suggest giving more details about the Agreement Index (AI).

The formula for AI calculation has been included in the revised version of the manuscript. Together with the Agreement Index, more validation metrics are used for precipitation. They are contained in Table 2.

R2C7. Line 577-578: This sentence is rather unclear. It is important to note that, in general, the adjustment introduced by GPS-ZTD could be a function of the height if variational approaches are considered, through the background error matrix.

Indeed, generalizing to other assimilation schemes is not possible from our study. This conclusion relating to the difficulties of the nudging scheme to correctly improve the vertical distribution of humidity when using GPS should be constrained to this type of observation and assimilation method, exclusively. In the sentence

mentioned by the reviewer it is explicitly said “GPS-ZTD nudging”. We agree, nevertheless, that it would be very interesting extending these experiments to other assimilation schemes. This was one of our initiatives in the project that could sadly not be finished due to missing forcing data from the ICON ensemble for the year 2012.

REFERENCIAS

Ducrocq, V. et al., 2014. HyMeX-SOP1: The Field Campaign Dedicated to Heavy Precipitation and Flash Flooding in the Northwestern Mediterranean. *Bulletin of the American Meteorological Society,* 7, Band 95, p. 1083–1100.

Gilleland, E. et al., 2009. Intercomparison of Spatial Forecast Verification Methods. *Weather and Forecasting,* 10, Band 24, p. 1416–1430.

Lamb, P. J., Portis, D. H. & Zangvil, A., 2012. Investigation of Large-Scale Atmospheric Moisture Budget and Land Surface Interactions over U.S. Southern Great Plains including for CLASIC (June 2007). *Journal of Hydrometeorology,* 12, Band 13, p. 1719–1738.

Röhner, L., Nerding, K.-U. & Corsmeier, U., 2016. Diagnostic study of a HyMeX heavy precipitation event over Spain by investigation of moisture trajectories. *Quarterly Journal of the Royal Meteorological Society,* 6, Band 142, p. 287–297.

Schraff, C. & Hess, R., 2012. *A Description of the Nonhydrostatic Regional COSMO-Model Part III: Data Assimilation,* DeutscherWetterdienst, P.O. Box 100465, 63004 Offenbach, Germany: s.n.

Wernli, H., Paulat, M., Hagen, M. & Frei, C., 2008. SAL—A Novel Quality Measure for the Verification of Quantitative Precipitation Forecasts. *Monthly Weather Review,* 11, Band 136, p. 4470–4487.

Assessing Atmospheric Moisture Effects on Heavy Precipitation During the HyMeX IOP16 Using GPS Nudging and Dynamical Downscaling

Alberto Caldas-Alvarez[1], Samiro Khodayar[1,2]

[1]Institute of Meteorology and Climate Research (IMK-TRO), Karlsruhe Institute of Technology, Karlsruhe, P.O. Box, 76131, Germany
[2]Mediterranean Centre for Environmental Studies (CEAM), Valencia, 46980, Spain

Correspondence to: Alberto Caldas-Alvarez (alberto.caldas-alvarez@kit.edu~~@email.com~~)

Abstract. Gaining insight on the interaction between atmospheric moisture and convection is determinant to improve the model representation of heavy precipitation, a weather phenomenon that every year brings casualties and ~~important~~ monetary losses in the western Mediterranean region. Given the large variability of atmospheric moisture, an accurate representation of its distribution is expected to reduce the errors related to the representation of moist convective processes. In this study, we use a diagnostic approach to assess the sensitivity of ~~precipitating convection~~convective precipitation and underlying mechanisms during a heavy precipitation event (Hydrological cycle in the Mediterranean eXperiment; HyMeX I~~i~~ntensive ~~o~~Observation P~~p~~eriod; IOP 16) to ~~corrections~~ variations of the atmospheric moisture spatio-temporal distribution. Sensitivity experiments are carried out by nudging a homogenised data set of Global Positioning System-derived Zenith Total Delays (GPS-ZTD) with sub-hourly frequency (10 minutes) in 7 km and 2.8 km simulations with the Consortium for Small scale Modelling in CLimate Mode (COSMO-CLM) model over the western Mediterranean region. The analysis shows that (a) large atmospheric moisture amounts (Integrated Water Vapour; IWV ~ 40 mm) precede heavy precipitation at the affected areas. This occurs 12 h ~~before~~ prior to initiation over southern France and 4 h over Sardinia, north eastern Italy and Corsica, which is ~~(~~ our main study area~~)~~. (b) We found that the moisture is ~~transported on the one hand,~~ swept from the Atlantic by a westerly large-scale front associated with an upper-level low on the one hand and ~~on the other hand~~ evaporated from the Mediterranean Sea and north Africa on the other. The latter moisture transport occurs in the <1 km to 4 km layer and has been identified for this event for the first time. (c) COSMO-CLM overestimated the atmospheric humidity ~~and precipitation amount~~ over the study region (Corsica) and this was, to a good extent, corrected by the GPS-ZTD nudging. This reduced drastically maximum precipitation (- 49 % for 7 km and -16 % for 2.8 km) considerably improving the precipitation representation in the 7 km. The convection permitting simulation (2.8 km) without the GPS-ZTD nudging already did a good job in representing the precipitation amount ~~by reducing noticeably both quantities, bringing results closer to observations~~. (d) The two processes that exerted the largest control on precipitation reduction were the ~~reduction~~ decrease of atmospheric instability over the island (Convective Available Potential Energy; CAPE -35 %) and the drying of the lower free troposphere bringing ~~more~~ additional dry air entrainment. Besides, the 7 km simulation showed a ~~stronger impact for large-scale dynamical lifting at the target area,~~

given a weakening of the represented low-pressure system and the associated cyclonic wind circulation. This reduced ultimately, the intensity and number of convective updrafts represented over the island. These results highlight the large impact exerted by moisture corrections on precipitating convection and the chain of related processes leading to it across scales. Additionally., Tthe modelling experiments demonstrated the benefit of sub-hourly GPS-ZTD nudging to improve the modelling of precipitation. Our approach is relatively easy to implement and we envisage that it may be fruitfully applied to other regions and heavy precipitation events.

1 Introduction

Heavy precipitating convection causes yearly serious damages and casualties in countries of the Western Mediterranean (WMed) basin especially by autumn (Llasat et al., 2010; Gilabert and Llasat, 2017). During these events, daily accumulated precipitation over 150 mm is not rare and precipitation rates can reach be well over 20 mm h^{-1}.(Ducrocq et al., 2014; Röhner et al., 2016)MISSING -- references of higher precip rates Rochern et al 2016 and Ducrocq et al 2014].. These are caused mainly by convective events ranging several temporal and spatial scales, from the mesoscale down to the micro-alpha (Ducrocq et al., 2016; Funatsu et al., 2018). Accurate representation of the convective processes interacting across scales is crucial to support forecasters and decision makers to prevent impacts on properties and communities. The WMed is especially prone to heavy precipitating convection by autumn because of the combination of the relatively high sea surface temperature of the Mediterranean and the Atlantic, the arrival of low-pressure systems such as extra-tropical cyclones or upper-level troughs and the interaction with the Mediterranean complex orography (Ducrocq et al., 2014). Former studies pointed out the synoptic situation conducive to heavy precipitation as usually dominated by a low-pressure system, inducing a south-westerly warm and moist inflow, building sufficient instability and moisture convergence (Jansa et al., 2001; Toreti et al., 2010; Nuissier et al., 2011; Ricard et al., 2012; Xoplaki et al., 2012, Khodayar et al. 2016). These studies also demonstrate the key role of aAtmospheric moisture plays a decisive role at all phases of convective development and therefore, hence and the need of gainingit is relevant to gain knowledge regarding its interaction with convection across scales on moist convective processes to improve the modelling of extreme phenomena (Sherwood et al., 2010; Ahrens and Samson, 2010). Given the high spatio-temporal variability of atmospheric moisture (Steinke et al., 2015; Girolamo et al., 2016), a deficient representation of its distribution (Steinke et al., 2015; Girolamo et al., 2016) has been pointed out as a source of uncertainty in current predictions (Chazette et al., 2015; Khodayar et al., 2016). That is why;, there is growing interest in developing forecast systems that assimilate humidity observations with sub-hourly frequency (Guerova et al., 2016). Given the novelty of such assimilation frequencies and the multiple methodologies applied, new insights are needed on their impact on simulated atmospheric conditions leading to heavy precipitation.

Determinant for the development of precipitating convectionheaviest precipitation events in the WMed are the vast moisture amounts associated with the heaviest precipitation events, which may originate from remote or local sources (Ricard et al., 2012; Krichak et al., 2014; Khodayar et al., 2016). Depending on the synoptic conditions, the Mediterranean Sea can account

for over~~>~~ 50 % of the transported moisture (Duffourg and Ducrocq, 2011). This is the case when an anticyclonic flow dominates the 3 to 4 days preceding heavy precipitation. Remote sources such as the Atlantic and the tropics also supply the needed moisture, especially for the heaviest precipitation events (Pinto et al., 2013; Winschall et al., 2014), whose transport is brought via tropical plumes (Chazette et al., 2015b) or extra-tropical cyclones (Xoplaki et al., 2012). Finally, north Africa has been also identified as a source by Duffourg and Ducrocq (2011). ~~Despite being less common, this source provides larger amounts of specific humidity when low pressure over the Iberian Peninsula induces cyclonic conditions.~~ Regions prone to convective development are correlated with areas of moisture convergence where building up of conditional instability takes place (Ricard et al., 2012; Khodayar et al., 2016). Given the correlation between the location of moisture convergence and precipitating convection, the complex Mediterranean orography plays a decisive role in setting areas prone to heavy precipitation. The high mountain ridges constrain the moisture transports in the basin favouring moisture gathering at the mountain foothills, the coasts and the valleys. Moreover, the elevated terrain provides dynamic lifting to the convergent moist air masses triggering convection.

In addition to the moisture transport, the ~~its~~~~The~~ variability and stratification ~~of atmospheric moisture~~ determine~~s~~ when, where and how intense, convection can be. Several studies (Duffourg and Ducrocq, 2011; Ricard et al., 2012; Khodayar et al., 2016, Maranan et al., 2019) have highlighted the moistening of the lower troposphere as a necessary factor for precipitating convection to develop with specific humidity values up to 10 g kg^{-1} below 850 hPa. A moist low-level, increases the Convective Available Potential ~~(CAPE-ML)~~ ~~e~~Energy (CAPE) of the lifted parcel. A second factor, crucial for convection intensity is the moisture at the Lower Free Troposphere (LFT). This is the moisture transport that occurs above the Planetary Boundary Layer (PBL~~) where the influence of the surface roughness can be considered negligible~~). Recent observational studies (Virman et al., 2018; Schiro and Neelin, 2019) concluded that the probability of intense convection increases rapidly with increasing LFT humidity, especially over land. ~~In this regard, a more humid LFT prevents larger dry air entrainment from happening. Khodayar et al. (2018) quantified relative humidity to be > 75 % at 700 hPa~~ in the hours prior to heavy precipitation at the locations ~~affected by convective systems~~ in the location of all convective systems during a~~n~~other ~~Heavy Precipitation Event (HPE)~~ of ~~the HymeX SOP1. In addition to an increased probability of transition to deep moist convection, a more humid LFT enhances convection intensity (Zhuang et al., 2018).~~ Whether this sensitivity of heavy precipitation to LFT moisture variations is well represented by current atmospheric models has been investigated by past sensitivity modelling studies using fine model resolutions, from Δx~ 500 m to Δx~7 km (Keil et al., 2008; Honda and Kawano, 2015; Lee et al., 2018). They demonstrated that convection enhancing (~~/~~weakening) happened ~~when~~ with increasing (~~/~~diminishing) moisture at the LFT in the simulations. These studies performed moisture sensitivity experiments modifying the water vapour distribution by adding or subtracting a prescribed water vapour amount at chosen heights. It is thus, of particular interest to investigate the aforementioned issues by performing corrections toward observations instead of using idealized experiments.

~~Given the correlation between the location of moisture convergence and precipitating convection, the complex Mediterranean orography plays a decisive role in setting areas prone to heavy precipitation. The high mountain ridges constrain the moisture transports in the basin favouring moisture gathering at the mountain foothills, the coasts and the valleys. Moreover, the elevated~~

terrain provides dynamic lifting to the convergent moist air masses triggering convection. The mountain slopes bring the low-level air masses to the level where they become buoyantly unstable. Therefore, the Alps (Italy, Switzerland, and Austria), the Massif Central (France) and Corsica (France) are focal regions for precipitating convection events (Ducrocq et al., 2014). The case of Corsica is especially characteristic given the complex distribution of valleys and ridges, which induces diurnal variations in the mountain atmospheric boundary layer coming from processes related to the terrain (Adler et al., 2015). This induces spatial inhomogeneities in the water vapour distribution that are crucial to determine the timing and location of deep convection (Adler et al., 2015) The linear composition of the highest peaks in the northwest to southeast direction render the island prone to heavy precipitation. Corsica is one of the main study regions of this paper where we assess relevant aspects of the moisture and convection interactions for a HPE coinciding the Intensive Observation Period (IOP) 16 of the Hydrological Cycle in the Mediterranean Experiment (HyMeX; Ducrocq et al. 2014) field campaign in autumn 2012.

A powerful technique to correct the atmospheric moisture distribution is Data Assimilation (DA). In relation to the problem of accurately representing heavy precipitation, the combination of rRecent advances in remote sensing techniques for atmospheric moisture measuring and the growing computational power hasve enabled the achievement of relevant improvements through data assimilation for heavy precipitation representation (Wulfmeyer et al., 2015). A well-established method to assimilate data is the Nudging scheme (Schraff and Hess, 2012). Nudging consists of relaxing the model's prognostic variables towards measurements (Schraff and Hess, 2012), where the main advantages are its simplicity (Guerova et al., 2016) and that it has shown good results especially in analysing humidity fields as compared to other schemes (Schraff et al., 2016). Nudging can be used to assimilate Global Positioning System (GPS) measurements that provide information on the total column atmospheric moisture. The demonstrated benefits of using GPS measurements are that it is an all-weather product (as opposite to other remote sensing integrated products), its large accuracy and its high temporal resolution (Cress et al., 2012; Guerova et al., 2016). The GPS data set used for nudging in this work is provided in the framework of the Hydrological Cycle in the Mediterranean Experiment (HyMeX; Ducrocq et al. 2014)HyMeX., which is This unique HyMeX GPS product is particularly interestingunique given the common processing of data from more than 25 European and African networks its bringing a dense coverage and of the area and its frequency of five minutes high temporal resolution of minutes (Bock et al., 2016). The total number of stations included in the nudging sums up to over 900 in the whole WMed and specifically over Corsica up to 20. In this sense, an open question is what the different impacts of nudging GPS data across resolution simulations are. Especially after reaching grid lengths that explicitly resolve convection (< 3 km). With this purpose, we use two horizontal different horizontal resolutions (7 km and 2.8 km) to quantitatively asses the different impacts of correcting the atmospheric moisture distribution depending on the corresponding model configurations.

Within this framework, this work is devoted to assessing the benefit of atmospheric moisture corrections with state of the art GPS derived measurements on sub hourly time frequencies for the modelling of heavy precipitation through realistic sensitivity experiments.

We analyse this issue first by understanding the role of local and remote atmospheric moisture contributions to the convection related processes leading to the occurrence of the event, and second through moisture sensitivity experiments nudging GPS

~~information. The IOP16 of the HyMeX Special Observation Period (SOP) 1 has been extensively investigated in the past by e.g. Thévenot et al. (2015), Duffourg et al. (2016) and Martinet et al. (2017). This study complements those previous publications providing a detailed analysis of the relevance and characteristics of atmospheric moisture for the same case.~~

Our study focuses on the Intensive Observation Period (IOP) 16 of the HyMeX field campaign in autumn 2012 (Ducrocq et al., 2014) taking Corsica as our study region. The event was selected due to the combination of propitious instability and moisture conditions interacting with the Corsican complex orography. It has been also selected given the large impact shown to GPS nudging in seasonal simulations of the complete autumn 2012 period performed in our working group. This on-going work revealed that the GPS nudging was able to reduce the existing wet bias in the model with a non-systematic response for heavy precipitation. HyMeX IOP16 was highlighted as one of the events where the GPS nudging was beneficial to reduce the precipitation overestimation.

Within this framework, this work is devoted to assess the sensitivity of convective precipitation and underlying mechanisms to variations of the atmospheric moisture spatio-temporal distribution~~impact of atmospheric moisture variations for precipitating convection representation~~. Our objectives are 1) to gain knowledge on the role of local and remote atmospheric moisture contributions to the convection-related processes leading to the occurrence of the event, 2) to assess the model sensitivity to continuous GPS nudging and 3) to quantify the impact of the GPS nudging depending on the model resolution.

The organization of the paper is as follows. Section 2 describes the model ~~set-ups and the modelling~~ experiments and presents the observational data sets used for model validation and~~or~~ nudging. Section 3 provides a description of the event including the synoptic situation, the convective evolution and the transport of moisture. Section 4 discusses the impact of the GPS nudging in precipitation, humidity and convective-related processes and Sect. 5 presents the conclusions.

2 Observations and Model Set-ups

2.1 Observations

GPS-Zenith Total Delay

The Zenith Total Delay (ZTD) is the "excess path length of GPS satellite emissions (in the L1 and L2-band) caused by the refractivity of the neutral atmosphere" (Businger et al., 1996). The refractivity definition for the neutral atmosphere depends on the partial pressures of water vapour and dry air and on the temperature as introduced in ground papers of GPS meteorology (Bevis et al., 1994). The ZTD is proportional to the Integrated Water Vapour (IWV) in the zenith direction. The ZTD is given in length units and the delay in the Zenith direction is usually preferred given it shows the shortest delays. It is obtained from the slanted path delays by means of mapping functions, $Z_m(\theta)$ dependent on the curvature of the Earth and the elevation angle (Duan et al., 1996). The dataset used for the sensitivity experiments, is provided by the LAboratoire de Recherche en Géodésie (LAREG) and the HyMeX community and its specifications can be found in Bock et al. (2016). It merges data from more than ~~25 European and African networks, with over~~ 900 stations with 20 stations over Corsica, our study region, is made available in temporal resolutions up to five minutes and it has a dense coverage of the western European countries (see Fig. 1). All

networks have been commonly processed by the GIPSY-OASIS II software to guarantee homogeneity. Data screening includes outliers, range and ambiguity checks to increase the accuracy. The comparison against radiosonde IWV measurements has shown no significant biases during night-time and biases in the range 0.5 – 1.4 mm during daytime (Bock et al., 2016).

Radiosondes

In the framework of the HyMeX SOP1 MétéoFrance provides the operational soundings containing more than 30 atmospheric parameters, including temperature, dew point temperature~~, wind speed~~, geopotential height, air pressure, wind direction and horizontal wind speed. In average, they contain ca. 30 levels between the surface and the 300 hPa level with about one measurement every 250 m. In addition to the operational soundings, supplementary soundings were launched during the HyMeX IOPs. Hence, the temporal resolution of the soundings lies between 12 h and 6 h. In total, 10 stations are used among which 3 (Gibraltar, Mallorca and Dar El Beïda) are used for process-understanding and 7 over the Italian Peninsula, Croatia, Corsica and Sardinia are used for validation of the specific humidity and IWV simulations. We perform the validation of the model data obtaining the nearest grid points to the location of the radiosondes. No height correction is applied for this purpose since the difference in height between the neighbouring grid points and the height of the radiosonde stations does not exceed 30 m in any case. The data is accessible at http://mistrals.sedoo.fr/?editDatsId=595&datsId=595&project_name=HyMeX.

Rain gauges

Météo-France and the HyMeX program provide the HyMeX domain precipitation amount (Nuret, 2013; SEDOO OMP. doi: 10.6096/mistrals-hymex.904) data set with hourly accumulated precipitation measured by rain gauges. Over 5000 stations are deployed over the WMed~~western Mediterranean~~ land parts with about 30 stations placed over the island of Corsica. The version used (V4) enjoys the newest quality control and checks for double stations. The data set spans the Sep-2012 to Mar-2013 period.

The NOAA CPC Morphing Precipitation (CMORPH)

CMORPH makes available precipitation measurements in a rectangular grid merging satellite microwave observations. These are combined using the Morphing technique (Joyce et al., 2004, https://doi.org/10.5065/D60R9MF6), that uses motion vectors, derived from infrared data to transport the microwave information to spots where no microwave data were available. It has a broad coverage (60°S - 60°N), and its spatial and temporal resolution at the equator is of 8 km and 30 minutes. The Climate Prediction Center (CPC) of the National Weather Service (NWS) in the USA provides the data and it spans the period 1998 to 2015. CMORPH has shown a good detection skill in validation studies (Bitew and Gebremichael, 2011; Habib et al., 2012) and high correlation rates with sub-daily rain gauge data (Sapiano and Arkin, 2009).

Global Land Evaporation Amsterdam Model (GLEAM)

GLEAM provides daily accumulated terrestrial evaporation (evapotranspiration) in a 0.25° x 0.25° grid, spanning the period 2003-2017. GLEAM computes the total evaporation over land from the sum of bare-soil evaporation (Eb), transpiration (Et), open-water evaporation (Ew), Snow sublimation (Es), snow sublimation (Es) and interception loss (Ei), as described in Martens et al. (2017) and Miralles et al., (2011). Four interconnected modules dealing with the rainfall interception, soil stress, soil state and the evaporation calculation, compute the aforementioned contributions. The four modules are forced by gridded global data which, in the version used in this work (v3b), is obtained mostly from remote sensing products, such as the Clouds and the Earth's Radiant Energy System (CERES) for radiation, the Tropical Rainfall Measurement Mission (TRMM) for precipitation, the Atmospheric Infrared Sounder (AIRS) for air temperature or European Space Agency Climate Change Initiative Soil Moisture (ESA CCI SM) for soil moisture. GLEAM version v3b has shown an average correlation with in-situ measurements of 0.78. In the validation, only 2 out of 63 stations showed differences with a level of significance of 10 % (Martens et al., 2017).

The Hybrid Single-Particle Lagrangian Integrated Trajectory Model (HYSPLIT)

The HYbrid Single-Particle Lagrangian Integrated Trajectory (HYSPLIT) computes air parcels, dispersion and chemical transformations (Stein et al., 2015; Rolph et al., 2017). In this paper, we use HYSPLIT to compute backward trajectories of moisture sources. The HYSPLIT model uses a hybrid approach combining lagrangian trajectories with the Eulerian methodology, using a fixed three-dimensional grid as a frame of reference (Stein et al., 2015). The free access internet-based platform READY (https://www.ready.noaa.gov/index.php) offers HYSPLIT trajectories calculation using eight different atmospheric model analyses of meteorological data. In this work, we use the half-degree archive of the National Centers for Environmental Prediction (NCEP) Global Data Assimilation System (GDAS) that spans the period 2007 to present and has a global coverage. The dataset is accessible in https://www.ready.noaa.gov/HYSPLIT_traj.php, last accessed 18-July-2019.

2.2 The COSMO-CLM Model and the GPS-ZTD Nudging Sensitivity Experiments

2.2.1 Consortium for Small-scale Modelling ~~(COSMO)~~ in Climate Mode (COSMO-CLM)

The COSMO model is based on the fully compressible, nonhydrostatic, hydro-thermodynamical equations of the atmosphere. COSMO-CLM simulates the atmosphere ~~Where the latter is considered~~ as a multicomponent continuum constituted by, liquid water, dry air, water vapour and solid water in the form of cloud droplets ice crystals, raindrops, rimed aggregates, hail and graupel (Schättler et al., 2016). We use t~~T~~he COSMO version ~~used in this study is the~~ 5.00 ~~and the model is used~~ in climate configuration ~~(COSMO-CLM)~~. This implies that the slow-changing variables (ozone concentration, aerosol concentration and canopy variables) evolve in time. This brings a more realistic representation for seasonal simulations such as the ones presented in this work. The dynamic solver is a third order Runge-Kutta split-explicit scheme following Wicker and Skamarock (2002). It uses an Arakawa-C/Lorenz grid with scalars defined at the centre of the grid box and the normal velocity components defined on the corresponding box faces. The grid is rotated, and the height coordinate shows a Gal-Chen terrain-following grid

stretching. The model uses a sponge layer with Rayleigh damping at the top boundary and three grid point lines for adaptation at the lateral boundaries. The boundary and initial states of the atmospheric prognostic variables are obtained by coarser resolution forcing models in a one-way nesting approach. The soil state and the surface-atmosphere interactions are simulated through the TERRA-Multi-Layer model (TERRA-ML; Doms et al., 2011). TERRA-ML has eight soil layers and is responsible for issuing the temperature and humidity conditions at the ground and considers the processes of evaporation, runoff, snow storage and interception storage. COSMO-CLM in the used ~~configurations for the~~ resolutions of this work (~~for a~~ 7 km and ~~a~~ 2.8 km ~~grid resolution~~), parameterizes the turbulent diffusion using a 1D diagnostic closure for the turbulent kinetic energy (Doms et al., 2011). The grid-scale clouds and precipitation are parameterized using a bulk scheme including several hydrometeor types (Doms et al., 2011). The radiation is parameterized following the formulation after Ritter and Geleyn (1992). In the case of grid spaces larger than 3 km sub-grid deep moist convection is parameterized using a mass-flux, low-level scheme with the equilibrium closure based on moisture convergence (Tiedtke, 1989). Shallow convection is parameterized using an adaptation of the Tiedtke scheme in the simulations using a 7 km and a 2.8 km grid.

The Nudging Scheme

Following Schraff and Hess (2012), "nudging or Newtonian relaxation consists of relaxing the model's prognostic variables towards prescribed values within a predetermined time window". The extent of the relaxation depends on the difference between the observed and the modelled variable ~~$((\varphi_k^{obs} - \varphi(x_k,t))[\varphi_k^{obs} - \varphi(x_k,t)])$~~, a weighting factor considering the measurement location and its representativeness ($W_k(x,t)$) and a coefficient that modulates the impact of the analysis increments (G_φ). This term is added to the result provided by the dynamics and numerics ($F(\varphi,x,t)$) ~~see Eq. (1.a)~~. These terms define the state of the prognostic variable ($\varphi(x,t)$) in the nudging equation (Eq. 1).

$$\frac{\partial}{\partial t}\varphi(\boldsymbol{x},t) = F(\boldsymbol{\varphi},\boldsymbol{x},t) + G_\varphi \cdot \sum_{k_{obs}} W_k(\boldsymbol{x},t) \cdot \left[\varphi_k^{obs} - \varphi(\boldsymbol{x}_k,t)\right] \quad (1.a)$$

For any observation type, the weighting factor considers the spatial and temporal distance to the ~~observed value~~ location of the observation by means of the horizontal (w_{xy}), vertical (w_z) and temporal weights (w_t). The weight for spreading in the horizontal direction ~~w_{xy}~~ is ~~performed following~~ a second-order autoregressive function ~~of~~ dependent on the distance between the ~~location of the~~ observation and the target point (Δr~~/s~~ ~~; see Eq. 1.b~~) and the correlation scale (s), see Eq. (2~~1.b~~). ~~The correlation scale is dependent on the pressure level and is largest for the stratosphere (100 km) and shortest for the PBL (58 km). This~~ This implies that the impact of the assimilated observation decreases with the distance to the station location. For example, the horizontal weight is halved ($w_{xy} = 0.5$) at a distance of 135 km at the 500 hPa level. ~~The vertical interpolation of the observed data is performed assuming a Gaussian decay in height differences.~~

$$w_{xy} = (1 + \Delta r/s) \cdot e^{-\Delta r/s} \quad (2)$$

~~1.b)~~

The vertical interpolation of the observed data is performed assuming a Gaussian decay in height differences (Eq. 3). The vertical interpolation is also applied in the case of GPS-ZTD nudging since a profile of specific humidity is constructed from the derived GPS-IWV value. This constructed profile shall be treated by the nudging scheme as an upper-air measurement in the remainder of the process. The applied vertical weight (Eq. 3) depends on the distance between the height of the model level and the height of the observation ($\Delta z = z - z_{obs}$), the virtual temperature at the height of the observation ($T_v^{z_{obs}}$) and the correlation scale for humidity (0.2).

$$w_z = exp\left\{-\left(\left(g/RT_v^{z_{obs}}\right)\cdot \Delta z/0.2\right)^2\right\} \quad (3)$$

~~$$\frac{\partial}{\partial t}\varphi(\boldsymbol{x},t) = F(\boldsymbol{\varphi},\boldsymbol{x},t) + G_\varphi \cdot \sum_{k_{obs}} W_k(\boldsymbol{x},t)\cdot\left[\varphi_k^{obs} - \varphi(\boldsymbol{x}_k,t)\right]$$~~ ~~(1.a)~~

~~$$w_{xy} = (1+\Delta r/s)\cdot e^{-\Delta r/s}$$~~ ~~(1.b)~~

Regarding temporal weighting, for hourly or even more frequent data measured from a stationary platform, the data are ~~temporally~~ linearly interpolated ~~linearly~~ to the model time. The observations are assigned to a grid point in the spatio-temporal space and the body of the report is evaluated. This is the step where gross error and consistency checks, quality control and redundancy checks dismiss suspicious observations.

In the case of GPS-ZTD observations, ~~these~~ they are converted to ~~Integrated Water Vapour (~~IWV~~)~~ following Bevis et al. (1994). Making use of run-time COSMO-CLM pressure and temperature values linearly interpolated to the station location~~,~~ ~~COSMO-CLM computes IWV from the issued ZTD~~ (Schraff and Hess, 2012). The observations are assigned to a grid point in the model space, provided the altitude difference of the GPS station and model surface lays within the range -150 ~~-~~to 600 m to allow for extrapolation and interpolation, respectively. Then they are ~~and are co~~converted to a specific humidity profile (q_v^{mod} ~~$q_{v_{obs}}$~~). ~~This is needed given~~given IWV is not a model prognostic variable as opposite to specific humidity. The profile is constructed ~~($q_{v_{mod}}$)~~ by means of an iterative process that scales the observed IWV (~~IWV_{obs}~~IWV^{obs}) with the modelled ~~IWV~~ one (~~IWV_{mod}~~IWV^{mod}) until a sufficiently low error is reached or alternatively ~~a~~ after 20 iterations. Eq~~, see Eq~~. (~~2~~4) describes the iterative formula. The first ~~constructed~~ profile ($q_{v_i}^{mod}$ ~~$q_{v_{mod}}$~~) used as the first guess for the iterative process, is the modelled specific humidity profile. Hence, the profile used for nudging depends on the vertical humidity distribution simulated by the model at the beginning of the nudging time-window.

~~$$q_{v_{obs}} = q_{v_{mod}}\cdot\frac{IWV_{obs}}{IWV_{mod}}$$~~ ~~(2)~~

$$q_{v_{i+1}}^{mod} = q_{v_i}^{mod}\cdot\frac{IWV^{obs}}{IWV_i^{mod}} \quad (42)$$

2.2.2 The GPS-ZTD Nudging Sensitivity Experiments

The Nudging scheme is used to assimilate GPS-ZTD data to assess the sensitivity of heavy precipitating convection to corrections of the spatio-temporal distribution of atmospheric ~~moisture. We use a diagnostic approach as opposite to commonly~~

use data-denial experiments. Hence, we do not provide in this study an assessment of the prognostic impact of nudging GPS-ZTD. moisture. We employ seasonal simulations of the autumn 2012 to profit from the full length of the GPS-ZTD data set.

The methodology is described as follows, we perform reference runs, hereafter referred to as CTRL, of the period 1-Sep 0000 UTC to 20-Nov 0000 UTC using two different horizontal resolutions (7 km and 2.8 km). Subsequently, we simulate the same period, keeping the same settings but nudging GPS-ZTD data continuously every 10 minutes. These runs are called NDG-7 and NDG-2.8. The 7 km runs (CTRL-7 and NDG-7) have been forced by European Centre for Medium-Range Weather Forecasts (ECMWF) analyses with a 6 hourly frequeneuncy. The 2.8 km runs (CTRL-2.8 and NDG-2.8) are forced by the CTRL-7 simulation in a one-way nesting strategy. CTRL-7 forces NUDG-2.8 to ensure a fair comparison between CTRL-2.8 and NDG-2.8 with the same different boundary and initial conditions. The simulation domains are contained in Fig. 1. We assimilate GPS data continuously to assess the differences in model representation from the free runs and the runs with an improved representation of the atmospheric column content. In this sense we a diagnostic approach and our experiments do not assess the impact of the assimilation on the subsequent first guess forecast.

Within the 80-day period of simulation, there are were several events, which are were largely affected by the GPS-ZTD nudging. IOP16, the case study of this paper, is one of them, which is especially interesting given the large reduction of maximum precipitation reductions (-49 %) induced by the GPS-ZTD nudging over the investigation area of Corsica in the course of 26 h. The remaining cases of the autumn 2012 period and analyses on the complete season are part of a series of modelling studies from our working group, including a PhD thesis by Caldas-Alvarez (2019). IOP16 is also suitable to assess the benefit of atmospheric moisture corrections with GPS-ZTD nudging given and the important role of the local orographic and instability factors in triggering and maintaining convection rather than the large-scale upper level forcing. We observed in the seasonal simulations that cases occurring undUnder a weak synoptic forcing are more impacted by the , the impact of the GPS-ZTD nudging given the strong is larger given the strongest correction of the lower to middle tropospheric humidity. We validate the model output against in-situ humidity measurements quantifying the Mean Absolute Error (MAE) and Mean Bias (MB) and the Agreement Index (AI, see Eq. 3) adaptedas fromdescribed in González-Zamora et al. (2015). More details on these validation metrics can be found in the Annex.

$$AI = 1 - \frac{\sum_{i=1}^{n}(obs_i - mod_i)^2}{\sum_{i=1}^{n}(|obs_i - \overline{obs}| + |mod_i - \overline{mod}|)^2} \quad (3)$$

. The precipitation fields are validated against rain gauges and the evapotranspiration over land using spatial averages of the GLEAM product.

To investigate the impact of moisture variations on convection-related processes, such as atmospheric latent and potential instability conditions, several convective related indices are examined. The CAPE -ML, providing information about the latent instability, is obtained through the mean layer parcel method, as described in (Leuenberger et al., 2010). KO-index is obtained as the differences in Equivalent Potential Temperature (-θe) between several levels of the atmosphere up to 500 hPa (Andersson et al., 1989) hence it bears information on potential instability and how the upper-levels introduce atmospheric instability.

Finally, the moisture flux is obtained by multiplying specific humidity and the horizontal wind following Ricard et al. (2012) but computed at each pressure level.

3 Atmospheric Moisture transport and Precipitating Convection during IOP16

During IOP16 ~~was an HPE that took place on the 26-Oct 2012 where~~ several convective systems affected regions in the north-WMed ~~.~~and ~~Radar measurements showed precipitation intensities over 100 mm in the course of 6 h, brought by large Mesoscale Convective Systems (MCSs) located close to the Spanish and French coasts displacing inland in the course of the day. R~~rain gauge stations measured totals up to 200 mm d^{-1} over southern France, 150 mm d^{-1} south of the western Alps and 250 mm d^{-1} at the gulf of Genoa (250 mm d^{-1}). Over Corsica, most precipitation occurred over the western side of the island for twelve hours, with maximum precipitation intensities reaching 25 mm h^{-1}. ~~Once the active systems reached land, the cold pools and the mesoscale moist south-westerly flow, as well as the local orographic lifting further promoted convection (Duffourg et al., 2016).~~

In this section, we use observations from radiosondes, the Evapotranspiration product GLEAM (see Sect. 2.1), CMORPH precipitation estimates, backward trajectories and the CTRL-7 simulation to understand the transport and distribution of moisture towards the WMed region. To validate the atmospheric moisture field of CTRL-7 we present in Table 1 the MAE, the AI and the MB of IWV between CTRL-7 and operational sounding measurements. In total, we selected 55 soundings from 7 stations (blue squares within the 2.8 km simulation domain in Fig. 1), during the period 26-Oct 0000 UTC to 28-Oct 0000 UTC with a temporal ~~. The temporal~~ resolution ~~of the radiosondes is~~ between 6 h and 12 h. ~~depending on the considered station. Table 1 represents the MAE, the AI and the MB of IWV for the comparison of the simulations against the 55 soundings.~~ CTRL-7 has a MAE of 2.7 mm, a MB of 0.61 mm and AI of 0.88. These values are within the acceptable range and are of the same order as the RMSE values found in other publications of IWV comparison between model data and GPS observations (Bock et al., 2016).

3.1 Synoptic conditions

The synoptic situation during the IOP16 was characterized by a cut-off low displacing westerly from the Iberian Peninsula toward southern France between 25-Oct 1200 UTC and 27-Oct 0000 UTC (Thévenot et al., 2015). The upper levels showed an associated diffluent flow with a south-westerly to southerly circulation at the low levels over the western part of the basin. Such a synoptic situation is prototypical for HPEs in the WMed (Jansa et al., 2001; Duffourg and Ducrocq, 2011). Over the Thyrrenean Sea on the morning of 26-Oct, the low-level flow induced convergence to the south of France. Figure 2 shows the geopotential height of the 500 hPa level (FI500), the Pressure at the Mean Sea Level (PMSL) and the spatial distribution of ~~the Equivalent Potential Temperature (~~ θ_e ~~)~~ at 850 hPa at three hours of the event as represented by CTRL-7. Figure 2.a shows the situation on the 26-Oct 0600 UTC where values of θ_e larger than 320 K take place. This moist and energetic southerly flow agrees with past publications referring values of the wet bulb temperature (θ_w) over 16 °C (Duffourg et al., 2016; Martinet

et al., 2017). Six hours later (Fig. 2.b) the cut-off Low progressed toward the border of France and Spain further deepening. On the 26-Oct 1800 UTC, the high values of θ_e (> 320 K) finally reached Corsica as well as extensive parts of the Thyrrenean Sea (see Fig. 2.c). Northerly cold winds terminated the event in the early morning of 27-Oct.

3.2 Convective evolution over Corsica

In the early morning of 26-Oct convection triggered and organized into a V-shape MCS close to the north-eastern coast of Spain. This MCS was named MCS0 by Thévenot et al. (2015) and hereafter we adopt the same nomenclature. This is shown by Fig. 3.a, depicting the convective cloud tops through brightness temperature images obtained with the Spinning Enhanced Visible Infrared Imager (SEVIRI) in a composite image at 0000 UTC, 0730 UTC and 1400 UTC. Northward, in the proximity of the Gulf of Lions, new convective cells triggered forming an MCS (MCS1) at 0500 UTC that would split into two defined MCSs (MCS1a and MCS1b). The two split MCSs moved toward southern France and eastward respectively in the course of 6 h (Duffourg et al., 2016). At the southern French region, the first MCS induced precipitation accumulations over 70 mm. South of the Alps, the second split MCS brought values over 90 mm (see Fig. 3.b, showing the accumulated precipitation between 26-Oct 1300 UTC and 27-Oct 1500 UTC for the whole WMed). Another MCS developed at the Liguria-Tuscany region in north-western Italy around 0730 UTC named MCS2 after Thévenot et al. (2015), not shown here. This area shows the highest precipitation rates of the event with over 245 mm in 24h (Duffourg et al., 2016). High convective cloud tops are also observed over the mid Mediterranean west of Corsica at 0730 UTC as shown by the brightness temperature (Fig. 3.a). This shows that convection is already happening offshore before the cells arrive at the island. At 1400 UTC over the island, the offshore convection is reinforced by orographic lifting of the moist low-level air masses.

Over Corsica, which is our study region, precipitation total values reach maximum accumulations between 75 mm and 100 mm, over the windward side of the mountains and over the mountain crests, between 50 mm and 75 mm (see Fig. 3.b). At the lee side of the mountain, the accumulated precipitation reaches 30 mm. The first convective cells occur over the island between 1300 UTC - 1500 UTC on the 26-Oct, forced by orographic lifting precipitating with intensities up to 11.5 mm h^{-1} over the windward side of the mountains (not shown). Between 26-Oct 1900 UTC and 27-Oct 0100 UTC, offshore ~~-size~~ convective systems arrive at the island (see Fig. 3.a). This stage has the largest precipitation intensities of the event (up to 16 mm h^{-1}, not shown) with precipitation falling mostly over the western part of the island, transitioning from the north at 2100 UTC to the south at 2300 UTC.

3.3 Atmospheric moisture transport

The transport of moisture feeding the convective systems ~~along~~ at Corsica, ~~and at~~ southern France and north-eastern Italy arises from the action of the upper-level pressure low through two mechanisms. First, the associated front swept atmospheric moisture from the Atlantic to the Mediterranean in the course of 36 h. Second, from intense evaporation over the Mediterranean and north-Africa between 25-Oct 1800 UTC and 26-Oct 1200 UTC transported by the southwesterly flow.

~~In this section, we use observations from radiosondes, the Evapotranspiration product GLEAM (see Sect. 2.1), CMORPH precipitation estimates, backward trajectories and the COSMO-CLM CTRL-7 simulation for understanding of the transport and distribution of moisture towards the WMed region. We use the CTRL-7 simulation given the good agreement against radiosonde measurements from the HyMeX database (discussed later in Sect. 4.2).~~

Figure 4 shows the CTRL-7 representation of IWV between 25-Oct 1200 UTC and 26-Oct 1200 UTC in the WMed~~western Mediterranean~~ at three hours with the simulated wind fields at 850 hPa. Given the overall good performance of CTRL-7 in representing IWV (Table 1) we use this simulation to study the moisture origins. At 25-Oct 1200 UTC (Fig. 4.a), the front associated with the pressure low west of the Iberian Peninsula ~~swept~~ carried ~~swept by the~~ large IWV amounts, up to ~~about~~ 40 mm over the strait of Gibraltar and along the southern Portuguese coast. Local areas at the Gulf of Lions (southern France) also showed values as large as 40 mm at about 12 h ~~00 UTC~~ before precipitation initiation. At 26-Oct 0000 UTC, the Atlantic moisture is already located over the Algerian coast and at the Gulf of Lions (see Fig. 4.b). Along the Algerian coast, these high moisture amounts at 26-Oct 0000 UTC were a combination of moisture ~~swept~~pushed by the low-pressure system from the Atlantic and moisture evaporated from north African land. The large moisture amount present at the Gulf of Lions originates partly from the Mediterranean Sea due to evaporation along the Spanish eastern coast , ~~A~~as introduced in Thevenot et al. (2015) and Martinet et al. (2017~~5~~), ~~the large moisture amount present at the Gulf of Lions originates partly from the Mediterranean Sea due to evaporation along the Spanish eastern coast~~. ~~Along the Algerian coast, these high moisture amounts at 26-Oct 0000 UTC were a combination of moisture swept by the low-pressure system from the Atlantic and moisture evaporated from north African land.~~ At the hour of precipitation initiation over Corsica (26-Oct 1200 UTC), vast IWV amounts surrounded the western and southern coasts of the island (see Fig. 4.c). These large IWV values (~ 40 mm) surrounded the island ~~about~~ 4 h prior to precipitation initiation. We have additionally validated these moisture transports against the Moderate Resolution Imaging Spectroradiometer (MODIS) daily product but we do not show it here given the presence of extensive cloud cover during the period hampering the quantitative validation. The visual comparison is included in the supplementary material (Fig. S.1).~~.~~

To better asses the timing and vertical stratification of the moisture transport the time-height cross-sections of Equivalent Potential Temperature (θ_e), specific humidity and horizontal winds measured by radiosondes between 24-Oct and 27-Oct 0000 UTC at Gibraltar (Spain), Dar el Beïda (Algeria) and Mallorca (Spain) are shown in Fig. 5. The cross-section of Gibraltar (Fig. 5.a) shows high specific humidity values throughout the complete atmospheric column (3 g kg^{-1} at 500 hPa and 11 g kg^{-1} at 950 hPa) between 24-Oct 1800 UTC and 25-Oct 0600 UTC, in agreement with the simulated IWV in Fig. 4.a. Further east, over Dar el Beïda (Algeria, see Fig. 5.b), high specific humidity and θ_e values are present between 500 hPa and 800 hPa on the 25-Oct 0000 UTC. The high humidity (6 g kg^{-1}) and θ_e (325 K) at this time come from the arrival of the moisture swept from the Atlantic. At lower levels (800 hPa to 1000 hPa), high humidity and θ_e only happens at the station 24 h later, at 26-Oct 0000 UTC. This is because below 800 hPa, the mesoscale circulation has a strong south-to-south-easterly component (Duffourg et al., 2016; Martinet et al., 2017) which delays the arrival of the moist air masses. This can also be seen in the wind direction over Dar el Beïda on the 25-Oct 1200 UTC below 850 hPa, where a south-easterly circulation takes place. Over

Mallorca, a similar vertical distribution can be observed (see Fig. 5.c.). On the 25-Oct 0000 UTC, specific humidity values as high as 6 g kg^{-1} exist between 500 hPa and 800 hPa. Twelve hours later, the high θ_e and specific humidity can be found in the layer 700 hPa to 800 hPa due to the delayed arrival of moisture at the low-levels. Finally, at 26-Oct 0000 UTC high θ_e and specific humidity is located at the marine boundary layer over Mallorca.

To further understand the extent of the moisture contribution ~~A relevant source of moisture~~ feeding convection from north Africa (NA)~~in our area of study originates in Algeria, from the Atlas Mountains and the Kasdir region (both regions are contained within the black box NA in~~ (Fig.1). ~~This moisture anomaly results from an intense episode of evapotranspiration over North African land between 20-Oct and 27-Oct as a result of heavy precipitation on the 19-Oct and 20-Oct. The resulting atmospheric moisture is transported by the south-westerly flow within the layer 500 m to 4 km during the evening of the 25 Oct merging with the Atlantic moisture swept by the large-scale front.~~, Fig. 6 shows the mechanisms of moisture evaporation and transport.

Figure~~s~~ 6.a ~~and 6.b~~ show~~s~~ the spatial distribution of hourly evapotranspiration simulated by CTRL-7 on the 25-Oct at 1200 UTC ~~and 1800 UTC~~ and the vertical updrafts of wind speed larger than 0.25 m s^{-1} ~~(Fig 6.a)~~. Hourly evaporation rates of 0.3 mm h^{-1} took place at the southern part of the NA box (North Africa) and of 0.2 mm h^{-1} over the Algerian Atlas (northern part of the NA black box). The moisture gathers in the PBL for several days until the first convective updrafts take place over the area on the ~~(~~25-Oct 1800 UTC~~, see Fig. 6.b)~~. The radiosondes over Dar el Beïda (Fig. 5.b) show the accumulation of moisture in the lower-atmosphere (about 10 g kg^{-1} close to 1000 hPa on the 25-Oct 1200 UTC). ~~The first convective activity over NA starts at about 25-Oct 1800 UTC (see Fig. 6.b).~~ Vertical transport of humidity is promoted by convection ~~and continues~~ during the evening of 25-Oct ~~(see Fig. 6.b)~~. At 26-Oct 0600 UTC, intense convective activity takes place over the Mediterranean Sea, between the coast of Algeria and the island (Corsica and Sardinia). This further promotes the moisture uptake form the Sea aided by the intensified drag of ~~the~~ low-level winds ~~convergence~~ associated with convection to ensure mass-continuity (Schneider et a., 2010; Peixoto and Oort, 1992).

Figure 6.b~~e~~ represents the evapotranspiration anomaly over North Africa showing the temporal evolution of spatially averaged precipitation measured by CMORPH and simulated by CTRL-7 and of evapotranspiration as shown by GLEAM and CTRL-7. CMORPH shows spatially averaged daily precipitation ~~up to~~over 15 mm d^{-1} ~~at~~ over North Africa on the 19-Oct and 20-Oct. Precipitation during these days coincided the IOP15 of HyMeX where a large band of south to north precipitation impacted regions of Africa, eastern Spain and southern France (Pantillon et al., 2015). CTRL-7 represents this precipitation but overestimates the amount. Suite to the precipitation event, daily evapotranspiration over the area reached daily spatial averages of 1.4 mm as shown by GLEAM, lasting for seven days, well above the mean evapotranspiration values during this season (0.5 mm). Albeit differences in the magnitude of evaporation, COSMO-CLM well captures this period of anomalous evapotranspiration.

Figure 6.c~~d~~ shows the 24h backward trajectories obtained with the HYSPLIT model, using reanalysis data from the GDAS model (see Sect. 2.1) with a resolution of 0.5°. We initialize the trajectories in a 3° x 2.5° box, ~~every 0.5°~~ at a height of 4000 m a.s.l., ~~representative of a height of convective activity~~over the study region CO, ~~. The trajectories start~~ on the 26-Oct at 1800

UTC. The trajectories confirm the moisture transport from northern Africa, as they are located over the intense evapotranspiration area "NA" black box on the 25-Oct 1800 UTC. ~~This is the hour when convective activity occurs over "NA" lifting the humid air masses (see Fig. 6.b).~~ Two sets of trajectories are distinguishable. The first set (ellipse A in Fig. ~~7~~6.c~~d~~) ~~shows faster trajectories, whose starting point is located over Morocco on the 25-Oct 1800 UTC and whose transport occurs at higher levels (between 2000 and 3000 m a.s.l). The second set (ellipse B in Fig. 7~~6.d) shows trajectories which are slower, that originate over northern Algeria at a height < 1000 m, representative of the well mixed diurnal layer (Garratt, 1994) and rise to 4000 m over the island.~~shows the trajectories, ~~reaching~~over the Moroccan shore on the 25-Oct 1800 UTC. These trajectories travel at height between 2000 and 3000 m a.s.l, as shown by the vertical section on the bottom of Fig.6.c. The second set (ellipse B in Fig. 6.c) shows trajectories ~~reaching~~located over northern Algeria at 25-Oct 1800 UTC. They travel at a lower height (< 1000 m) in the well mixed diurnal layer. Further trajectory analysis can be found in the supplement of this paper.

Figure 7 shows the temporal evolution of the spatially averaged moisture budget terms over the investigation areas NA and MED (see Fig. 6). The moisture budget terms have been obtained as in Lamb et al. (2012). Precipitation is considered a moisture sink, whereas evapotranspiration is a source. Moisture Flux Convergence (MFC) can be a sink or a source depending on its sign. The temporal evolution over NA (Fig. 7.a) shows that on the 25-Oct 1200 UTC the contribution of the Evaporation to IWV reaches 0.~~2~~1 mmh^{-1}, due to the wetter than usual soil over NA and the intense solar radiation. This moisture contribution is almost as large as the evaporation from the Mediterranean Sea over the MED area (0.~~2~~15~~5~~ mmh^{-1}). On the 25-Oct 1800 UTC an increase in IWV takes places reaching 0.8 mmh^{-1} over NA (Fig.1.a) due to strong Moisture Flux Convergence (MFC) associated with the Atlantic moisture brought by the south-westerly flow. Over MED (Fig 7.b) we can see a stable Evaporation during the period as well as an enhanced MCF, especially after 25-Oct 1800 UTC. These two contributions build up overseas until the 26-Oct 0600 UTC when convection triggers.

4 Nudging Effects on Convection

~~The present section examines the sensitivity of the precipitation field and the underlying convection-related processes responsible for the IOP16 event, to realistic atmospheric moisture corrections through GPS-ZTD nudging.~~

4.1 Precipitation

The COSMO-CLM simulations were able to represent the event over the island on both the 7 km and the 2.8 km configurations at the right time. ~~, albeit they overestimated the amount. Indeed, the maximum accumulated precipitation simulated by CTRL-7 was between 125 mm and 200 mm and for CTRL 2.8 was between 100 mm and 125 mm, both of which are too large in comparison with the measurements (between 75 mm and 100 mm, see Fig. 3.b).~~

CTRL-7 performed well in representing the location of maximum precipitation~~;~~ over the windward slope of the Corsican mountains (see Fig. 8~~7~~.a and Fig. 3.b). ~~The represented precipitation was mostly orographically triggered together with an~~

offshore convective line west of the island triggered by low-level convergence (not shown). Offshore precipitation accumulations at this location brought by the convective line are between 50 mm and 75 mm. CTRL-2.8 showed a worse representation of the location of the maximum as it shifted it towards the crests of the mountain mainly and also to the lee side (see Fig. 87.c), but represented better the amount than CTRL-7. CTRL-2.8 represented more isolated precipitation structures, located over the mountain crests. Representing more localized structures is a well identified effect of reaching convection permitting resolutions (Chan et al., 2012; Fosser et al., 2016)

The main differences in precipitation representation of CTRL-2.8 (Fig. 7.c) in comparison with CTRL-7 (Fig. 7.a) are the location of maximum precipitation over the crests, the missing of the offshore convective line at 26-Oct 2100 UTC and the much more localized heavy precipitation structures. The latter is a well identified effect of reaching convection permitting resolutions (Chan et al., 2012; Fosser et al., 2016).

The GPS-ZTD nudging induced for both model resolutions a decrease in the accumulated totals, bringing values closer to the observations. In the case of NDG-7, it showed maximum precipitation totals between 100 mm and 125 mm (-20 % variation), rain gauges showed precipitation between 75 mm and 100 mm (see Fig. 7.b). The location of the maximum was very similar to that of CTRL-7, totals. In the case of NDG-7 this occurred over the windward side of the mountain, improving the in good agreement with the observations (Fig. 3.b). NDG-2.8 showed the same location of the maxima as CTRL-2.8 but an overall with a too large reduction elsewhere with values below 20 mm. However, the convective line ahead of the island is not captured by the NDG-7 simulation because of relevant changes in the low-level mesoscale wind circulation (not shown). These differences in wind circulation arise partly due to changes in the pressure distribution of the event, as explained in Sect. 4.4. The NDG-2.8 showed maximum accumulated precipitation in the range 75 mm to 100 mm (-25 %) over one of the mountain peaks in better agreement with observations (Fig. 7.d). The location of precipitation maxima did not change however significantly as it erroneously remained over the mountain crests.

To validate quantitatively our simulations against rain gauges, Table 2 shows the scores of Root Mean Square Error (RMSE), the hourly standard deviation difference ($\boldsymbol{OBS_\sigma - MOD_\sigma}$), the spatially averaged differences ($\overline{\boldsymbol{OBS}} - \overline{\boldsymbol{MOD}}$), the accumulated precipitation standard deviation difference ($\boldsymbol{OBS_\sigma - MOD_\sigma}$) and the difference of maximum precipitation ($\boldsymbol{OBS_{max} - MOD_{max}}$). A description of the metrics can be found in the Annex. The results show the overestimation of maximum and spatially average precipitation by CTRL-7 in excess of 185 mm and 10.4 mm, respectively, as well as of the standard deviations (-32 mm). The RMSE for hourly precipitation was of 3.1 mm. The reduction caused by the GPS-ZTD nudging was beneficial for the representation of maximum accumulated precipitation in NDG-7, now in excess of 58 mm compared to the observations, of the accumulated precipitation standard deviation (-0.7 mm) and of the RMSE (2.6 mm). CTRL-2.8 showed a good performance with better values than CTRL-7 for maximum (excess of 3 mm) and spatially averaged accumulated precipitation (14.6 mm) as well as of the standard deviation differences with, however, the same RMSE (3.1 mm). The GPS-ZTD dried excessively the NDG-2.8 simulations bringing worse scores. Only the RMSE was improved (2.7 mm), similarly to NDG-7, possibly due to a better representation of the location of precipitation relevant for the interpolation of the COSMO-CLM simulations to the rain gauges location.

4.2 Atmospheric Moisture

As introduced in Section 3, we ~~To~~ assess the accuracy of model moisture outputs and the impact of nudging GPS-ZTD, comparing ~~-~~ independent humidity measurements from radiosondes ~~profiling of the atmosphere are compared with the CTRL and NDG simulations~~. ~~In total, we selected 55 soundings from 7 stations (blue squares within the 2.8 km simulation domain in Fig. 1), during the period 26 Oct 0000 UTC to 28 Oct 0000 UTC. The temporal resolution of the radiosondes is between 6 h and 12 h depending on the considered station. Table 1 represents the MAE, the AI and the MB of IWV for the comparison of the simulations against the 55 soundings.~~ The reference run~~s~~, ~~CTRL-7 and~~ CTRL-2.8, has ~~show~~ MAE values of 2.7 mm, with M~~ean~~ B~~iases~~ of ~~0.61 mm and~~ 0.38 mm and AI of ~~to 0.88 and~~ 0.89~~, respectively~~. These values are similar to those of CTRL-7 albeit a slight improvement of the MB and the AI.~~-~~ ~~The values of Mean Biases are of the same order as the RMSE values found in other publications of IWV comparison between model data and GPS observations (Bock et al., 2016). We can see that the 2.8 km slightly outperforms 7 km in representing IWV.~~

Nudging GPS-ZTD data, improves further the scores bringing t~~. T~~he MAE of IWV ~~is~~ to 2 mm for NDG-7 and NDG-2.8 and the MB to ~~is of~~ -0.04 mm and -0.08 mm, respectively. In this sense, both the 7 km and the 2.8 km simulations endure an improvement.

Figure 9~~8~~.a shows the spatially averaged temporal evolution of IWV over the study region CO~~Corsica~~. The hours prior to precipitation initiation (26-Oct 1300 UTC) were characterized by an IWV pick up starting at 26-Oct 0000 UTC. All simulations show~~ed~~ this, albeit the IWV amount over ~~Corsica~~ CO for NDG-7 and NDG-2.8 was 5 mm higher than for CTRL-7 and CTRL-2.8. This was due to represented precipitation over the island until the night of 24-Oct in the NDG runs, hence inducing a much wetter boundary layer (not shown). By 26-Oct 1000 UTC, an intense moisture increase takes place over the island. As described in Sect. 3.3, this is the time when the Atlantic, Mediterranean and African moisture reached CO~~the island~~. At this time, all simulations show the same mean IWV (27 mm) which lasts for 4 hours. ~~This is so since only after the moist air masses reach the island the GPS nudging has a noticeable impact on the simulated IWV.~~ Given no GPS stations are located over Africa or the Mediterranean Sea, the south-westerly moisture ~~flow~~ is only weakly impacted by the GPS-ZTD nudging during these first four hours ~~stages~~ of the event over ~~Corsica~~CO. At 26-Oct 1400 UTC, the CTRL and NDG runs start to diverge and between 26-Oct 1600 UTC and 27-Oct 0600 UTC, NDG-7 and NDG-2.8 show ca. 4 mm less than their CTRL counterparts do. This is due to the impact of the GPS measurements over the island. ~~This has stringent consequences for the intensity of convection and precipitation with a vast decrease of precipitation amount, as discussed in Sect. 4.1.~~

To understand at which levels the humidity reduction was most effective Figure 9.b shows box and whiskers plots between 500 hPa and the surface. ~~The humidity reduction between 26-Oct 1600 UTC and 27-Oct 0600 UTC takes place below 500 hPa (see Fig 8.b and Fig 9). Fig. 8.b shows how median IWV decreases from 30 mm to 27 mm as a result of the GPS-ZTD nudging in the 7 km simulations (~ 10 %) and from 30 mm to 28 mm in the 2.8 km (~7 %).~~ At 500 hPa, a specific humidity reduction of 0.2 g kg^{-1} took place for median values in the 7 km simulation (-13 %). The decrease was weaker in the 2.8 km grid with a reduction of 0.05 g kg^{-1} (~~3~~-3 %). At ~~5~~700 hPa the specific humidity decrease ~~ranged~~ was about ~~between~~ 0.~~54~~ g kg^{-1} ~~and 1 g kg^{-1}~~

~~1~~ for median values (-8 %) for both resolutions. At 950 hPa, the humidity reduction was larger in the 7 km (-8 %) than in the 2.8 km run (-2%). Finally, at 2 m height the reduction was of -7 % for 7 km and of -3 % for 2.8 km

Figure 10~~9~~ represents the MAE and the MB of specific humidity profiles between 500 hPa and 950 hPa for the same set of radiosondes. The period of validation is 26-Oct 0000 UTC to 28-Oct 0000 UTC and the area is larger than that of Corsica. This is done to assess the overall performance of the model with as many radiosondes as possible (Fig. 1). Between 600 hPa and 950 hPa, the MAE of specific humidity of CTRL-7 and CTRL-2.8 is between 0.7 g kg^{-1} (600 hPa) and 1.3 g kg^{-1} (925 hPa). The MB of the profile shows that this error comes from an underestimation of specific humidity by COSMO-CLM below 650 hPa, which is largest below 900 hPa. Over 650 hPa, the simulations overestimated the specific humidity. The GPS-ZTD nudging improves the MAE of the humidity profile between 650 hPa and 925 hPa for both resolutions. The MAE of NDG-7 is now within the range 0.6 g kg^{-1} (600 hPa) and 1.1 g kg^{-1} (925 hPa) and the improvement reaches the 950 hPa level. For NDG-2.8, the MAE is between 0.8 g kg^{-1} (650 hPa) and 1.2 g kg^{-1} (900 hPa) but an improvement is only achieved down to 925 hPa. The MB is closer to zero at the same atmospheric layers (650 hPa to 900 hPa) for both resolutions albeit showing better results for the 7 km simulation. The correction for LFT moisture is larger in the 7 km runs than in the 2.8 km, probably due to the larger number of observations included in the nudging in this simulation because of larger simulation domains (see Fig. 1). These values of the MAE and Mean Bias are of the same order as the validation of the RMSE of specific humidity profiles between reanalyses data and Lidar measurements from Duffourg et al. (2016).

Below 900 hPa, the GPS-ZTD nudging was not able to ~~bring such a clear correction, especially for NDG-2.8 where the MAE and MB showed very similar values to the CTRL-2.8 runs. The GPS-ZTD is not able to~~ correct sufficiently the dry bias of the model. ~~below 900 hPa because the radiosondes showed a steeper gradient of increasing humidity at the lowest levels.~~ Both CTRL runs show difficulties in representing the steeper~~is~~ gradient shown by the radiosondes and the correction induced by the GPS-ZTD nudging is not enough to moist sufficiently the PBL during this event. Overall, COSMO-CLM shows a good performance in representing the integrated atmospheric moisture fields and humidity over 900 hPa at both model resolutions. The 2.8 km simulation was initially more accurate, but the nudging brings both to similar accuracy ~~rates~~values.

4.3 Instability reduction and increase of free-tropospheric mixing

The two affected processes, which exerted the largest control on precipitation reduction, were atmospheric latent instability reduction and dry air entrainment, both investigated in this section. ~~The drying brought by the GPS-ZTD nudging over Corsica dried the atmosphere below 500 hPa. In this section, we will discuss how the impact was primarily reducing CAPE-ML and additionally enhancing mixing with dry air above the PBL.~~ The changes in these two processes start to play a role immediately after the first hour of large IWV differences i.e. after 26-Oct 1600 UTC this is so for both the 7 km and the 2.8 km simulations. Figure 1~~0~~ shows the ~~height-surface~~vertical cross-sections of Equivalent Potential Temperature (θ_e), specific humidity and the wind ~~in the vertical-horizontal direction~~ along the direction of the mean horizontal wind (purple transect in Fig. 1) over the island at 26-Oct 1700 UTC. CTRL-7 and CTRL-2.8 show θ_e values over 322 K from the surface up to 500 hPa showing the upward transport of moist low-level air masses. After applying the GPS-ZTD nudging, NDG-7 shows reduced values of θ_e

(310 K) close to the ground (see 2 m specific humidity in Fig.9.b) over the island and at 700 hPa (312 K) showing a less favourable environment for convection development. The 2.8 km simulation, for its part, showed a weak reduction of θ_e at the windward side of the mountain (316 K) as a result of the GPS-ZTD nudging compared to the NDG-7. However, at the lee side between 600 hPa and 900 hPa, θ_e is reduced in NDG-2.8 by -8 K (compared to CTRL-2.8, 318 K), this is shown in Fig. 11~~0~~.c and Fig. 11~~0~~.d. The consequence for the updrafts was a change in their timing location and intensity with less penetrating updraughts (see Fig. 11~~0~~.d). ~~For the time shown, the drier environment in the NDG-7 and NDG-2.8 runs impedes the development of deeper updraughts.~~

Figure 1~~1~~2 shows that median ~~CAPE-ML~~CAPE is reduced as a result of the GPS-ZTD nudging for both resolutions from 310 J kg^{-1} in CTRL-7 to 190 J kg^{-1} in NDG-7 (-39 %) and from 600 J kg^{-1} in CTRL-2.8 to 410 J kg^{-1} in NDG-2.8 (-32 %). Since COSMO-CLM selects the lowest 50 hPa as the mean layer to compute CAPE~~-ML~~ (mixed layer), a decrease of humidity close to ground implies a relevant impact on atmospheric instability conditions. COSMO-CLM in the 2.8 km resolution represented larger latent instability than 7 km for this event. Median KO-index increased from -2.7 K, in CTRL-7 to -1.5 K in NDG-7 (+ 44 %) where lower KO-index indicates more potential for storm development under favourable large-scale conditions. The narrower simulation domains of the 2.8 km simulations (see Sect. 2.2.2) render the impact of the GPS-ZTD nudging on KO-index weaker given the inability to represent changes on the large-scale pressure distribution. The overall decrease in the median moisture flux implies a drier ground level and a drier LFT. This means that the air entrained in the convective updrafts is drier than that of the reference runs (CTRL). The median moisture flux is reduced by about 13 % in NDG-7 and about 5% in CTRL-2.8 at 700 hPa. At the PBL, the moisture flux is also reduced. The changes in moisture flux between CTRL-7 and NDG-7 are larger than their 2.8 km counterparts. This is due to two factors, first, the changes in specific humidity are slightly weaker in the 2.8 km runs as compared to 7 km and second, the horizontal wind speed and direction in the 7 km runs are modified as a result of the GPS-ZTD nudging. For instance, at 950 hPa, extreme horizontal wind speeds are reduced by -8 % from CTRL-7 to NDG-7. This impact is not observed in the 2.8 km runs.

Overall, the humidity reduction caused by the GPS-ZTD nudging, locally over Corsica, reduced the amount of instability (as shown by ~~CAPE-ML~~CAPE and KO-index) as well as humidity at the LFT (demonstrated by the changes in specific humidity and moisture flux).

4.4 Impact on the low-pressure system and mesoscale winds

Besides impacting the representation of the local conditions of humidity, instability and buoyancy, the GPS-ZTD nudging affected the representation of the low-pressure system. ~~This section shows how a large humidity reduction over the Iberian Peninsula and France weakened the intensity of the pressure Low and its associated circulation. This brought, in turn, stringent modifications of the wind fields close to Corsica down to the ground and hence on dynamic lifting. This effect was observed in the 7 km resolution runs exclusively given the broader extent of the simulation domains. Hence, for the analysis of the impact of the GPS-ZTD nudging on the large-scale surface pressure distribution we focus in the 7 km resolution simulations.~~

In the early morning of 26-Oct-2016, the centre of the upper-level low was located over the north-western part of the Iberian Plateau. The GPS-ZTD nudging induced moisture reductions of 7 mm in IWV at that location in the NDG-7 simulations, with very large reductions in the range 1-2 g kg^{-1} from the ground up to 700 hPa (not shown). The progression of the pressure-low toward southern France was effective in twelve hours and at 1500 UTC, the PMSL was of 995hPa at the Rhône Valley (CTRL-7). The centre of the Low extended toward the Alps at 2300 UTC. Drying of the atmospheric column, due to the GPS-ZTD nudging, also took place at this region between the 25-Oct and the 28-Oct (not shown). At 2300 UTC on the 20-Oct, over the Cévennes-Vivarais area, differences in IWV were of 3 mm between CTRL-7 and NDG-7. Figure 1~~2~~3 shows the differences in PMSL on the 26-Oct 2300 UTC between NDG-7 and CTRL-7 as well as the wind fields at 950 hPa. The GPS-ZTD nudging increased by 10 hPa the PMSL at the centre of the system and up to 2 hPa between Brittany (France) and the Balearic Islands (Spain). The drying over France and the Iberian Peninsula induced a weaker low-pressure system in NDG-7, this changed ~~impact for~~ the cyclonic wind circulation ~~was a veering~~ from a south-westerly to west-south-westerly flow and a reduction of the horizontal wind speeds. The largest impact was observed at the 950 hPa level albeit relevant differences affecting Corsica exist between 850 hPa and 1000 hPa. The reduction of the horizontal wind speeds is demonstrated through box-whisker plots in Fig. 1~~1~~2. This difference in horizontal wind speed does not exist in the 2.8 km runs. ~~The consequence for convection initiation was that weaker low-level convergence was represented in the NDG-7. Either for offshore convergence or convergence forced by the orography.~~ This hampered orographic lifting at the mountain foothills and ahead of the island reducing triggering of new cells and weakening the convective updrafts.

4.5 10-min vs. 1-hour nudging

To discern the added value of nudging GPS-ZTD with a 10-minute frequency with respect to lower nudging frequencies, we carried out additional simulations with COSMO-CLM with a 1 h frequency initialized on the 20-Oct-2012~~0~~ 0000 UTC. These simulations have the same model settings as the original simulations (Section 2.2.2) except for the changes in nudging frequency (named with the suffix 1h). The initialization time is also different to avoid the computational cost of running the whole autumn season but is early enough to mind the Atlantic and African moisture transports described in Section 3.3. They show analogue features to those presented in Section 2.2.2 and hence are used for validation of the 1 h frequency nudging impacts~~.~~

Table 3 shows a validation of the additional runs against rain gauges, as in Table 2. Nudging GPS-ZTD data with a 1h frequency brings a slightly larger reduction of the precipitation maximum and the hourly standard deviation for NDG-7-1h as compared to the 10-minute frequency (NDG-7). The RMSE, the standard deviation and the mean of accumulated precipitation showed no relevant differences between NDG-7 and NDG-7-1h. This aspect is even clearer in the case of 2.8 km. No perceptible differences exist for the validation metrics between NDG-2.8-1h and NDG-2.8. Similarly to the validation metrics, the spatial distribution shows no relevant differences between the 1 h and the 10 min frequency nudging. The spatial distributions are shown in Fig. S.4 of the supplementary material.

5 Conclusions

Further knowledge of the pathways of moisture and convection interaction is neededThe pathways of moisture and its interaction with convection are not fully understood (Stevens, 2005; Sherwood et al., 2010; Ahrens and Samson, 2010). A deeper understanding of moist processes is relevant to improve the representation of heavy precipitation by numerical atmospheric models in order to support the mitigation and prevention of its hazards. The presented workThis study aimed at assessing the sensitivity of the precipitating convectionconvective precipitation and underlying mechanisms to realistic variationscorrections of the atmospheric moisture distribution. We did this by, first understanding the role of local and remote atmospheric moisture contributions to the occurrence of the event and second, through moisture sensitivity experiments nudging GPS ZTD observations. The unique opportunity provided by the synergy of high resolution atmospheric modelling, very frequent data nudging and high resolution humidity datasets enables the study of moisture and convection interactions in a selected case study of heavy precipitation. With this purpose, we presented an in-depth analysis of HyMeX IOP16 with special focus on the complex orographic region of Corsica. We showed .

The results showed novel insights on the role of remote and local moisture transports for this event and the sensitivity of precipitation representation to high frequency GPS-ZTD nudging. moisture distribution pre-conditioning heavy precipitation at the WMed and over Corsica during IOP16. These results supplement the findings by (Thévenot et al., 2015; Duffourg et al., 2016; Martinet et al., 2017), focusing in southern France and the Gulf of Lions as study region. The main findings of this diagnostic study are summarized in the following:

- Large atmospheric moisture amounts (IWV~ 40 mm) precondition the areas of convective activity, namely, southern France, and theFrance, the Gulf of Lions, Corsica, and SardiniaCorsica, Sardinia, the middle Mediterranean and northeastern Italy, in agreement with previous investigations in the region (Khodayar et al., 2016). These very wet air masses reach southern France and the Gulf of Lions about 12 h prior to precipitation initiation and about 4h for the central Mediterranean about 4 h prior to initiation. A low-level convergence line southerly located between France and the Balearic Islands (Duffourg et al., 2016; Martinet et al., 2017) to southeasterly flow at the low levels over the Mediterranean Sea delays the arrival of low-level moisture at Corsica and the Italian Peninsula. in the eastat the easterly locations.
- The transport of moisture feeding the convective cells arises from the action of the upper-level pressure low through two mechanisms. On the one handFirstly, the associated front, sweeps atmospheric moisture from the Atlantic to the Mediterranean in the course of 36 hours. . These large-scale moisture transports are delayed 24 h at the layers below 800 hPa with respect to the higher levels due to the southerly flow bringing low-level convergence south of the Gulf of Lions as referred in Martinet et al. (2017) and in Duffourg et al. (2016). This was demonstrated by the radiosondes in the region (Gibraltar in Spain, Dar el Beida in Algeria and Mallorca in Spain). Secondly, evaporated moisture over the Mediterranean and north Africa between 25-Oct 1800 UTC and 26-Oct 1200 UTC is transported by the south-westerly flow towards Corsica, contributed to the feeding of the convective systems.

- NFor the first time, to the authors' knowledge, this evapotranspiration anomaly over northern Africa has been identified as a source of moisture for this eventfeeding HPE in the WMed during this event., caused by Iintense evapotranspiration over the Algerian Atlas and NA takes place between 21-Oct and 28-Oct due to as a result of intense solar radiation and precipitation impacting the region two days earlier on the 19-Oct and 20-Oct. SubsequentlyAfter 25-Oct, the intense south-westerly flow and the convective activity across the WMed Sea broughtings the moisture up north in the course of 24 h to 30 hours as shown by backward trajectories and model output.

COSMO-CLM was able to represent theis event over Corsica with a good agreement on the timing for both resolutions but an overestimation of precipitation in CTRL-7, well corrected by the GSP-ZTD nudging. Overall, the representation of humidity during the event was good and the GPS-ZTD nudging helped to further reduce the model humidity biases. and an overall good performance in humidity representation. In this regard

- The precipitation overestimation in the 7 km run was well corrected by the GPS-ZTD nudging. Regarding the 2.8 km simulations, CTRL-2.8 This was not the case for the 2.8 km since the reference runs (CTRL-2.8) performed well in representing the maximum and the spatial averages but the GPS-ZTD nudging reduced excessively the total precipitation. The impact of nudging GPS-ZTD with a 1 h frequency or a the 10-minute frequency showed no relevant differences.

- The reference runs (CTRL-7 and CTRL-2.8) The reference runs using both a 7 km and a 2.8 km grid performed overall well in reproducing the moisture distribution during the event. The GPS-ZTD nudging improved the representation of IWV reducing the MAE of IWV to 2 mm. Regarding the vertical distribution of humidity, the GPS-ZTD nudging improved by 25 % the MAE from below 650 hPa down to the ground in the 7 km simulation and by 8% between 650 hPa and 925 hPa in the 2.8 km resolution. The weaker improvement at the PBL (PBL) below 925 hPa in the 2.8 km resolution is because the model is unable to represent the abrupt humidity gradient of the lowest layers. Even if the GPS-ZTD correction is beneficial, it is not enough sufficient to overcome the humidity biases at this level. The accumulated precipitation amount was overestimated by the reference runs of both resolutions, most notably by CTRL-7 with totals between 125 mm and 200 mm at the windward side of the mountains. CTRL-2.8 also overestimated the maximum accumulated precipitation (between 100 mm and 125 mm) this time at the mountain crests. The GPS-ZTD reduced the maximum accumulated precipitation to 100 mm in NDG-7 and to 75 mm in NDG-2.8, bringing closer values to the rain gauges observations (between 75 mm and 100 mm). The CTRL-7 and NDG-7 better captured the location of precipitation than the 2.8 km simulations. The nudging did not improve this aspect in the 2.8 km resolution.

The impact of the GPS-ZTD nudging during the case study has been assessed with the following conclusions:

- Heavy precipitation showed a large sensitivity to the moisture variations, implying a strong reduction of the maximum totals (-49 % for 7 km and -16 % for 2.8 km) arising from less intense convection and a lower number of triggered

cells. ~~This is related to the reduction of specific humidity below 500 hPa by -10 % in the 7 km and by -7 % in the 2.8 km.~~

- The two affected processes which exerted the largest control for precipitation reduction were the reduction of atmospheric instability over the island (-35 % ~~CAPE ML~~CAPE) and the drying of the LFT bringing more dry air entrainment into the convective updrafts (-13 % moisture flux at 700 hPa for 7 km and -5 % for 2.8 km).

- Additionally, the 7 km simulations showed an impact on the large-scale surface pressure and the associated circulation given the larger simulation domains. The GPS-ZTD nudging dried the atmospheric levels over Iberia and France, weakening the Low-Pressure system ~~(~10 hPa higher for PMSL)~~. This induced in turn a decrease in horizontal wind speed ~~(7 %)~~ and a veering of the direction toward a west-south-westerly.

The unique opportunity provided by the synergy of high-resolution atmospheric modelling, very frequent data nudging and high-resolution humidity datasets enables the study of moisture and convection interactions in a selected case study of heavy precipitation. We showed the benefit ~~This study highlights the added value~~ of nudging GPS-ZTD ~~adequate corrections of atmospheric moisture~~ for the simulation ~~modelling~~ of the vertical profile and integrated amount of atmospheric humidity and for precipitation in a convection parameterized set-up (7 km). This is relevant since coarse resolution simulations will still be needed as providers of forcing data and therefore GPS-ZTD nudging can reduce moisture uncertainties at these grid ~~lengths to improve the precipitation forecasts~~. The performance of CTRL-2.8 was acceptable without the GPS-ZTD nudging. This highlights the added value of convection permitting resolutions for this case able to provide a fair precipitation forecast even in the presence of the addressed humidity biases. ~~convective processes, in this case through sub-hourly GPS-ZTD nudging. The high-temporal resolution of the GPS-ZTD observations facilitate a better representation of the water vapour variability and a better regulation of the accumulated precipitation. This was shown to be the case for HyMeX-IOP16 at convection permitting and convection parameterized grid lengths. This is especially relevant since, in spite of the consensus in the scientific community that convection permitting is the future of NWP, coarser resolution simulations will still be needed as providers of forcing data and therefore reducing moisture uncertainties at these grid lengths is needed to improve the precipitation forecasts.~~ Also noteworthy is the large sensitivity to variations of the LFT moisture showed by the model. Recent observational studies have highlighted the linkage between intense convective precipitation and a humid ~~free troposphere~~LFT (Schiro and Neelin, 2019; Virman et al., 2018), hence the relevance of the ability to represent such sensitivity. ~~Just as the high-temporal resolution, the dense spatial coverage and the accuracy are the clear benefits of GPS-ZTD nudging, this~~This study also points out one of ~~its~~ the GPS-ZTD nudging drawbacks. Being an integrated quantity, GPS-ZTD nudging struggles to correct the vertical distribution of humidity, in this case particularly in the lower-troposphere. Lastly, this study focuses on a single case study; therefore, the results presented here should be extended to other events of the region to allow for

generalization ~~prove their general applicability~~. In a further publication, the authors evaluate the impact of GPS-ZTD nudging on the SOP1 period of the HyMeX campaign considering the sensitivity of all IOPs in this autumn season.

6. Code Availability

The COSMO-CLM model is only accessible to members of the Climate Limited-area Modelling Community and access is granted upon request. Parts of the model documentation are freely available at http://www.cosmo-model.org/content/model/documentation/core/default.htm

7. Data Availability

Two further publications using these nudging simulations are on-going. Therefore, these are not yet available for the open public. However, the data used to produce the figures showing results on the nudging simulations (Figures 2, 4, 6.a, 6.b, 8, 9, 10, 11, 12, 13; and Tables 1, 2 and 3) are accessible in at https://doi.org/10.5445/IR/1000097457. The observational data used in the figures within this manuscript are obtained from the referenced data sets and their access depends on the restrictions of the producing institutions.

8. Author Contributions

SK designed and planned the experiments. ACA carried out as part of his PhD the nudging experiments under the supervision of SK. ACA and SK analysed the results and wrote the manuscript.

9. Competing Interests

The authors declare that they have no conflict of interest.

10. Acknowledgements

We acknowledge Oliver Bock and the LAboratoire de Recherche En Géodésie (LAREG) of the French Institute of the Geographic and Forest Information (IGN) for their providing of the GPS-ZTD data set. We also acknowledge Météo-France and the HyMeX program for supplying the Rain gauges and radiosonde data supported by grants MISTRALS/HyMeX and ANR-11-BS56-0005 IODA-MED. We would like to thank the German Weather Service (DWD) and the CLM-Community for their providing of the COSMO-CLM model, and especially Ulrich Schättler and Christoph Schraff for their support in carrying out the nudging experiments. We are also thankful to the European Centre for Medium-Range Weather Forecasts

(ECMWF) for their Integrated Forecasting System (IFS) analyses. We thank as well the teams of HYSPLIT at the NOAA Air Resources Laboratory, CMORPH at the Climate Prediction Center (CPC) and GLEAM for their data sets. We thank the reviewers for their fruitful comments. Finally, we would like to thank the hosting institution, the Karlsruhe Institute of Technology (KIT).

11. Financial support

This research work has been supported by the Bundesministerium für Bildung und Forschung (BMBF; German Federal Ministry of Education and Research) project PREMIUM 01LN1319A.

12. References

Adler, B., Kalthoff, N., Kohler, M., Handwerker, J., Wieser, A., Corsmeier, U., Kottmeier, C., Lambert, D., and Bock, O.: The variability of water vapour and pre-convective conditions over the mountainous island of Corsica, Quarterly Journal of the Royal Meteorological Society, 142, 335–346, https://doi.org/10.1002/qj.2545, 2015.

Ahrens, C. D. and Samson, P. J.: Extreme Weather and Climate, Cengage Learning, 2010.

Andersson, T., Andersson, M., Jacobsson, C., and Nilsson, S.: Thermodynamic indices for forecasting thunderstorms in southern Sweden, Meteorological Magazine, 118, 1989.

Bevis, M., Businger, S., Chiswell, S., Herring, T. A., Anthes, R. A., Rocken, C., and Ware, R. H.: GPS Meteorology: Mapping Zenith Wet Delays onto Precipitable Water, Journal of Applied Meteorology, 33, 379–386, https://doi.org/10.1175/1520-0450(1994)033<0379:gmmzwd>2.0.co;2, 1994.

Bitew, M. M. and Gebremichael, M.: Evaluation of satellite rainfall products through hydrologic simulation in a fully distributed hydrologic model, Water Resour. Res., 47, 45, https://doi.org/10.1029/2010WR009917, 2011.

Bock, O., Bosser, P., Pacione, R., Nuret, M., Fourrié, N., and Parracho, A.: A high-quality reprocessed ground-based GPS dataset for atmospheric process studies, radiosonde and model evaluation, and reanalysis of HyMeX Special Observing Period, Quarterly Journal of the Royal Meteorological Society, 142, 56–71, https://doi.org/10.1002/qj.2701, 2016.

Businger, S., Chiswell, S. R., Bevis, M., Duan, J., Anthes, R. A., Rocken, C., Ware, R. H., Exner, M., VanHove, T., and Solheim, F. S.: The Promise of GPS in Atmospheric Monitoring, Bulletin of the American Meteorological Society, 77, 5–18, https://doi.org/10.1175/1520-0477(1996)077<0005:tpogia>2.0.co;2, 1996.

Caldas-Alvarez. A.: Atmospheric Moisture Effects on Deep Convection in the Western Mediterranean, KIT Scientific Publishing, VI, 237, http://dx.doi.org/10.5445/KSP/1000097100, 2019.

Chan, S. C., Kendon, E. J., Fowler, H. J., Blenkinsop, S., Ferro, C. A. T., and Stephenson, D. B.: Does increasing the spatial resolution of a regional climate model improve the simulated daily precipitation?, Climate Dynamics, 41, 1475–1495, https://doi.org/10.1007/s00382-012-1568-9, 2012.

Chazette, P., Flamant, C., Shang, X., Totems, J., Raut, J.-C., Doerenbecher, A., Ducrocq, V., Fourrié, N., Bock, O., and Cloché, S.: A multi-instrument and multi-model assessment of atmospheric moisture variability over the western Mediterranean during HyMeX, Quarterly Journal of the Royal Meteorological Society, 142, 7–22, https://doi.org/10.1002/qj.2671, 2015.

Chazette, P., Flamant, C., Raut, J.-C., Totems, J., and Shang, X.: Tropical moisture enriched storm tracks over the Mediterranean and their link with intense rainfall in the Cevennes-Vivarais area during HyMeX, Quarterly Journal of the Royal Meteorological Society, 142, 320–334, https://doi.org/10.1002/qj.2674, 2015b.

Cress, A., Anlauf, H., Bitzer, H. W., Rhodin, A., Schraff, C., Helmert, K., and Stephan, K. (Eds.): Global and regional impact studies at the German Weather Service (DWD), Sedona (USA), 2012.

Di Girolamo, P., Flamant, C., Cacciani, M., Richard, E., Ducrocq, V., Summa, D., Stelitano, D., Fourrié, N., and Saïd, F.: Observation of low-level wind reversals in the Gulf of Lion area and their impact on the water vapour variability, Q.J.R. Meteorol. Soc., 142, 153–172, https://doi.org/10.1002/qj.2767, 2016.

Doms, G., Förstner, J., Heise, E., Herzog, H. -J., Mironov, D., Raschendorfer, M., Reinhardt, T., Ritter, B., Schrodin, R., Schulz, J. -P., and Vogel, G.: A Description of the Nonhydrostatic Regional COSMO Model Part II: Physical Parameterization, P.O. Box 100465, 63004, Offenbach, Germany, 2011.

Duan, J., Bevis, M., Fang, P., Bock, Y., Chiswell, S., Businger, S., Rocken, C., Solheim, F., van Hove, T., Ware, R., McClusky, S., Herring, T. A., and King, R. W.: GPS Meteorology: Direct Estimation of the Absolute Value of Precipitable Water, Journal of Applied Meteorology, 35, 830–838, https://doi.org/10.1175/1520-0450(1996)035<0830:gmdeot>2.0.co;2, 1996.

Ducrocq, V., Braud, I., Davolio, S., Ferretti, R., Flamant, C., Jansa, A., Kalthoff, N., Richard, E., Taupier-Letage, I., Ayral, P.-A., Belamari, S., Berne, A., Borga, M., Boudevillain, B., Bock, O., Boichard, J.-L., Bouin, M.-N., Bousquet, O., Bouvier, C., Chiggiato, J., Cimini, D., Corsmeier, U., Coppola, L., Cocquerez, P., Defer, E., Delanoë, J., Di Girolamo, P., Doerenbecher, A., Drobinski, P., Dufournet, Y., Fourrié, N., Gourley, J. J., Labatut, L., Lambert, D., Le Coz, J., Marzano, F. S., Molinié, G., Montani, A., Nord, G., Nuret, M., Ramage, K., Rison, W., Roussot, O., Said, F., Schwarzenboeck, A., Testor, P., van Baelen, J., Vincendon, B., Aran, M., and Tamayo, J.: HyMeX-SOP1: The Field Campaign Dedicated to Heavy Precipitation and Flash Flooding in the Northwestern Mediterranean, Bulletin of the American Meteorological Society, 95, 1083–1100, https://doi.org/10.1175/bams-d-12-00244.1, 2014.

Ducrocq, V., Davolio, S., Ferretti, R., Flamant, C., Santaner, V. H., Kalthoff, N., Richard, E., and Wernli, H.: Introduction to the HyMeX Special Issue on 'Advances in understanding and forecasting of heavy precipitation in the Mediterranean

through the HyMeX SOP1 field campaign', Quarterly Journal of the Royal Meteorological Society, 142, 1–6, https://doi.org/10.1002/qj.2856, 2016.

Duffourg, F. and Ducrocq, V.: Origin of the moisture feeding the Heavy Precipitating Systems over Southeastern France, Natural Hazards and Earth System Science, 11, 1163–1178, https://doi.org/10.5194/nhess-11-1163-2011, 2011.

Duffourg, F., Nuissier, O., Ducrocq, V., Flamant, C., Chazette, P., Delanoë, J., Doerenbecher, A., Fourrié, N., Di Girolamo, P., Lac, C., Legain, D., Martinet, M., Saïd, F., and Bock, O.: Offshore deep convection initiation and maintenance during the HyMeX IOP 16a heavy precipitation event, Quarterly Journal of the Royal Meteorological Society, 142, 259–274, https://doi.org/10.1002/qj.2725, 2016.

Fosser, G., Khodayar, S., and Berg, P.: Climate change in the next 30 years: What can a convection-permitting model tell us that we did not already know?, Climate Dynamics, 48, 1987–2003, https://doi.org/10.1007/s00382-016-3186-4, 2016.

Funatsu, B. M., Rysman, J.-F., Claud, C., and Chaboureau, J.-P.: Deep convective clouds distribution over the Mediterranean region from AMSU-B/MHS observations, Atmospheric Research, 207, 122–135, https://doi.org/10.1016/j.atmosres.2018.03.003, 2018.

~~Garratt, J. R.: The Atmospheric Boundary Layer, Cambridge atmospheric and space science series, Cambridge University Press, 1994.~~

Gilabert, J. and Llasat, M. 4C.: Circulation weather types associated with extreme flood events in Northwestern Mediterranean, International Journal of Climatology, 38, 1864–1876, https://doi.org/10.1002/joc.5301, 2017.

González-Zamora, Á., Sánchez, N., Martández, J., Gumuzzio, Á., Piles, M.ggg, and Olmedo, E.: Long-term SMOS soil moisture products: A comprehensive evaluation across scales and methods in the Duero Basin (Spain), Physics and Chemistry of the Earth, Parts A/B/C, 83-84, 123–136, https://doi.org/10.1016/j.pce.2015.05.009, 2015.

Guerova, G., Jones, J., Douša, J., Dick, G., Haan, S. d., Pottiaux, E., Bock, O., Pacione, R., Elgered, G., Vedel, H., and Bender, M.: Review of the state of the art and future prospects of the ground-based GNSS meteorology in Europe, Atmospheric Measurement Techniques, 9, 5385–5406, https://doi.org/10.5194/amt-9-5385-2016, 2016.

Habib, E., Haile, A. T., Tian, Y., and Joyce, R. J.: Evaluation of the High-Resolution CMORPH Satellite Rainfall Product Using Dense Rain Gauge Observations and Radar-Based Estimates, J. Hydrometeor., 13, 1784–1798, https://doi.org/10.1175/JHM-D-12-017.1, 2012.

Honda, T. and Kawano, T.: How does mid-tropospheric dry air affect the evolution of supercellular convection?, Atmospheric Research, 157, 1–16, https://doi.org/10.1016/j.atmosres.2015.01.015, 2015.

Jansa, A., Genoves, A., Picornell, M. A., Campins, J., Riosalido, R., and Carretero, O.: Western Mediterranean cyclones and heavy rain. Part 2: Statistical approach, Meteorological Applications, 8, 43–56, https://doi.org/10.1017/s1350482701001049, 2001.

Joyce, R. J., Janowiak, J. E., Arkin, P. A., and Xie, P.: CMORPH: A Method that Produces Global Precipitation Estimates from Passive Microwave and Infrared Data at High Spatial and Temporal Resolution, Journal of Hydrometeorology, 5, 487–503, https://doi.org/10.1175/1525-7541(2004)005<0487:camtpg>2.0.co;2, 2004.

Keil, C., Röpnack, A., Craig, G. C., and Schumann, U.: Sensitivity of quantitative precipitation forecast to height dependent changes in humidity, Geophysical Research Letters, 35, https://doi.org/10.1029/2008gl033657, 2008.

~~Khodayar, S., Czajka, B., Caldas-Alvarez, A., Helgert, S., Flamant, C., Di Girolamo, P., Bock, O., and Chazette, P.: Multi-scale observations of atmospheric moisture variability in relation to heavy precipitating systems in the northwestern Mediterranean during HyMeX IOP12, Quarterly Journal of the Royal Meteorological Society, 144, 2761–2780, https://doi.org/10.1002/qj.3402, 2018.~~

Khodayar, S., Fosser, G., Berthou, S., Davolio, S., Drobinski, P., Ducrocq, V., Ferretti, R., Nuret, M., Pichelli, E., Richard, E., and Bock, O.: A seamless weather-climate multi-model intercomparison on the representation of a high impact weather event in the western Mediterranean: HyMeX IOP12, Q.J.R. Meteorol. Soc., 142, 433–452, https://doi.org/10.1002/qj.2700, 2016.

Khodayar, S., Kalthoff, N., and Kottmeier, C.: Atmospheric conditions associated with heavy precipitation events in comparison to seasonal means in the western mediterranean region, Climate Dynamics, 51, 951–967, https://doi.org/10.1007/s00382-016-3058-y, 2016.

Krichak, S. O., Barkan, J., Breitgand, J. S., Gualdi, S., and Feldstein, S. B.: The role of the export of tropical moisture into midlatitudes for extreme precipitation events in the Mediterranean region, Theoretical and Applied Climatology, 121, 499–515, https://doi.org/10.1007/s00704-014-1244-6, 2014.

Lamb, P. J. and Ports, D. H.: Investigation of Large-Scale Atmospheric Moisture Budget and Land Surface Interactions over U. S. Southern Great Plains including for CLASIC (June 2007), Journal of Hydro Meteorology, https://doi.org/10.1175/JHM-D-12-01.1, 2012.

Lee, K.-O., Flamant, C., Duffourg, F., Ducrocq, V., and Chaboureau, J.-P.: Impact of upstream moisture structure on a back-building convective precipitation system in south-eastern France during HyMeX IOP13, Atmospheric Chemistry and Physics, 18, 16845–16862, https://doi.org/10.5194/acp-18-16845-2018, 2018.

Leuenberger, D., Stoll, M., and Roches, A.: Description of some convective indices implemented in the COSMO model, Deutscher Wetterdienst (DWD), http://www.cosmo-model.org/content/model/documentation/techReports/docs/techReport17.pdf, last access: 22 July 2019, 2010.

Llasat, M. C., Llasat-Botija, M., Prat, M. A., Porcú, F., Price, C., Mugnai, A., Lagouvardos, K., Kotroni, V., Katsanos, D., Michaelides, S., Yair, Y., Savvidou, K., and Nicolaides, K.: High-impact floods and flash floods in Mediterranean countries: The FLASH preliminary database, Advances in Geosciences, 23, 47–55, https://doi.org/10.5194/adgeo-23-47-2010, 2010.

Maranan, M., Fink, A. H., Knippertz, P., Francis, S. D., Akpo, A. B., Jegede, G., and Yorke, C.: Interactions between Convection and a Moist Vortex Associated with an Extreme Rainfall Event over Southern West Africa, Mon. Wea. Rev., 147, 2309–2328, https://doi.org/10.1175/MWR-D-18-0396.1, 2019.

Martens, B., Miralles, D. G., Lievens, H., van der Schalie, R., Jeu, R. A. M. d., Fernández-Prieto, D., Beck, H. E., Dorigo, W. A., and Verhoest, N. E. C.: GLEAM v3: Satellite-based land evaporation and root-zone soil moisture, Geoscientific Model Development, 10, 1903–1925, https://doi.org/10.5194/gmd-10-1903-2017, 2017.

Martinet, M., Nuissier, O., Duffourg, F., Ducrocq, V., and Ricard, D.: Fine-scale numerical analysis of the sensitivity of the HyMeX IOP16a heavy precipitating event to the turbulent mixing-length parametrization, Quarterly Journal of the Royal Meteorological Society, 143, 3122–3135, https://doi.org/10.1002/qj.3167, 2017.

Miralles, D. G., Holmes, T. R. H., Jeu, R. A. M. de, Gash, J. H., Meesters, A. G. C. A., and Dolman, A. J.: Global land-surface evaporation estimated from satellite-based observations, Hydrol. Earth Syst. Sci., 15, 453–469, https://doi.org/10.5194/hess-15-453-2011, 2011.

~~Nuissier, O., Joly, B., Joly, A., Ducrocq, V., and Arbogast, P.: A statistical downscaling to identify the large-scale circulation patterns associated with heavy precipitation events over southern France, Quarterly Journal of the Royal Meteorological Society, 137, 1812–1827, https://doi.org/10.1002/qj.866, 2011.~~

Nuret, M.: HyMeX domain precipitation amount, SEDOO OMP. Doi: 10.6096/mistrals-hymex. 904, 2013.

Pantillon, F., Chaboureau, J. P. and Richard, E.: Remote impact of North Atlantic hurricanes on the Mediterranean during episodes of intense rainfall in autumn 2012, Q. J. R. Meteorol. Soc., 141, 967-978, https://doi.org/10.1002/qj.2419, 2015.

Peixoto, J. P. and Oort, A. H.: Physics of Climate. American Inst. Of Physics, 1992.

Pinto, J. G., Ulbrich, S., Parodi, A., Rudari, R., Boni, G., and Ulbrich, U.: Identification and ranking of extraordinary rainfall events over Northwest Italy: The role of Atlantic moisture, Journal of Geophysical Research: Atmospheres, 118, 2085–2097, https://doi.org/10.1002/jgrd.50179, 2013.

Röhner, L, Nerding, K. U. and Corsmeier, U.: Diagnostic Study of a Heavy Precipitation Event over Spain by investigation of moisture trajectories. Q. J. R. Meteorol. Soc., 142, 287-297, https://doi.org/10.1002/qj.2825, 2016.

Ricard, D., Ducrocq, V., and Auger, L.: A Climatology of the Mesoscale Environment Associated with Heavily Precipitating Events over a Northwestern Mediterranean Area, Journal of Applied Meteorology and Climatology, 51, 468–488, https://doi.org/10.1175/jamc-d-11-017.1, 2012.

Ritter, B. and Geleyn, J.-F.: A Comprehensive Radiation Scheme for Numerical Weather Prediction Models with Potential Applications in Climate Simulations, Monthly Weather Review, 120, 303–325, https://doi.org/10.1175/1520-0493(1992)120<0303:acrsfn>2.0.co;2, 1992.

Rolph, G., Stein, A., and Stunder, B.: Real-time Environmental Applications and Display sYstem: READY, Environmental Modelling & Software, 95, 210–228, https://doi.org/10.1016/j.envsoft.2017.06.025, 2017.

Sapiano, M. R. P. and Arkin, P. A.: An Intercomparison and Validation of High-Resolution Satellite Precipitation Estimates with 3-Hourly Gauge Data, J. Hydrometeor, 10, 149–166, https://doi.org/10.1175/2008JHM1052.1, 2009.

Schättler, U., Doms, G., and Schraff, C.: A Description of the Nonhydrostatic Regional COSMO-Model Part VII: User's Guide, DeutscherWetterdienst, P.O. Box 100465, 63004 Offenbach, Germany, 2016.

Schiro, K. A. and Neelin, J. D.: Deep Convective Organization, Moisture Vertical Structure, and Convective Transition Using Deep-Inflow Mixing, Journal of the Atmospheric Sciences, 76, 965–987, https://doi.org/10.1175/jas-d-18-0122.1, 2019.

Schneider, M., Romero, P. M., Hase, F., Blumenstock, T., Cuevas, E., Ramos, R.: Continuous quality assessment of atmospheric water vapor measurement techniques: FTIR, Cimel, MFSR, GPS, and Vaisala RS92, Atmos. Meas. Tech., 3, 323-338, https://doi.org/10.5194/amt-3-323-2010, 2010.

Schraff, C. and Hess, R.: A Description of the Nonhydrostatic Regional COSMO-Model Part III: Data Assimilation, DeutscherWetterdienst, P.O. Box 100465, 63004 Offenbach, Germany, 2012.

Schraff, C., Reich, H., Rhodin, A., Schomburg, A., Stephan, K., Periáñez, A., and Potthast, R.: Kilometre-scale ensemble data assimilation for the COSMO model (KENDA), Quarterly Journal of the Royal Meteorological Society, 142, 1453–1472, https://doi.org/10.1002/qj.2748, 2016.

Sherwood, S. C., Roca, R., Weckwerth, T. M., and Andronova, N. G.: Tropospheric water vapor, convection, and climate, Reviews of Geophysics, 48, https://doi.org/10.1029/2009rg000301, 2010.

Stein, A. F., Draxler, R. R., Rolph, G. D., Stunder, B. J. B., Cohen, M. D., and Ngan, F.: NOAA's HYSPLIT Atmospheric Transport and Dispersion Modeling System, Bull. Amer. Meteor. Soc., 96, 2059–2077, https://doi.org/10.1175/BAMS-D-14-00110.1, 2015.

Steinke, S., Eikenberg, S., Löhnert, U., Dick, G., Klocke, D., Di Girolamo, P., and Crewell, S.: Assessment of small-scale integrated water vapour variability during HOPE, Atmos. Chem. Phys., 15, 2675–2692, https://doi.org/10.5194/acp-15-2675-2015, 2015.

Stevens, B.: Atmospheric Moist Convection, Annual Review of Earth and Planetary Sciences, 33, 605–643, https://doi.org/10.1146/annurev.earth.33.092203.122658, 2005.

Thévenot, O., Bouin, M. -N., Ducrocq, V., Brossier, C. L., Nuissier, O., Pianezze, J., and Duffourg, F.: Influence of the sea state on Mediterranean heavy precipitation: A case-study from HyMeX SOP1, Quarterly Journal of the Royal Meteorological Society, 142, 377–389, https://doi.org/10.1002/qj.2660, 2015.

Tiedtke, M.: A Comprehensive Mass Flux Scheme for Cumulus Parameterization in Large-Scale Models, Monthly Weather Review, 117, 1779–1800, https://doi.org/10.1175/1520-0493(1989)117<1779:acmfsf>2.0.co;2, 1989.

~~Toreti, A., Xoplaki, E., Maraun, D., Kuglitsch, F. G., Wanner, H., and Luterbacher, J.: Characterisation of extreme winter precipitation in Mediterranean coastal sites and associated anomalous atmospheric circulation patterns, Natural Hazards and Earth System Science, 10, 1037–1050, https://doi.org/10.5194/nhess-10-1037-2010, 2010.~~

Virman, M., Bister, M., Sinclair, V. A., Järvinen, H., and Räisänen, J.: A New Mechanism for the Dependence of Tropical Convection on Free-Tropospheric Humidity, Geophysical Research Letters, 45, 2516–2523, https://doi.org/10.1002/2018gl077032, 2018.

Wicker, L. J. and Skamarock, W. C.: Time-Splitting Methods for Elastic Models Using Forward Time Schemes, Monthly Weather Review, 130, 2088–2097, https://doi.org/10.1175/1520-0493(2002)130<2088:tsmfem>2.0.co;2, 2002.

Winschall, A., Sodemann, H., Pfahl, S., and Wernli, H.: How important is intensified evaporation for Mediterranean precipitation extremes?, Journal of Geophysical Research: Atmospheres, 119, 5240–5256, https://doi.org/10.1002/2013jd021175, 2014.

Wulfmeyer, V., Hardesty, R. M., Turner, D. D., Behrendt, A., Cadeddu, M. P., Di Girolamo, P., Schlüssel, P., van Baelen, J., and Zus, F.: A review of the remote sensing of lower tropospheric thermodynamic profiles and its indispensable role for the understanding and the simulation of water and energy cycles, Reviews of Geophysics, 53, 819–895, https://doi.org/10.1002/2014rg000476, 2015.

Xoplaki, E., Trigo, R. M., Garcández, R., Kuglitsch, F. G., Mariotti, A., Nieto, R., Pinto, J. G., Pozo-Vázquez, D., Saaroni, H., Toreti, A., Trigo, I. F., Vicente-Serrano, S. M., Yiou, P., and Ziv, B.: Large-Scale Atmospheric Circulation Driving Extreme Climate Events in the Mediterranean and its Related Impacts, in: The Climate of the Mediterranean Region, Elsevier, 347–417, https://doi.org/10.1016/b978-0-12-416042-2.00006-9, 2012.

~~Zhuang, Y., Fu, R., and Wang, H.: How Do Environmental Conditions Influence Vertical Buoyancy Structure and Shallow-to-Deep Convection Transition across Different Climate Regimes?, J. Atmos. Sci., 75, 1909–1932, https://doi.org/10.1175/JAS-D-17-0284.1, 2018.~~

Table 1. Mean Absolute Error (MAE), Agreement Index (AI), and Mean Bias (MB) of IWV between the model and the observations. The selected observations are all radiosondes available in the period 26-Oct 0000 UTC to 28-OCT 0000 UTC at the 7 stations within the 2.8 km simulation domain (see red box in Fig. 1). All model values have been interpolated to the location of the radiosonde station from the nearest neighbours. The difference between model and station height never exceeded 30 m.

Rads vs. COSMO-CLM (IWV)	MAE [mm]	AI	MB [mm]
CTRL-7	2.7	0.88	0.61
NDG-7	2	0.93	-0.04
CTRL-2.8	2.7	0.89	0.38
NDG-2.8	2	0.92	-0.08

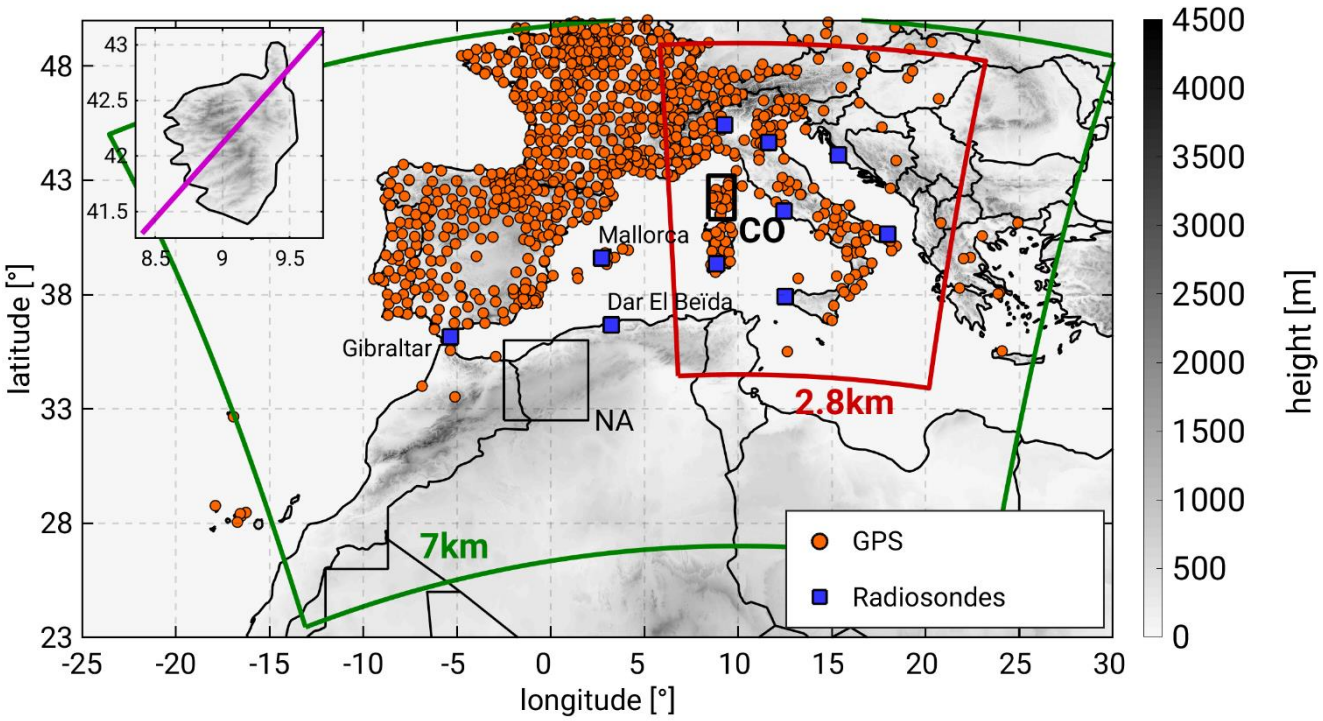

Figure 1: Simulation domains for the CTRL-7 and NDG-7 runs (green line) and for the CTRL-2.8 and NDG-2.8 (red line). The investigation area ~~Corsica (~~CO~~)~~ is depicted by the thick lined black box. The box over North Africa (NA) denotes the region of intense evapotranspiration between 20-Oct and 27-Oct (see Sect. 4.1). The orange scatter points show the location of the GPS receivers used for nudging and the blue squares the location of the radiosondes used for validation and process-understanding. The upper left corner shows a detail of the orography over CO with a purple transect used for representation of the humidity vertical distribution in Fig. 5.

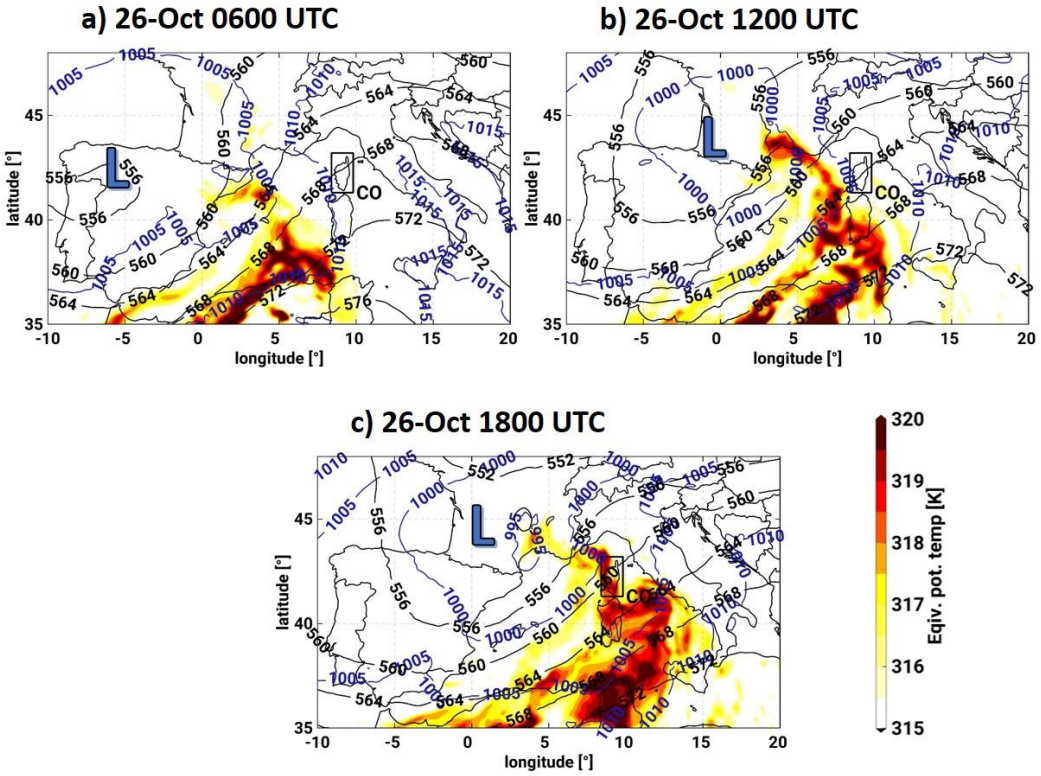

Figure 2. CTRL-7 simulation of 500 hPa geopotential height in black isolines (gpdam), mean sea-level pressure in blue isolines (hPa) and equivalent potential temperature at 850 hPa in colour scale (K) on the 26-Oct-2012 at 0600 UTC (a), 1200 UTC (b) and 1800 UTC (c).

1025

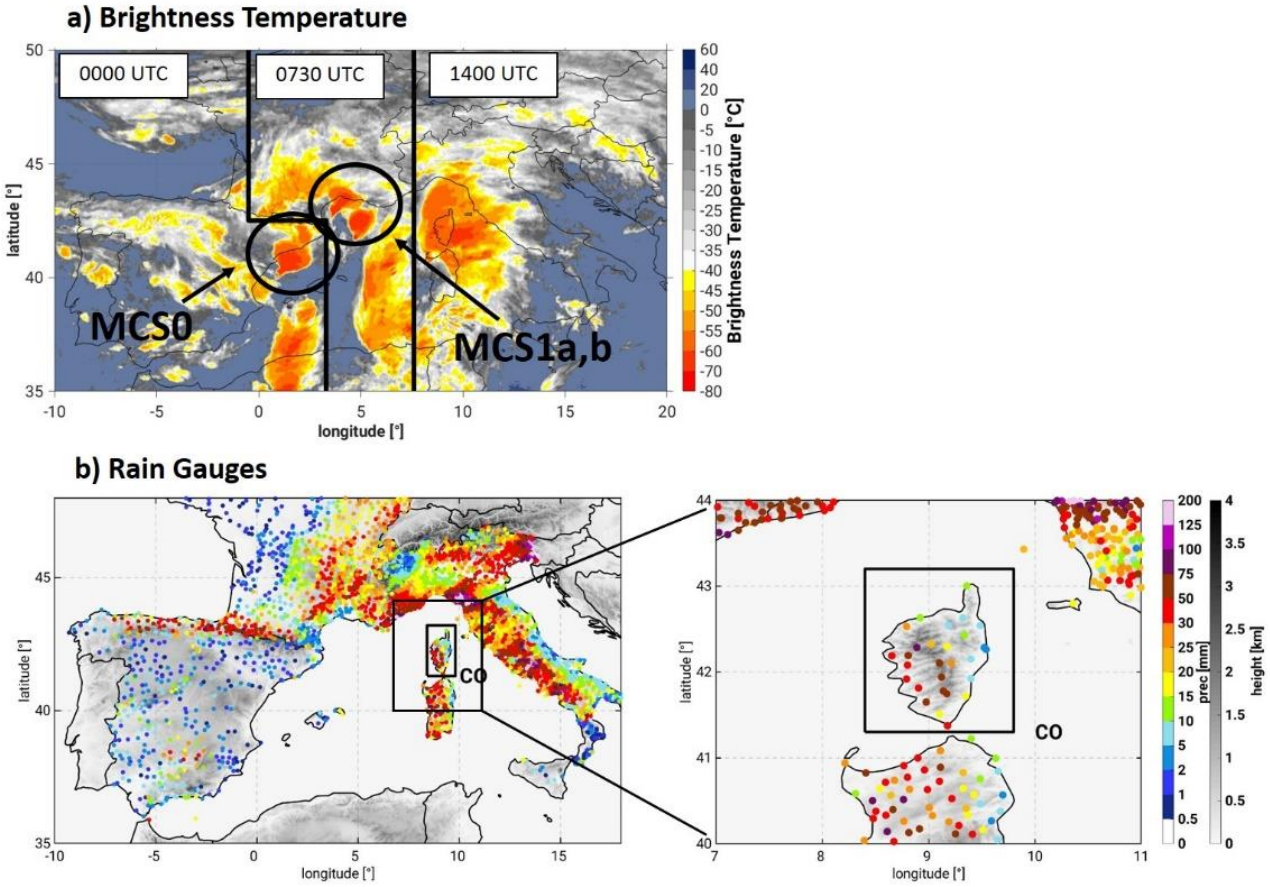

Figure 3. Composite image of brightness temperature as measured by the SEVIRI instrument~~satellite~~ on the 26-Oct-2012, at 0000 UTC, at 0730 UTC and at 1400 UTC (a). Rain gauge accumulated precipitation over the complete ~~Western Mediterranean (~~WMed~~)~~ region between 26-Oct 1300 UTC and 27-Oct 1500 UTC and zoomed over the study region of Corsica (b). The accumulation period shown is the period of heavy precipitation over our main study region, the island of Corsica (black box), during this event.

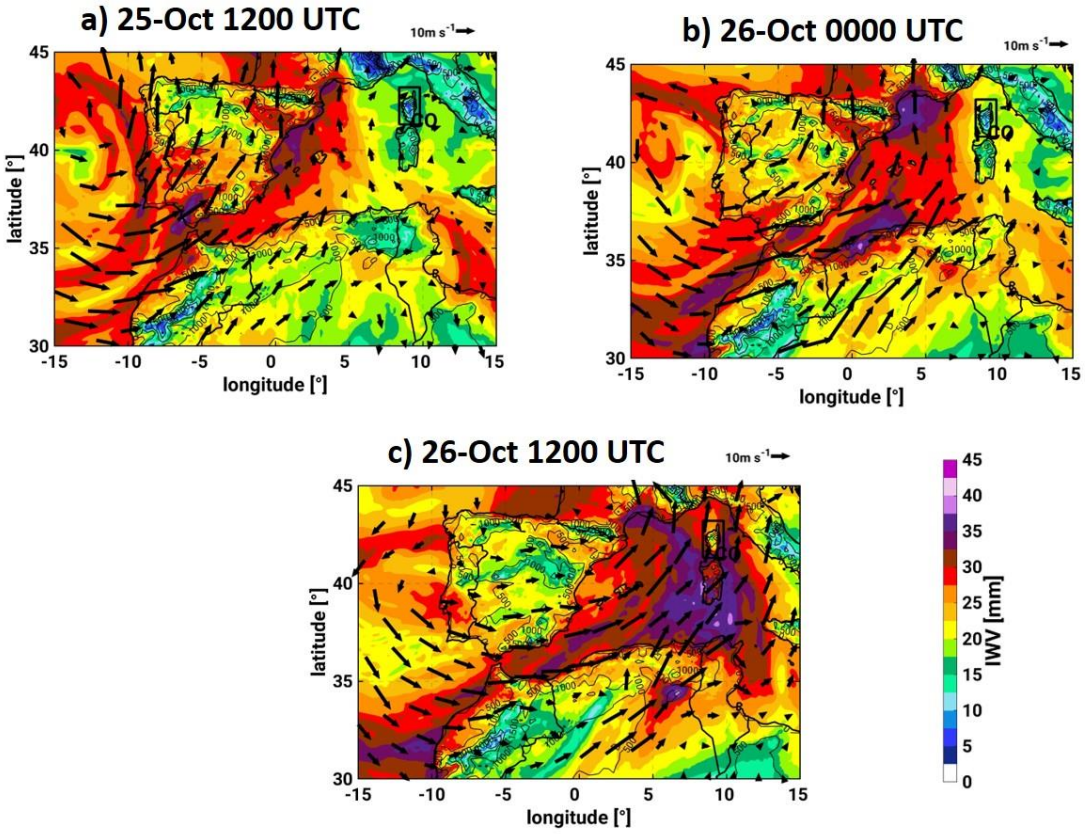

Figure 4. Spatial ~~d~~Distribution of ~~Integrated Water Vapour (~~IWV~~)~~ and winds at 850 hPa as represented by CTRL-7 on the 25-Oct-2012 at 1200UTC (a), 26-Oct 0000UTC (b) and on the 26-Oct-2012 at 1200UTC (c).

1035

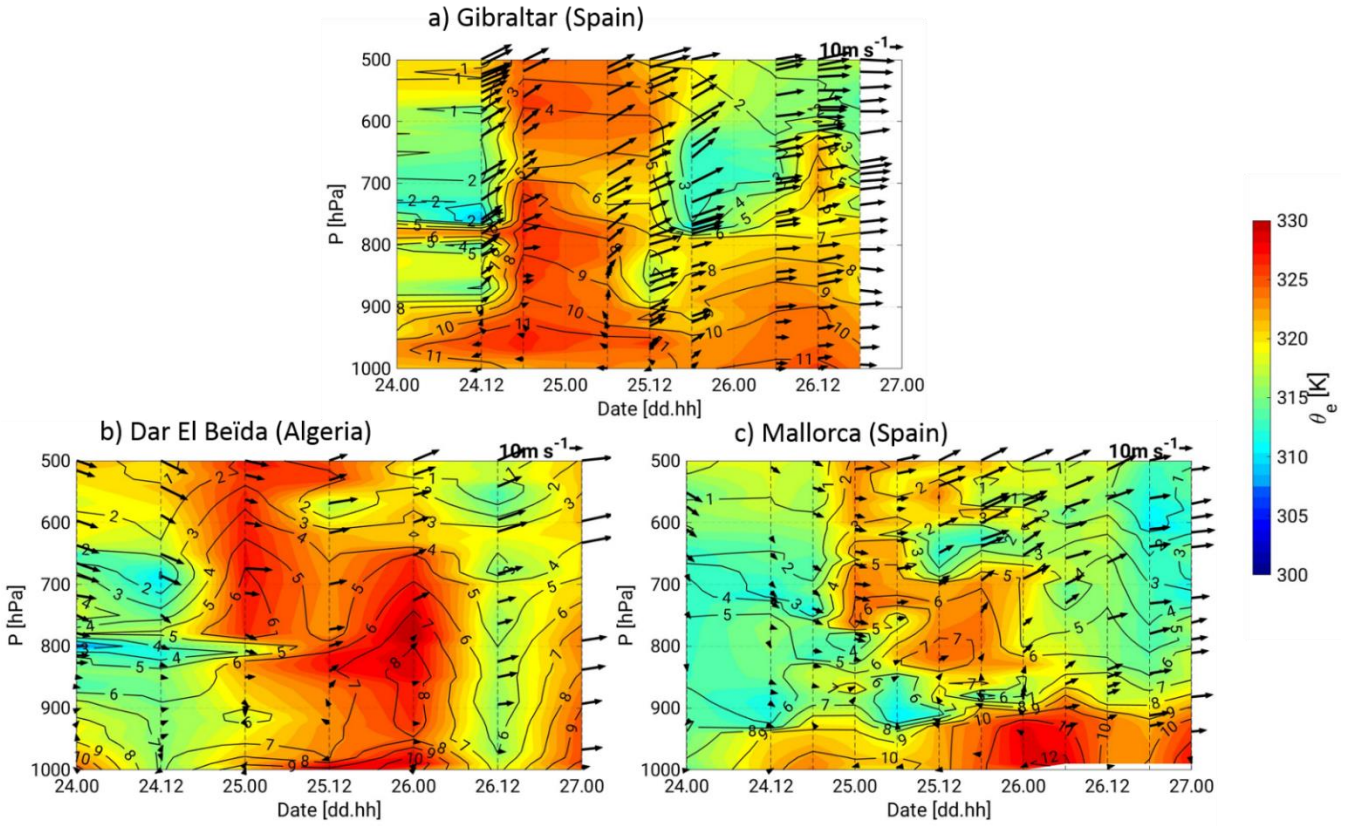

Figure 5. Height-time cross-sections at Gibraltar (a), Dar el Beïda (b) and Mallorca (c) between 24-Oct 0000UTC and 27-Oct 0000UTC. The colour shading stands for Equivalent Potential Temperature (θ_e), the contours denote specific humidity and the arrows show the direction and speed of horizontal wind at the stations. The location of the radiosondes can be seen in Fig. 1.

1040

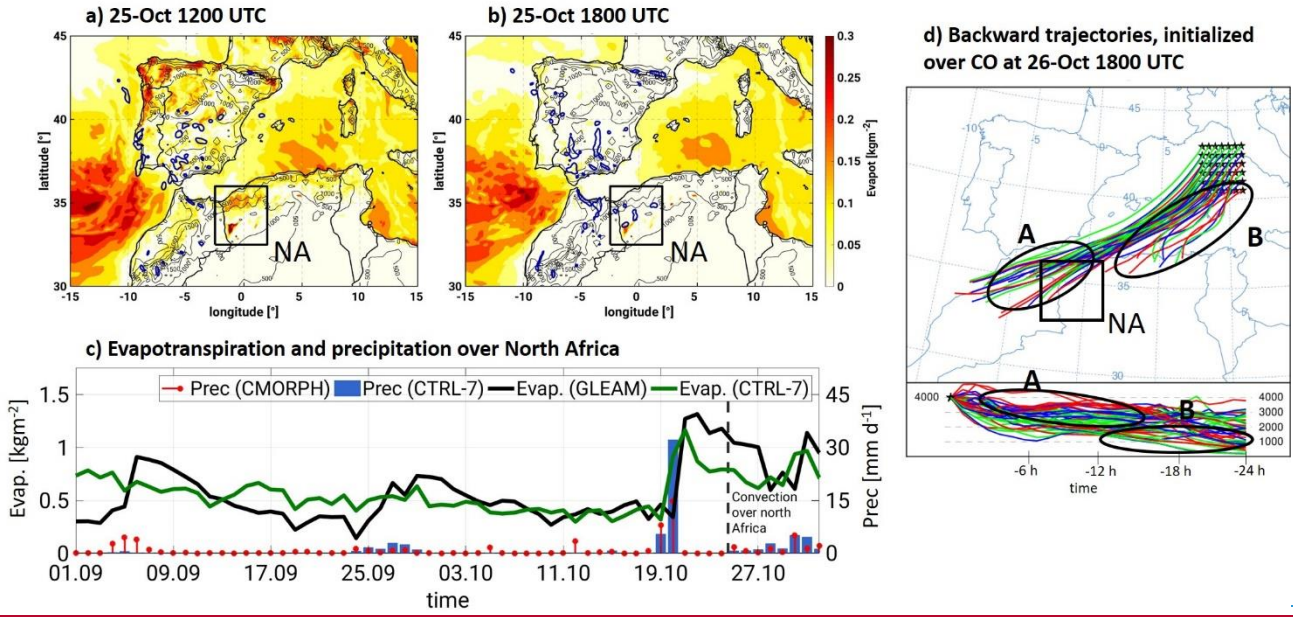
a) 25-Oct 1200 UTC
b) 25-Oct 1800 UTC
d) Backward trajectories, initialized over CO at 26-Oct 1800 UTC
latitude [°]
longitude [°]
Evapot [kgm-2]
NA
A
B
time
-6 h
-12 h
-18 h
-24 h
c) Evapotranspiration and precipitation over North Africa
Prec (CMORPH)
Prec (CTRL-7)
Evap. (GLEAM)
Evap. (CTRL-7)
Evap. [kgm-2]
Prec [mm d-1]
Convection over north Africa
01.09
09.09
17.09
25.09
03.10
11.10
19.10
27.10
time

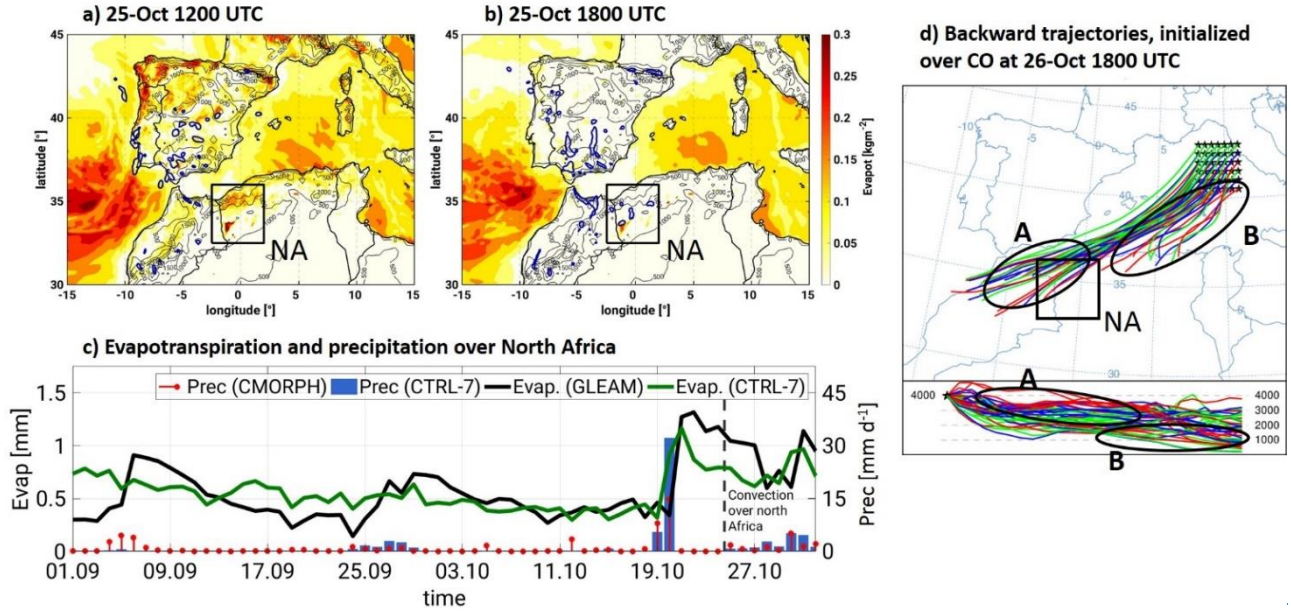
a) 25-Oct 1200 UTC
b) 25-Oct 1800 UTC
d) Backward trajectories, initialized over CO at 26-Oct 1800 UTC
latitude [°]
longitude [°]
Evapot [kgm-2]
NA
A
B
c) Evapotranspiration and precipitation over North Africa
Prec (CMORPH)
Prec (CTRL-7)
Evap. (GLEAM)
Evap. (CTRL-7)
Evap [mm]
Prec [mm d-1]
Convection over north Africa
01.09
09.09
17.09
25.09
03.10
11.10
19.10
27.10
time

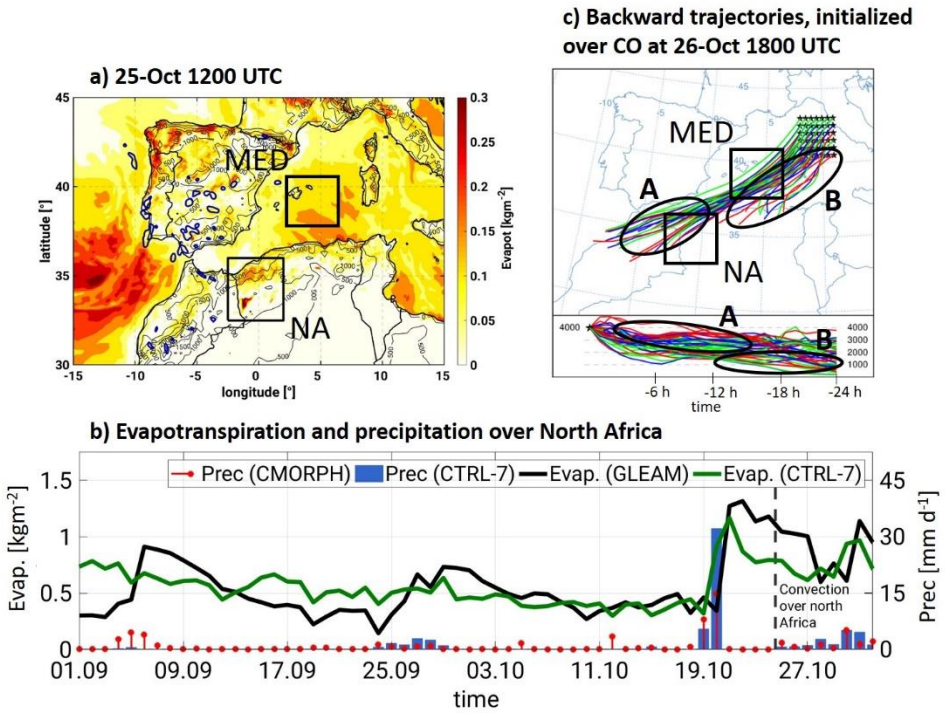

Figure 6. Spatial distribution of evapotranspiration (colour shading) and vertical updrafts with vertical wind speeds larger than 0.25 m~~/s~~$^{-1}$ (blue contours) simulated with CTRL-7 on the 25-Oct at ~~(a)~~ 1200UTC (a)~~and at (b) 1800UTC~~. The black box~~es~~ denote~~s~~ the region~~s~~ of intense evaporation ~~between 20-Oct and 27-Oct~~. (~~c~~b) Spatially averaged daily evapotranspiration (GLEAM and CTRL-7) and daily precipitation (CMORPH and CTRL-7) over north Africa (black box) between 01-Sep-2012 and 02-Nov-2012. The CTRL-7 precipitation has been upscaled to the coarser grid of CMORPH (0.0727°). Likewise, CTRL-7 evapotranspiration has been upscaled to the coarser grid of GLEAM of 0.25 °. (~~d~~c) Lagrangian backward trajectories obtained with the HYSPLIT model, starting on the 26-Oct-2012 1800 UTC (initiation of the event over Corsica) back to for 24 h.

a)

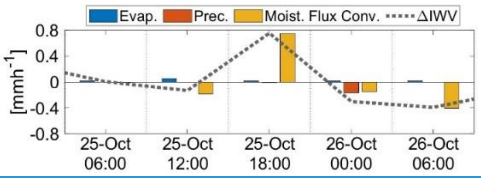

b)

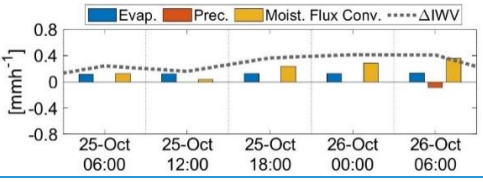

Figure 7. Temporal evolution of the moisture budget terms, variation of IWV (ΔIWV), Moisture Flux Convergence, Evapotranspiration and Precipitation. Hourly values are given. The spatial averages are performed over the investigation areas NA (a) and MED (b). The values are obtained from CTRL-7.

1055

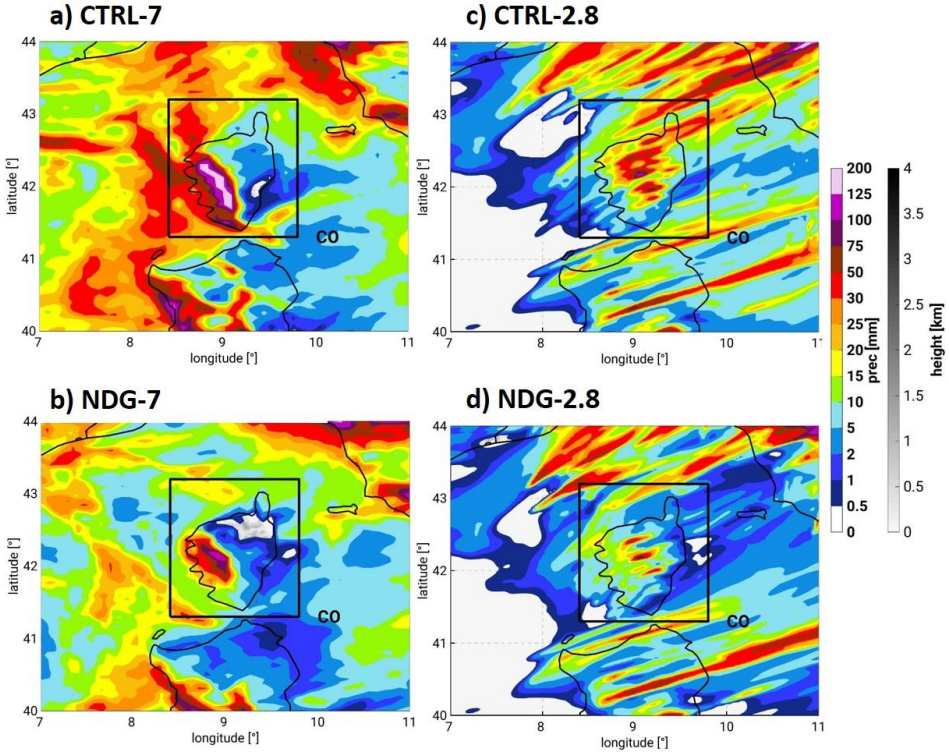

Figure 87. COSMO-CLM accumulated precipitation over Corsica between 26-Oct 1300 UTC and 27-Oct 1500 UTC i.e. during the period of precipitation over the island.

Table 2. Model precipitation validation against Rain Gauges (RG). COSMO-CLM has been interpolated to the location of the RG for the first three metrics Root Mean Square Error (RMSE), hourly standard deviation difference ($OBS_\sigma - MOD_\sigma$) and spatially averaged differences ($\overline{OBS} - \overline{MOD}$). On the contrary, all precipitation values simulated by COSMO-CLM over the island of Corsica are used in the last two metrics, standard deviation difference ($OBS_\sigma - MOD_\sigma$) and difference of maximum precipitation ($OBS_{max} - MOD_{max}$). The temporal resolution of each metric is given in brackets. The description of the validation metrics can be found in the Annex.

[mm]	Interp. To RG location			Distributions without interpolation	
	RMSE (1h)	$OBS_\sigma - MOD_\sigma$ (1h)	$\overline{OBS} - \overline{MOD}$ (27h)	$OBS_\sigma - MOD_\sigma$ (27h)	$OBS_{max} - MOD_{max}$ (27h)
CTRL-7-Init1Sep	3.1	-0.35	-10.4	-~~56~~32	-185
NDG-7- Init1Sep	2.6	1.07	15.4	-0.7	-58
CTRL-2.8-Init1Sep	3.1	0.55	14.6	6	-3
NDG-2.8-Init1Sep	2.7	1.03	21.5	12	11

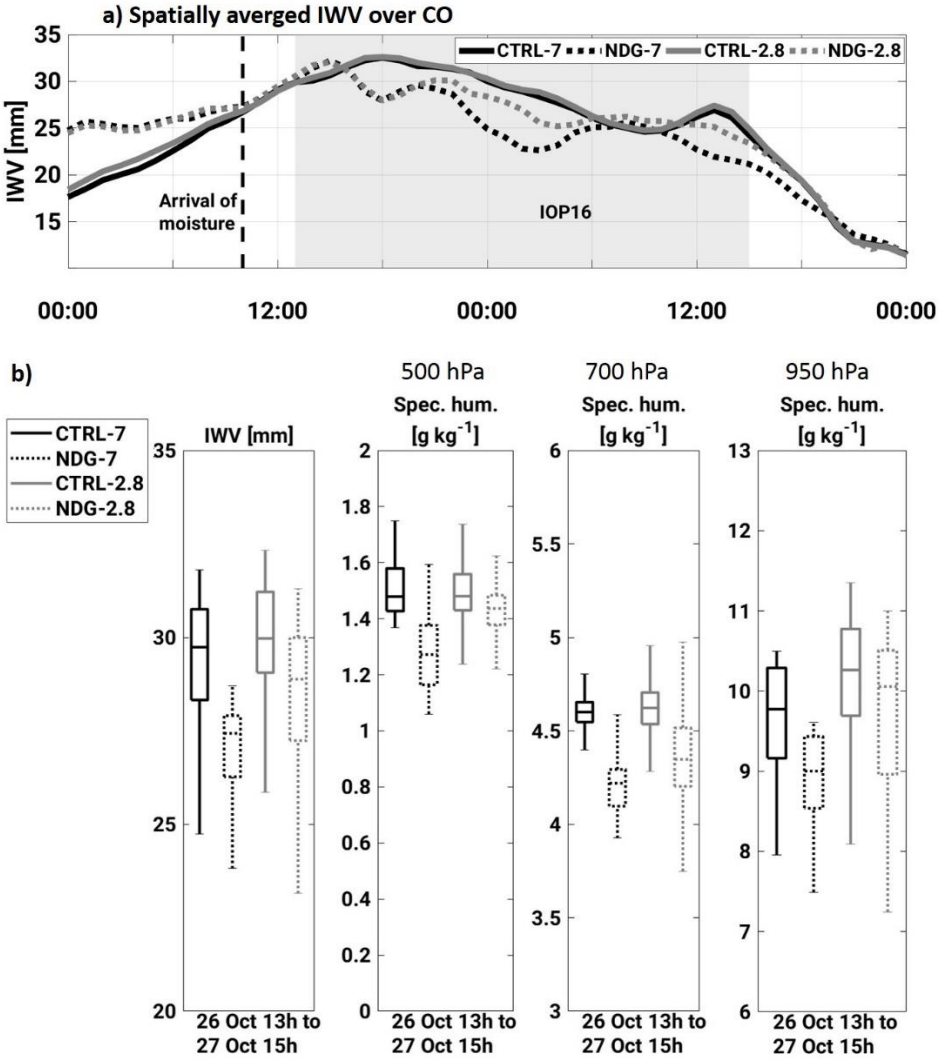
a) Spatially averged IWV over CO
CTRL-7
NDG-7
CTRL-2.8
NDG-2.8
IWV [mm]
Arrival of moisture
IOP16
00:00
12:00
00:00
12:00
00:00
b)
500 hPa
700 hPa
950 hPa
IWV [mm]
Spec. hum. [g kg-1]
26 Oct 13h to 27 Oct 15h

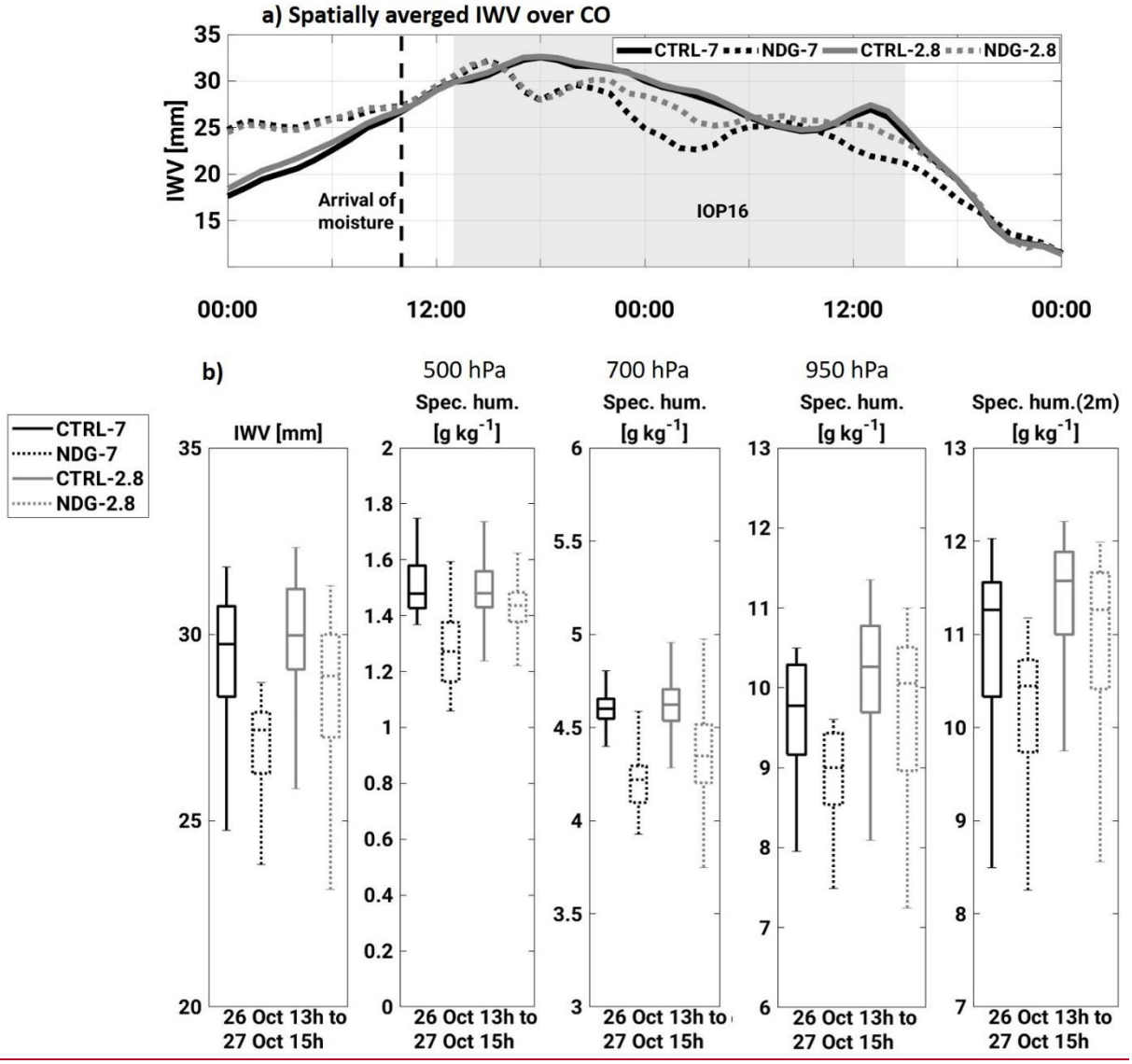

Figure 98. Spatially averaged IWV for all simulations during the event. The area for averaging is shown in Fig. 1 (CO) and the model output has been upscaled to a common coarser grid. The period shown is 26-Oct 0000 UTC to 28-Oct 0000 UTC. (b) Box and whiskers plots showing the median, the percentiles 25 and 75 and the extreme values of IWV and specific humidity at 500 hPa, 700 hPa, ~~and~~ 950 hPa and at 2m height. All box and whiskers are obtained from the distribution of values for the shown quantities between the 26-Oct 1300 UTC and 27-Oct 1500 UTC over the study region CO.

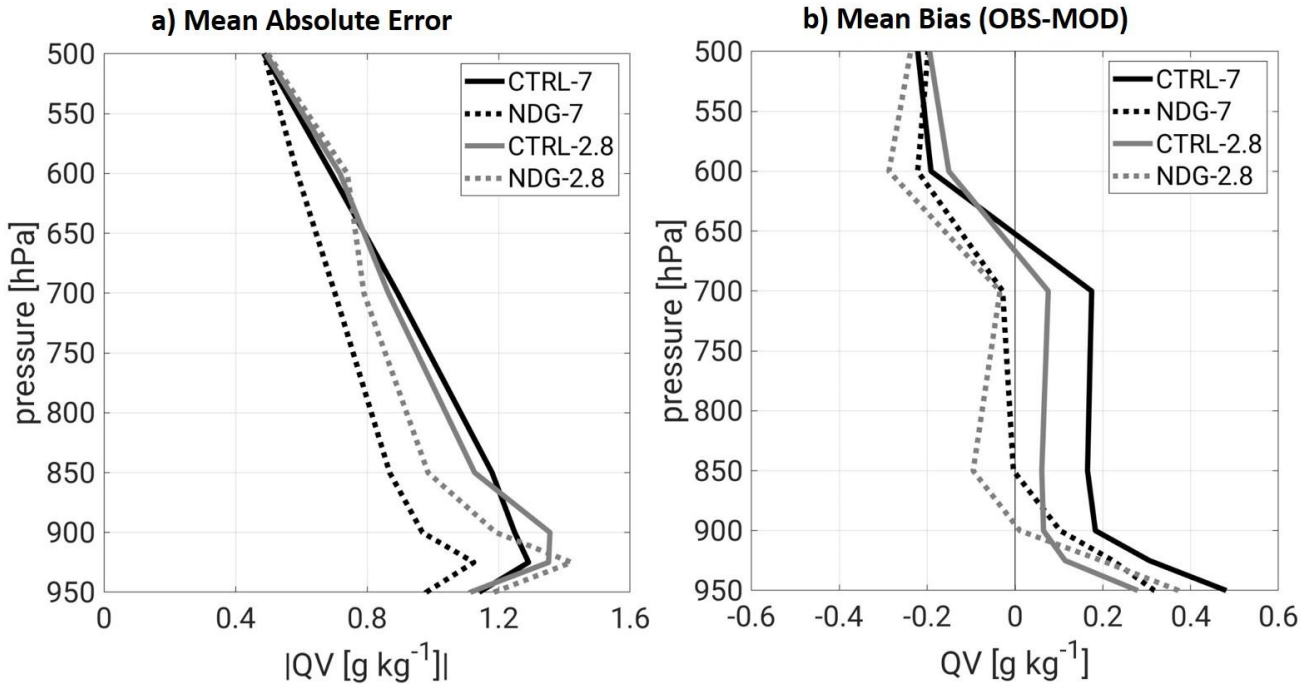

Figure 109. Validation of the model representation of the vertical distribution of specific humidity quantified by the Mean Absolute Error (a) and the Mean Bias as the OBS-MOD (b). All model values are validated against the radiosondes available in the period 26-Oct 0000 UTC to 28-OCT 0000 UTC at the 7 stations within the 2.8 km simulation domain (see red box in Fig. 1). All model values have been interpolated to the location of the radiosonde station from the nearest neighbours and the vertical specific humidity values have been interpolated to eleven pressure levels between 950 and 500 hPa. No values are shown below 950 hPa given the lack of available data for several stations below this level.

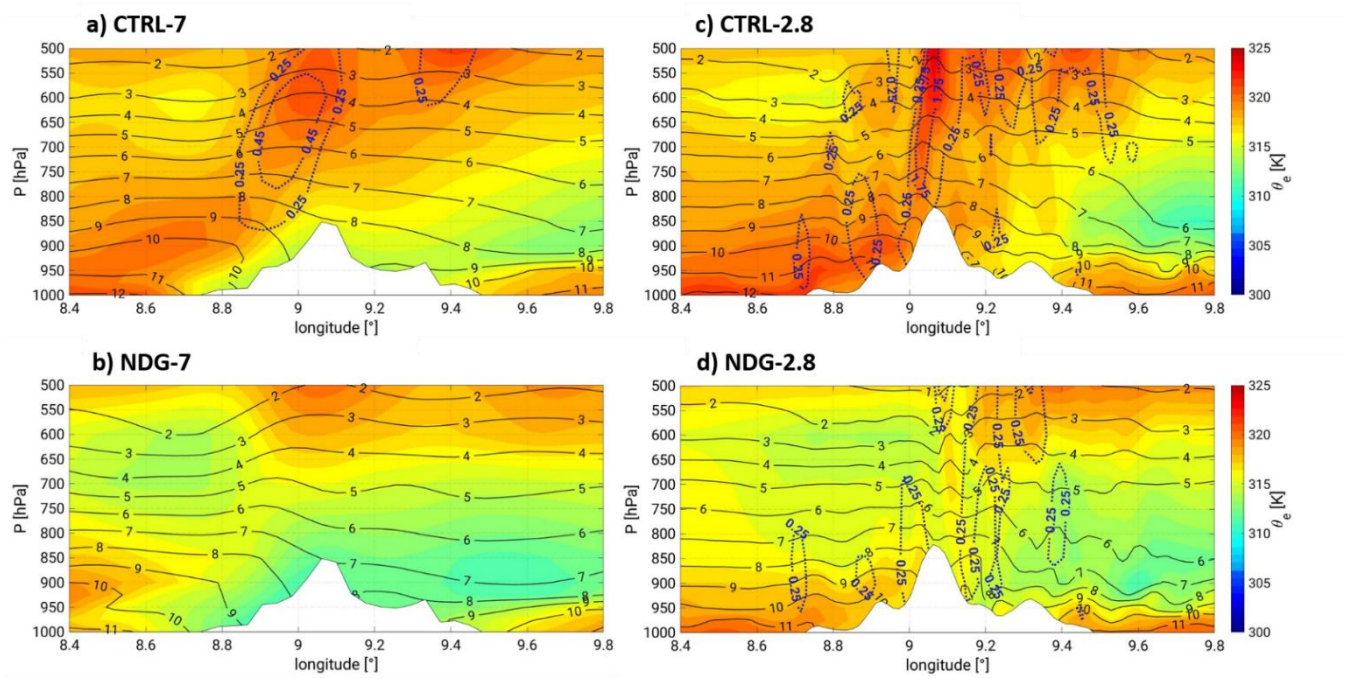

Figure 1~~0~~1. Vertical cross sections along the mean wind direction between 700 hPa and 1000 hPa (see transect in Fig. 1) on the 26-Oct 1700UTC. The selected hour corresponds to the first precipitation maximum represented over Corsica by the COSMO-CLM simulations. The position of the transect is represented in Fig. 1. The specific humidity values are represented as black contour lines, the colour shading represents equivalent potential temperature (θ_e). Vertical windspeed is represented in blue dashed contours, where isolines start at 0.25 m/s.

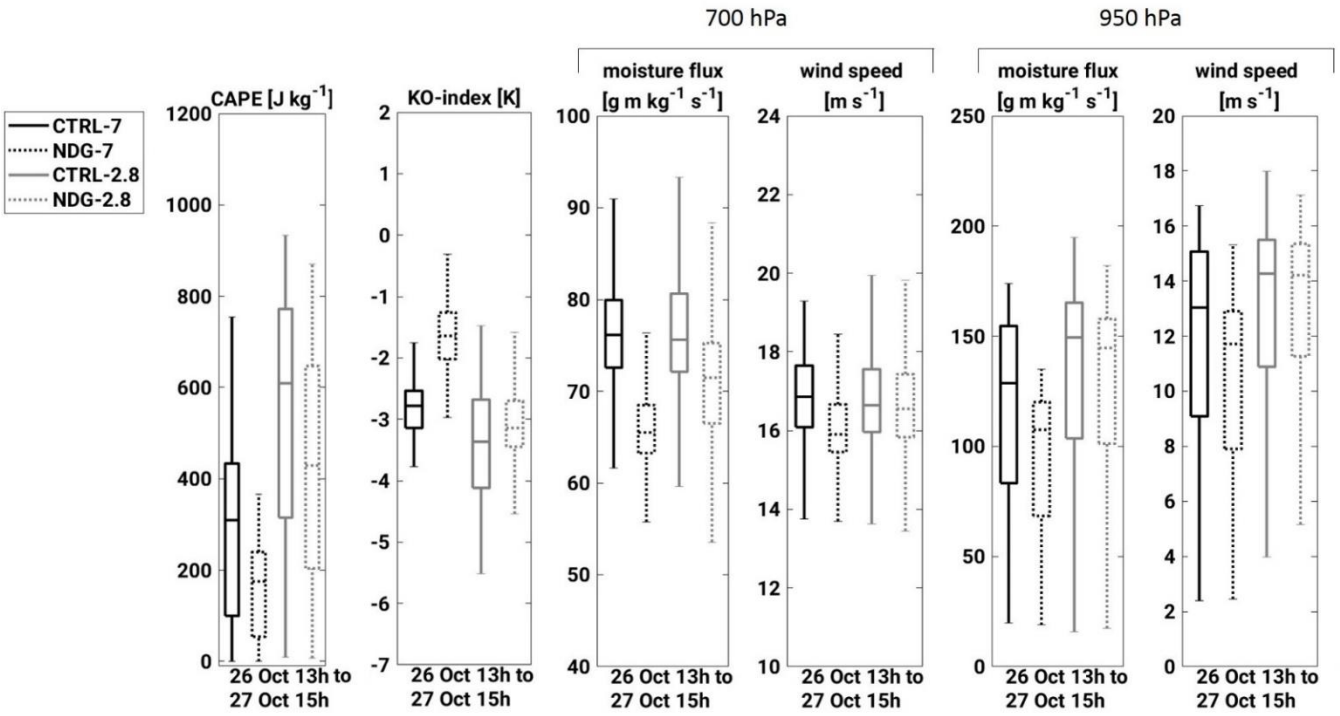

Figure 1~~2~~1. Box and whiskers plots showing the median, the percentiles 25 and 75 and the extreme values of ~~CAPE-ML~~CAPE, KO-index, moisture flux and horizontal wind speeds. All box and whiskers are obtained from the distribution of values for the shown quantities between the 26-Oct 1300 UTC and 27-Oct 1500 UTC over the study region CO.

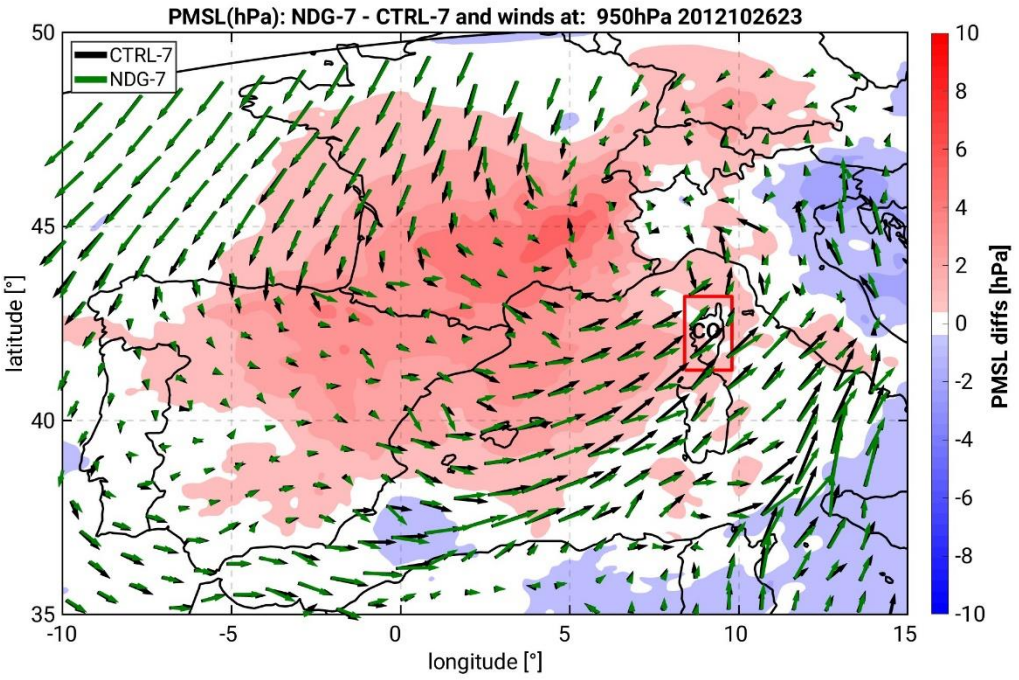

Figure 1~~2~~3. Spatial distribution of the differences in Pressure at the Mean Sea Level (PMSL) between NDG-7 and CTRL-7 on the 26-Oct 2300 UTC. Red colours indicate larger PMSL in NDG-7. Horizontal winds at 950 hPa are represented by black (CTRL-7) and green (NDG-7) arrows.

Table 3. Metrics for precipitation validation for the additional simulations initialized on the 20-Oct-2012. A description of the used metrics can be found in the Annex.

[mm]	Interp. To RG location			Distributions without interpolation	
	RMSE (1h)	$OBS_{\sigma} - MOD_{\sigma}$ (1h)	$\overline{OBS} - \overline{MOD}$ (27h)	$OBS_{\sigma} - MOD_{\sigma}$ (27h)	$OBS_{max} - MOD_{max}$ (27h)
CTRL-7	3.3	-0.85	-19.1	-33	-170
NDG-7	2.5	0.73	12.5	-5	-79
NDG-7-1h	2.5	0.95	12.2	-4	-50
CTRL-2.8	3.6	-0.15	9.5	-3	-74
NDG-2.8	2.6	1.64	23.8	11	-16
NDG-2.8-1h	2.5	1.64	23.6	10	-17

13. Annex

Table A.1 Precipitation validation metrics used in Tables 2 and 3. N are the total numbers of measurements at the rain gauges stations, hourly (1 h) or accumulated (27 h). M are all model grid points over land. For the first two metrics all hourly values between 26-Oct 1300 UTC and 27-Oct 1500 UTC are considered and COSMO-CLM is interpolated to the station's location. The third metric is an average of accumulated precipitation with COSMO-CLM values interpolated to the station's location. The last two metrics considered all observed and simulated precipitation values over land.

	Formula
RMSE (1h)	$\sqrt{\sum_{i(1h)}^{N}((OBS_i - \overline{OBS}) - (MOD_i - \overline{MOD}))^2}$
$\boldsymbol{OBS_\sigma - MOD_\sigma}$ (1h)	$\sqrt{\frac{1}{N}\sum_{i(1h)}^{N}(OBS_i - \overline{OBS})^2} - \sqrt{\frac{1}{N}\sum_{i(1h)}^{N}(MOD_i - \overline{MOD})^2}$
$\boldsymbol{\overline{OBS} - \overline{MOD}}$ (27h)	$\frac{1}{N}\sum_{i(27h)}^{N} OBS_i - \frac{1}{N}\sum_{i(27h)}^{N} MOD_i$
$\boldsymbol{OBS_\sigma - MOD_\sigma}$ (27h)	$\sqrt{\frac{1}{N}\sum_{i(27h)}^{N}(OBS_i - \overline{OBS})^2} - \sqrt{\frac{1}{M}\sum_{j(27h)}^{M}\left(MOD_j - \overline{MOD}\right)^2}$
$\boldsymbol{OBS_{max} - MOD_{max}}$ (27h)	$\max(OBS_{i(27h)}) - \max(MOD_{j(27h)})$

Table A.2 IWV Validation metrics used in Table 1 and Fig. 10 in Section 4.2

	Formula
Absolute Error (MAE)	$\frac{1}{N}\sum_{i=1}^{n}\lvert obs_i - mod_i\rvert$
Mean Bias (MB)	$\frac{1}{N}\sum_{i=1}^{n}(obs_i - mod_i)$
Agreement Index (AI)	$1 - \frac{\sum_{i=1}^{n}(obs_i - mod_i)^2}{\sum_{i=1}^{n}\left(\lvert obs_i - \overline{obs}\rvert + \lvert mod_i - \overline{mod}\rvert\right)^2}$

14. Supplementary Figures

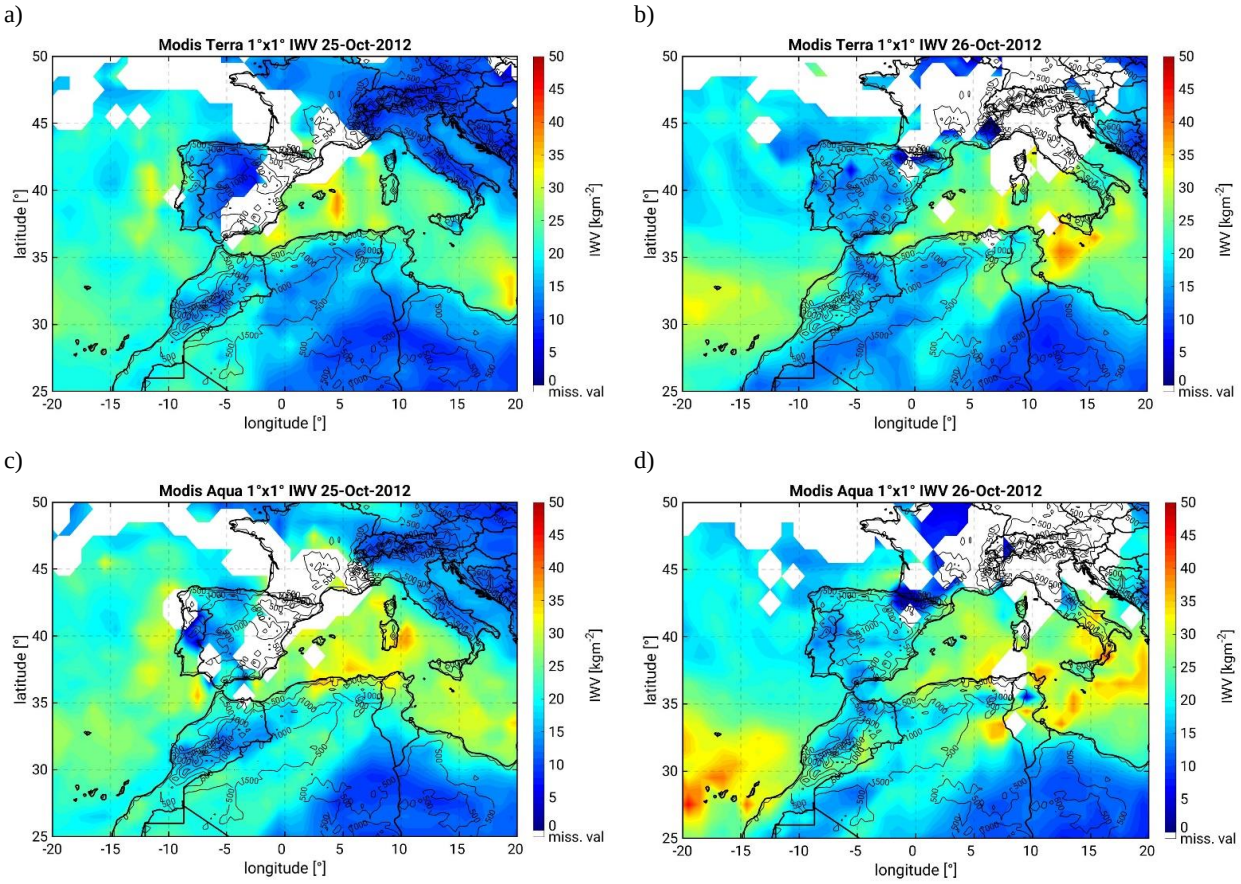

Figure S.1 Daily averaged IWV, measured by MODIS onboard the Terra (a,b) and Aqua (c,d) satellites. The spatial resolution is 1°x1°. The shown dates are 25-Oct-2012 (a, c) and 26-Oct-2012 (b, d). The products used are MOD08_D3 and MYD08_D3.

a)

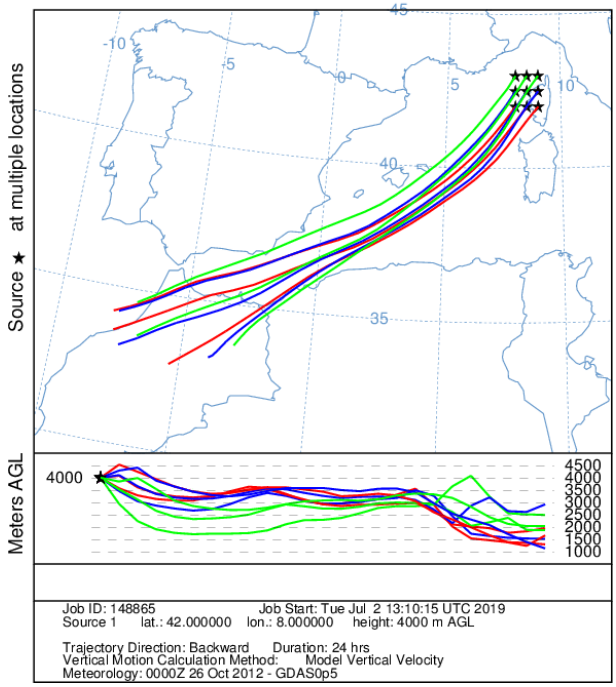

b)

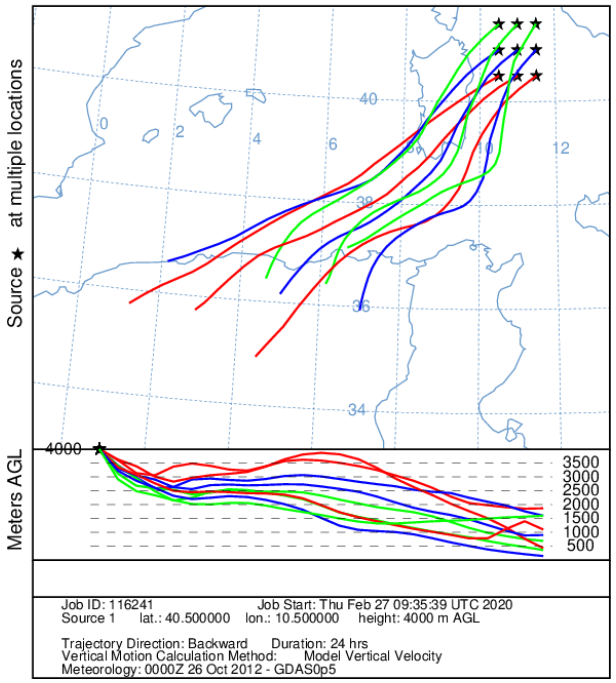

Figure S.2. HYSPLIT 24h backward trajectories initialized on 26-Oct-2012 1800 UTC supplementing the results of Fig. 6.c. They show the height levels at which ellipse A (a) and ellipse B (b) trajectories travel.

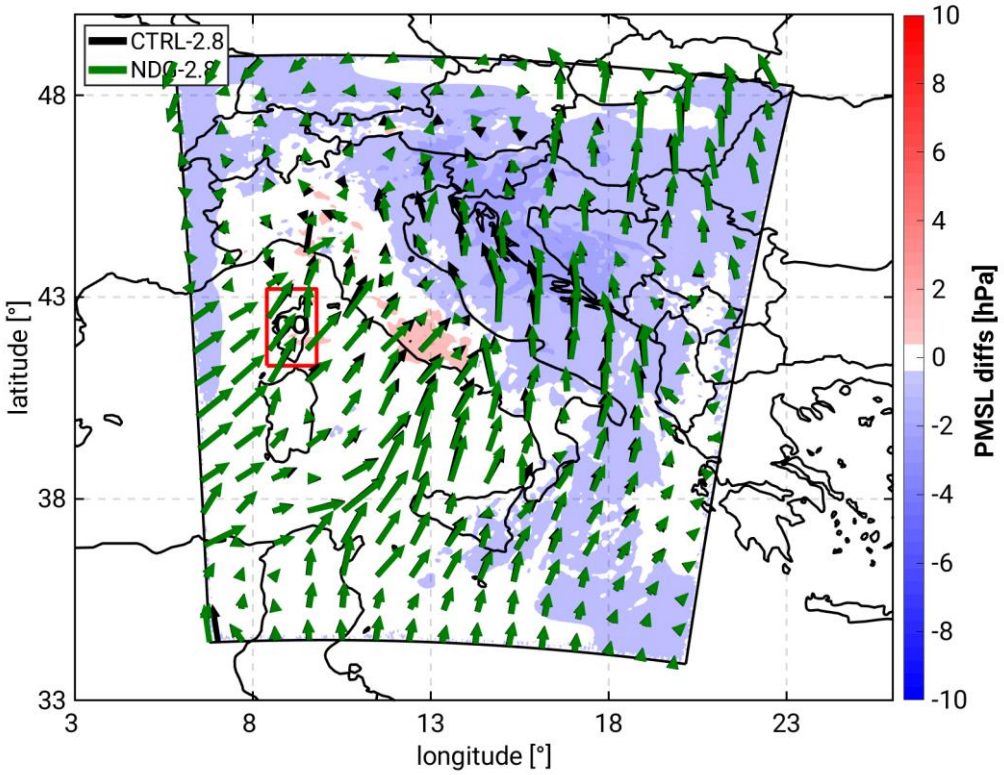

Figure SA.31 Spatial distribution of the differences in Pressure at the Mean Sea Level (PMSL) between NDG-2.8 and CTRL-2.8 on the 26-Oct 2300 UTC. Blue colours represent higher PMSL in CTRL-2.8. Horizontal winds at 950 hPa are represented by black (CTRL-2.8) and green (NDG-2.8) arrows.

~~Figure S.4. Precipitation amount as in Fig. 8 for the additional simulations initialized on the 20-Oct-2012 to study the dependency on the nudging temporal resolution. The accumulation time window is 26-Oct 1300 UTC to 27-Oct 1500 UTC.~~

a) CTRL-7 b) NDG-7 c) NDG-7-1h

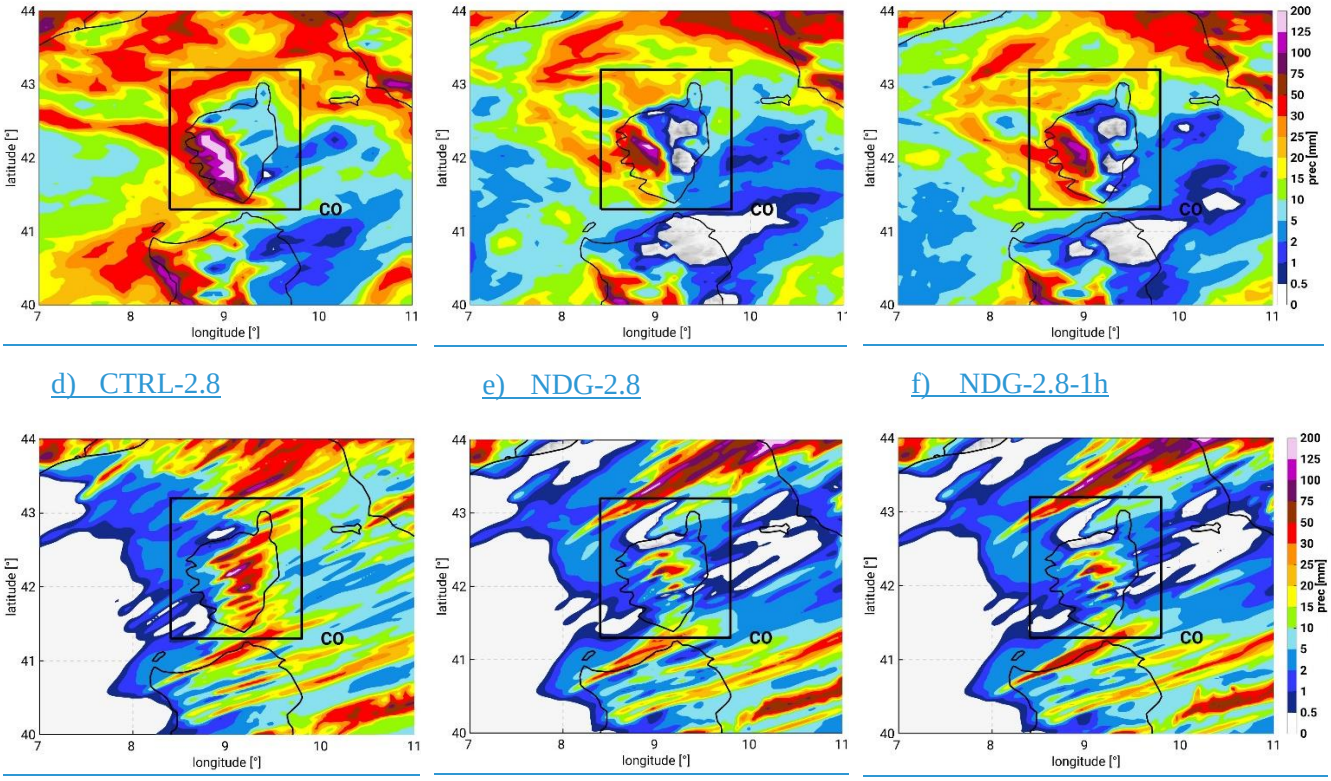

d) CTRL-2.8 e) NDG-2.8 f) NDG-2.8-1h

Figure S.4. Precipitation amount as in Fig. 8 for the additional simulations initialized on the 20-Oct-2012 to study the dependency on the nudging temporal resolution. The accumulation time window is 26-Oct 1300 UTC to 27-Oct 1500 UTC.